Ben-Gurion University of the Negev
Department of Electrical and Computer Engineering

Piezoelectric Transformers in Power Electronics

Thesis submitted in partial fulfillment
of the requirements for the degree
DOCTOR OF PHILOSOPHY

by

Svetlana Bronstein

Submitted to the Senate of Ben-Gurion University of the Negev

October 2005 תשרי תשס"ו

Beer-Sheva

ABSTRACT

The increasing utilization of piezoelectric transformers (PT) in power electronics requires fundamental analysis and design of PT power converters. In addition, the possibility of overcoming the essential limitations of PT power ability by a combined operation of PTs needs to be examined. These studies could provide wide opportunities for PT exploitation in power electronic circuits.

The main objective of this research is to develop generic models of PT power converters. We examine the output and input networks of the PT converter by utilizing a PT equivalent circuit.

Obtaining PT equivalent circuit parameters from physical measurements is a problematic issue. Therefore, the first concern of the present work is to try to improve the earlier published methods of PT parameters determination in order to make them suitable for every kind of PT and to the conditions under which the given PT operates. The study proposes and verifies two novel methods for extracting PT equivalent parameters from measurements.

A comparative analysis of the different types of rectifiers connected to the PT output is carried out in order to obtain generic models of PT AC/DC power converters. The methodology applied in this study follows the approach in which the PT output rectifier network is represented by an equivalent circuit that loads the PT as the corresponding rectifier.

The unique nature of a PT allows innovative circuit design that ensures soft switching without matching inductors. This design substantially reduces the costs of electronic components in the circuit. Therefore another aim of the research is to develop a generic approach for achieving soft switching with no additional reactive elements at the input.

To complete the work, the general requirements for the combined operation of several PTs are investigated.

Keywords: piezoelectric transformer, equivalent circuits, parameter estimation, generic approach, rectifiers, soft switching, power supplies.

CONTENTS

ASKNOWLEDGEMENTS

I would like to thank first and foremost my Ph.D. advisor Prof. Sam Ben-Yaakov, for his invaluable guidance and continued support during the course of this research work.

I am also extremely grateful to Prof. Gregory Ivensky for his help and encouragement. Without his assistance, I would have never accomplished this work.

Special thanks go to all the PEL students and staff for their help during my graduate career.

Last, I would like to express my profound gratitude to my family for their constant support and encouragement in my educational pursuits.

CHAPTER 1

INTRODUCTION

Power electronic circuits have traditionally been based on magnetic technology, and until recently, have not been part of the tide of miniaturization and integration advances from which signal-processing integrated circuits have benefited. The transformers and inductors in conventional converters are usually bulky compared to other elements. In an effort to miniaturize power components a piezoelectric, rather than a magnetic transformer could be employed in the power supplies. Utilization of piezoelectric transformers in power electronics became possible owing to new piezoelectric materials that have recently been developed. These materials exhibit improved piezoelectric ceramic characteristics. In the past few decades piezoelectric transformers used widely in many applications, such as DC/DC converters, adapters, and electronic ballasts for fluorescent lamps.

1.1. BACKGROUND

A. Piezoelectric Elements

Piezoelectric ceramics are characterized as smart materials and have been widely used in the area of actuators and transducers. Both piezoelectric actuators and transducers are made of piezoelectric ceramic elements. A piezoelectric element is composed of two electrode plates and a piezoelectric ceramic material. It can be side or end-plated and may be built as single or multi-layer structure (Fig. 1.1). Multi-layer construction increases entire capacitance of the ceramic element and decreases the volume of each layer and thus mechanical losses.

Generally speaking, piezoelectric elements can operate in either a longitudinal or transverse mode with a corresponding resonant frequency. In the longitudinal mode, the direction of the mechanical stress, T, is parallel to the electric or polarization direction, P, as shown on Fig. 1.2. In the transverse mode the direction of the mechanical stress, T, is perpendicular to the electric or polarization direction, P, as shown in Fig. 1.3. A piezoelectric element can operate as either an actuator or a transducer.

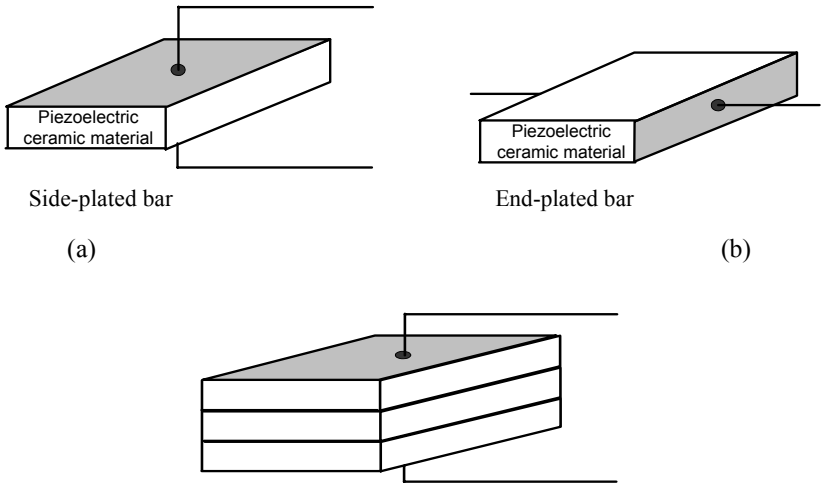

Fig. 1.1 Piezoelectric element. This element is composed of two electrode plates (side (a) or end plated (b)), made out of a piezoelectric ceramic material. The plate can be single (a, b) or multi-layered (c).

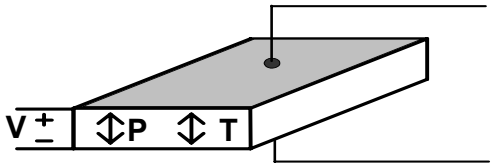

Fig. 1.2 Longitudinal mode piezoelectric element. In this type of element, the direction of the operating stress, T, is parallel to the polarization direction, P, with a corresponding resonant frequency.

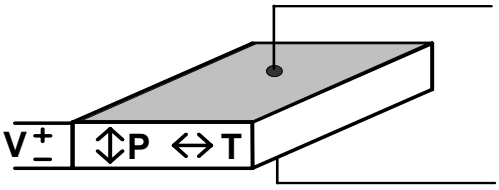

Fig. 1.3 Transverse mode piezoelectric element. In this type of element, the direction of the operating stress, T, is perpendicular to the polarization direction, P, with a corresponding resonant frequency.

B. Operational Principles

The operation principle of a piezoelectric transformer (PT) is that actuators and transducers function together so that energy can be transformed from an electrical form to an electrical form via mechanical vibration. In other words, in a piezoelectric transformer the converse and direct piezoelectric effects (in the actuator and transducer, correspondingly) are used to acoustically transform power from one voltage and current level to another through a vibrating structure. The converse piezoelectric effect, in which an applied electric field produces a resulting strain in a body, is used to convert an oscillating electric field to the primary part of a structure into a vibration mode of the entire bar. When driven at resonance, almost standing wave distributions of large amplitudes of stress and strain result. The resonantly amplified strain in the primary half of the ceramic bar is converted to a voltage across the output terminals by a direct piezoelectric effect. Depending upon the geometrical and material parameters, voltage amplifications of various magnitudes can be obtained, with associated step-ups/downs in current levels.

C. Physical Structure of PTs

On the whole, piezoelectric transformers can be classified into different categories based on their vibration modes or operating frequencies. They are commonly classified into three main groups: high voltage or Rosen-type PT [1-7], low voltage or thickness vibration mode PT [8-13], and radial vibration mode PT [14-16] (Figs. 1.4, 1.5, and 1.6 respectively).

The Rosen-type PT is made by a combination of a transverse mode piezoelectric actuator and a longitudinal mode piezoelectric transducer. Vibration occurs along its length direction and its resonant frequency is rather low. Because of the inherent high voltage gain associated with the Rosen-type PTs, they are commonly referred to as high voltage PTs. To achieve even higher voltage gain, the actuator, or transducer, or both of the Rosen-type PT may be made multi-layered [1, 3, 5-6]. The most suitable application for a Rosen-type PT is a driver for high voltage lamps, such as cold cathode fluorescent lamps used as a backlight sources for flat panel displays of notebook computers [4-5, 17-18].

The thickness vibration mode PT is a combination of a longitudinal mode actuator and a longitudinal mode transducer and both can be constructed as a single or a multi-layered structure. This type of PT is also known as a low voltage PT because of its inherent low

voltage gain. Since the vibration is occurs along its height the resonant frequency is high. Its main applications include DC/DC converters and adapters [19-22].

The radial vibration mode PT is a combination of piezoelectric actuator and transducer (single or multi-layer) both of which operate in the transverse mode. This type of PT can be used in different applications such as DC/DC converters, adapters, and electronic ballasts [23-25].

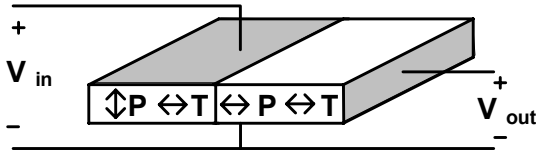

Fig. 1.4. Rosen-type piezoelectric transformer.

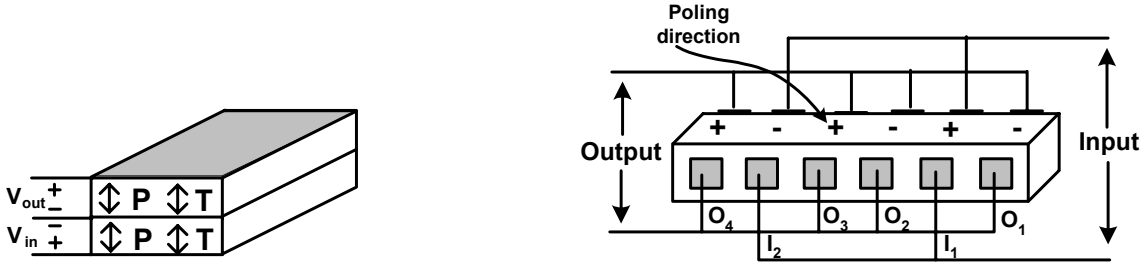

(a) (b)

Fig. 1.5. Thickness vibration piezoelectric transformer: (a) – single-layer, (b) – example of a multi-layer structure.

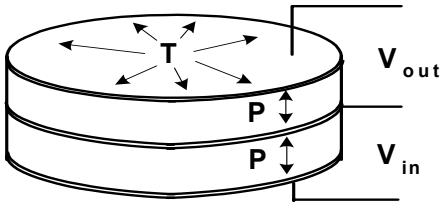

Fig. 1.6. Radial mode piezoelectric transformer.

1.2. MODELS FOR PIEZOELECTRIC TRANSFORMER POWER CONVERTERS

A. Electric Equivalent Circuit

It is obvious that to analyze and design a PT-based converter, a PT model has to be created in the form of a simple electric circuit. Generally, the behavior of PT can be represented by a transmission line with distributed parameters, which in turn would be transferred into a lamped parameters circuit [5-6, 16, 24, 26].

Since a PT is a non-linear element and its parameters are strongly dependent on the operational conditions such as the electric field, mechanical stress, temperature, depolarization, aging etc., creating a convenient electrical equivalent circuit that will represent the PT behavior, is not a simple matter. Such a circuit could estimate the equivalent PT parameters only under the very narrow range of frequencies and electrical loads.

Several studied describe the non-linear behavior of piezoelectric materials [27-29], but the models are quite complicated. The PT is represented as an electro-mechanical system that is described by a high order system of differential equations. This approach is essentially theoretical and does not attempt to obtain the simple electrical equivalent circuit.

Because of the different vibration modes and mechanical structures, the various PT categories have different mechanical and electrical characteristics. However, for a specific frequency bandwidth around the corresponding mechanical resonant frequency and a narrow load range, a single-branch equivalent circuit model can be developed (as shown in Fig. 1.7), which can characterize different types of PTs. In this model the circuit is identical to a series-parallel resonant network, which has been widely applied to a resonant converter, inverter or electronic ballast circuits. The parameters L_r, C_r, and R_m represent the mechanical behavior of the PT; C_{in} and C_o are the input and output dielectric capacitances; and n is the gain that represents electrical-mechanical and mechanical-electrical energy transformations. In general, these transformations can be represented by either of two equivalent circuits as shown on Fig. 1.8, both of which avoid DC coupling shorting as occurs in PT. However, the Type 2 network puts an inductance L_r in series with a dependent current source, as well as a capacitance C_o in parallel to a dependent voltage source, which may lead to convergence

problems in PSPICE simulations. Since this study uses PSPICE simulations for supporting analytical models of PT converters, the Type 1 equivalent network was applied.

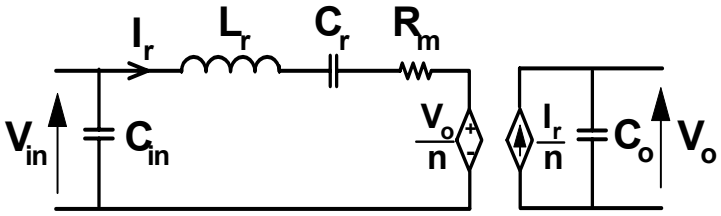

Fig. 1.7 Equivalent circuit of PT. C_r-L_r-R_m are the equivalent electrical parameters that represent the mechanical resonant circuit of PT, C_{in} and C_o are the input and the output capacitances, n is the gain.

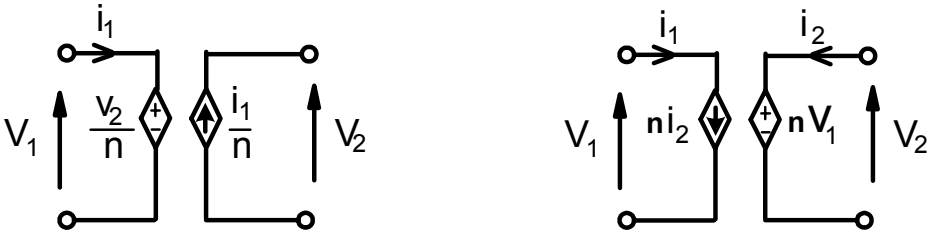

Type 1 **Type 2**

Fig. 1.8 Models for ideal transformer.

Different mechanical structures associated with different types of PT result in different equivalent circuit parameters. Various studies [5, 24, 26] have demonstrated how to obtain this equivalent circuit and how to estimate its parameters from the mechanical dimensions and ceramic material constants. However the non–linearity of the parameters of piezoelectric ceramic materials confines these results to a very narrow voltage-temperature-load range. In addition, there are some uncertainties regarding the estimation of electrodes resistance and disposition. All these factors indicate that for estimating PT behavior in the electric circuit, its equivalent parameters need to be obtained experimentally.

The problem of obtaining PT equivalent parameters from physical measurements has been widely discussed in the literature, but still remains an open issue. The majority of the proposed methods are based on the short-circuit test, which creates conditions that hardly resemble real operational conditions. Some works [30-31] use the transfer function test, but the process of extracting the equivalent parameters from experimental results with this test is far too complicated.

One of the objectives of the present investigation is to develop a simple process to find equivalent PT parameters from voltage gain and phase measured under practical operational conditions.

B. General Operation Characteristics of PT

A generic PT model was developed in [32]. The model consists of a system of closed form approximate equations that describe the main PT characteristics (efficiency, voltage ratio, output power) as a function of load and all PT parameters. This generic model proved to be very useful in engineering design. The present study uses this approach for further development of generic models of PT power converters and inverters.

C. Input Networks

A general approach to designing input and output matching networks is presented in [24, 32]. The main requirement for input network is that there are minimal losses in the switches. This can be achieved by soft switching. Most of the applications use additional inductive or capacitive-inductive networks at the input in order to achieve zero-voltage switching conditions [19, 22, 33-34]. However, a disadvantage when using this approach is that PT specific properties are not fully utilized. The unique nature of PT provides the opportunity for innovative circuit design that allows soft switching without compensating inductors. This means that PTs can be employed without any additional magnetic devices. Recent publications [23-24] have shown the effectivity of PT power converters built with no additional inductance in the input network.

The issue of a generic approach to achieve soft switching with no additional reactive elements at the input is still an open problem and is one of the focuses of the present study.

D. Output Networks

Low output voltage PT converters are usually built on a thickness or radial vibration mode PTs with two diode rectifier network. The converters use either a half-way or a current doubler rectifier with an inductive-capacitive filter (Figs. 1.9, 1.10). Converters for high output voltage typically use a Rosen-type PT and rectifier with capacitive filter as shown on Figs. 1.11 and 1.12. Different kinds of rectifiers were widely discussed in the literature [4-5, 33, 35-36], but there were no publications exist on the general operational characteristics of a PT AC/DC converter.

The advantages and disadvantages of each type of output networks and their characteristics when operating in a PT converter is another issue we address.

E. Power Limitations

PTs are especially suitable for low power applications, since its power ability is limited by mechanical losses. For higher power transform, in this research we suggest using the combined operation of several PTs. Its possibilities and general requirements are examined in this work.

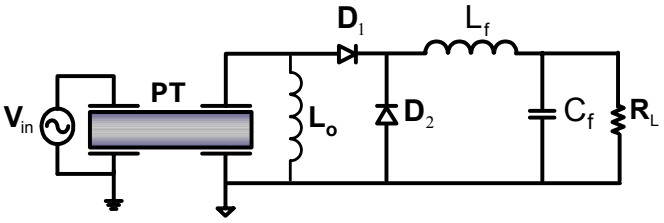

Fig. 1.9 Low voltage PT converter with half-way two diodes rectifier.

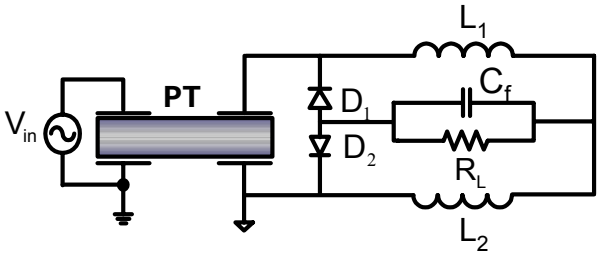

Fig. 1.10 Low voltage PT converter with current doubler rectifier.

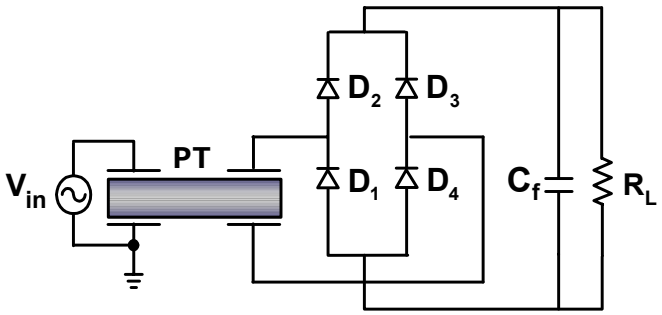

Fig. 1.11 High voltage PT converter with full way rectifier and capacitive filter.

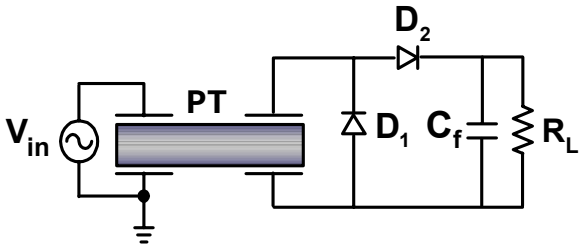

Fig. 1.12 High voltage PT converter with voltage doubler rectifier.

1.3. MOTIVATION

The miniaturization of power supplies has been an important issue in the power electronics industry during the last decade. The transformers and inductors used in conventional converters are usually bulky compared to other elements. Therefore low-profile transformers [38] were integrated to reduce the height and size of converters. PTs have several inherent advantages over low-profile transformers, such as a very low profile, high power density, no winding (which means suitability for automated manufacturing), high insulation properties, and potentially low cost.

Numerous studies have concentrated on the problem of how to substitute an electromagnetic transformer with a PT in power supplies. Because of the radically different nature of PT (resonant tank with high quality factor and essential capacitances at the input and the output) direct replacement of an electromagnetic transformer by PT in the electric circuit is impossible. As such, DC-DC converters' models are not appropriate for PT power supplies.

Prevailing models of PT converters usually relate to a concrete PT and hence present only partial solutions to the problem.

The increasing popularity of PTs in power electronics requires fundamental analysis and design of PT power converters, based on generic characteristics of the device. In addition, the essential limitation of PT power ability could be overcome by the combined operation of PTs. By realizing these conditions PT technology can be widely exploited in power electronic circuits.

1.4. Objective of the Research and Methods of Approach

The objective of the present research is to develop a generic model of PT power converters and to overcome the problem of PT power transfer limitations by combined operation of a number of PTs. We adhere to generic PT model and utilize the generic PT converter model for analysis and design of a PT converter with the desired characteristics – soft switching, maximum efficiency, and adequate voltage gain.

This approach motivated the following plan:

1) To complete the methods of PT parameters determination that will suit to every kind of PT and to the specific operational conditions of a given PT.
2) To develop generic analytical models of the prevailing rectifiers. A comprehensive comparison of the different rectifiers in PT power converters is to be carried out resulting in a recommendation of the preferred applications areas for each rectifier in terms of output current and voltage, power handling capability, and load resistance. The results of this study will be useful for optimal design of PT output networks or for the optimal design of PT for converters with desired characteristics.
3) To analyze the inherent soft switching capability of PTs. A generic analytical model should estimate the boundaries of soft switching in a power inverter/converter built around a given PT and should provide a PT design for soft-switching with no additional elements at the input.
4) To study the methods for combining identical and non-identical PTs, and to delineate the requirements for combined operation of PTs. In particular, we identify and quantify

the effect of non-identities in the PT parameters on current sharing and overall efficiency. This will prevent overheating of one or more of the combined PTs.

1.5. Dissertation Outline and Major Results

This dissertation is divided into six chapters, conclusions, and references. On the following we offer a brief description of each chapter.

Chapter 1 briefly reviews the background and application of piezoelectric transformers. Then, we set for the objectives and research plan.

Chapter 2 is devoted to obtaining equivalent circuit parameters from the physical measurements.

Chapters 3-4 discuss the behavior of a PT power converter with different kinds of output rectifiers as a particularly models of PT converters operating at either mechanical resonant frequency or frequency of maximum output power.

Chapter 3 studies steady-state processes in a power PT converter with a halfway two diodes output rectifier run at a mechanical resonant frequency. It is shown that such a power converter can operate in two modes: with or without overlap of the conduction intervals of the diodes. The analytical equations and characteristics derived in this study were found to be in good agreement with simulation and experimental results. The study highlights the effect of load and parasitic resistances on output voltage and the losses for both modes. Expressions obtained in the study can be used in engineering design.

Chapter 4 presents a comparative analysis of PT-based power converters that apply current doubler and voltage doubler types of rectifiers and operate at the frequency of maximum output voltage. The comparison methodology follows an approach developed earlier by which the output capacitor of PT and the rectifier sections are represented by an equivalent circuit. The equivalent circuit is linear and is composed of a parallel RC network that loads the PT as the corresponding rectifier does. We applied generic analysis to compare two types of rectifier, yielding generic models of PT AC/DC power converters.

Chapter 5 presents a general procedure for maintaining soft switching in an inductorless half-bridge PT inverter. Soft switching capability of the PT was examined and detailed guidelines are given for the load and frequency boundaries, voltage transfer function and

output voltage to maintain operation under ZVS conditions. The analysis takes into account the maximum power dissipation of the PT that is used to control the permissible power transfer through the device. The analytical results for the half-bridge inductorless PT inverter are verified by simulation and experiments for a radial vibration mode PT.

In **Chapter 6** the behavior of parallel-connected PTs was analyzed by applying a generic PT model that represents a combined network. The influence of a deviation in each of the PT parameters was examined with respect to total output power and losses. It was found that the requirements for identifying the equivalent circuit parameters R_m and C_o are not strong. The most critical parameter for equal loss in the PTs is ω_r – the mechanical resonant frequency of PTs, which has to be equal in the parallel units, even though the values of the parameters C_r and L_r can differ. Since resonant LCC-type inverters are practically identical to PT equivalent electrical circuit, the results of this study are relevant to combined connected LCC inverters. The analytical model verified by SPICE simulation and experiments. The experiments were done on parallel-connected PTs (T1-2, Face Co., VA, USA) and LCC inverters.

We complete the study with a summary of the main results and some suggestions for future research.

1.6. PUBLICATIONS

The thesis is based on material presented in papers published in refereed journals and in proceedings of international conferences, reference numbers [39-42, 44, 46].

CHAPTER 2

ESTIMATING THE PARAMETERS OF THE PT EQUIVALENT CIRCUIT

2.1. SHORT-CIRCUIT TEST

A single-branch equivalent circuit model (shown in Fig. 1.7) can characterize all types of PTs within a specific frequency bandwidth around the corresponding mechanical resonant frequency. The mechanical dimensions and material parameters of PT determine the parameters of this circuit [5-6, 16, 24, 26]. However, equivalent parameters should be obtained experimentally. The problem of obtaining PT equivalent parameters from physical measurements has been widely discussed in the literature, but still remains an open issue.

Considering the fact that a PT is a non-linear element, a linear network can describe its behavior only over small frequency and current/voltage (load) ranges. Measurement procedures for parameter extraction should therefore be carried out around the operational frequency of the device and at nominal current levels when the particular device is not that sensitive to the voltage level. The proposed method [39] extends the methods presented earlier [5, 24, 31].

When the input or output terminals of a PT are shorted, the electrical equivalent circuit is identical to the Y-parameter circuit model shown in Fig. 2.1. This Y-parameter circuit has been used to measure and characterize PT equivalent circuit parameters.

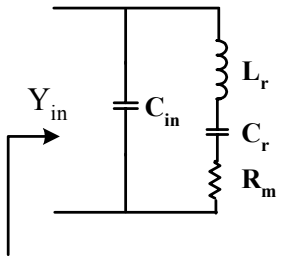

Fig. 2.1 Y-parameter equivalent circuit of PT with short circuited output terminals.

2.2. MEASUREMENT PROCEDURE

Measurements have to be carried out from the input and output sides of the PT while the complementary terminals are shorted. The equivalent circuit parameters of an experimental PT are obtained as follows:

1) The total input and output capacitances C_{Tin} and C_{To} are measured at low frequencies. These capacitances include in addition to C_{in} and C_o the series capacitance C_r and all parasitic capacitances in parallel to the series network C_r-L_r-R_m.
2) The input admittance Y_{in} (magnitude and phase) can be obtained by the setup shown in Fig. 2.2 applying the HP Network Analyzer. The input voltage of the PT should be chosen so as to keep the input current within the operational range of the device. The frequency is swept around the mechanical resonant frequency. The measured data V_A/V_R is recalculated to find the actual magnitude of admittance of the PT using the following expression:

$$Y_{in} = \frac{\frac{50+R_i}{(50+R_{ref})R_i}\frac{V_A}{V_R}}{1-\frac{50}{50+R_{ref}}\frac{V_A}{V_R}} \qquad (2.1)$$

3) The resonant f_r and anti-resonant f_a frequencies, corresponding to the zero imaginary part of the admittance, are found for both input and output terminals (in/o), respectively.
4) Input and output capacitances are estimated from the measured values of C_T, f_r and f_a [5], as follows:

$$C_{(in/o)} = \left(\frac{f_{r(in/o)}}{f_{a(in/o)}}\right)^2 C_{T(in/o)} \qquad (2.2)$$

This equation is valid when the quality factor Q_m of the PT is sufficiently high (Q_m>300), and if the parasitic capacitances parallel to the R_m-C_r-L_r and C_{in} network are negligibly small.

5) The series circuit parameters C_r-L_r-R_m (in/o) are calculated from the measured magnitude and the phase of the PT admittance by the method presented in [31] for the piezoelectric resonant blade elements. The method is based on two admittance values $Y_{in}(f_i)$, measured slightly before the resonant frequency. We calculate

$$R_{eq_i} = \frac{1}{\mathrm{Re}\{Y_{in}(f_i)\}}; \quad C_{eq_i} = \frac{\mathrm{Im}\{Y_{in}(f_i)\}}{\omega_i}$$
$$C_{p_i} = C_{eq_i} - C_T; \qquad C_{s_i} = \frac{\left[1 + (\omega_i C_{p_i} R_{eq_i})^2\right]}{(\omega_i C_{p_i} R_{eq_i})^2} C_{p_i} \tag{2.3}$$

Applying f_1 and f_2 in (2.3), we obtain parameters C_r-L_r-R_m:

$$L_r = \frac{C_{s_1} - C_{s_2}}{C_{s_1} C_{s_2} (\omega_1^2 - \omega_2^2)}; \quad C_r = \frac{C_{s_i}}{1 + \omega_i^2 C_{s_i} L_r}; \quad R_m = \frac{R_{eq_i}}{1 + (\omega_i C_{p_i} R_{eq_i})} \tag{2.4}$$

6) The transfer ratio "n" is extracted from the calculated values of the series inductances obtained from the input and output measurements as follows:

$$n = \sqrt{\frac{L_{r(out)}}{L_{r(in)}}} \tag{2.5}$$

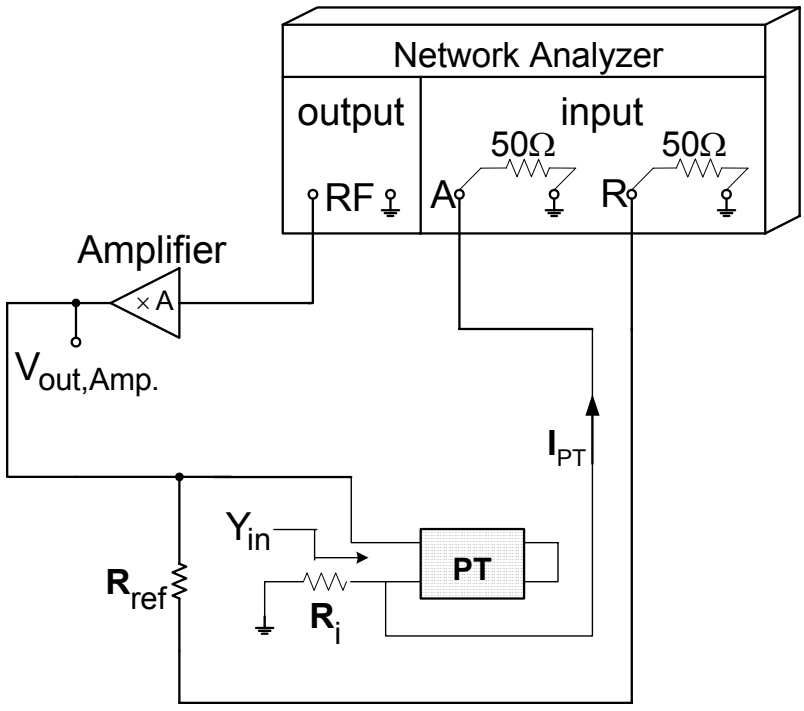

Fig. 2.2 Experimental setup.

2.3. MEASUREMENT OF THE RADIAL VIBRATION MODE PT SAMPLE

The experimental setup used a HP4395A Network Analyzer. The experimental sample was a radial vibration mode PT, Face Co., VA, USA.

The input rms voltage was approximately V_{in}=3V to keep the input current within operational range (250mA).

The measured data V_A/V_R (Fig. 2.3) was recalculated to find the actual magnitude of admittance by using the experimental R_i=1Ω and R_{ref}=466Ω.

The frequency was swept from 100 to 150 kHz.

Following the procedure described above, the equivalent parameters of the experimental PT were found to be as follows:

C_{in}=1.72nF, C_o=1.33nF, L_r=10.5mH, C_r=172.5μF, R_m=21Ω, n=1.08.

Fig. 2.3 shows the measured admittance (magnitude and phase) and the reconstructed admittance obtained by PSPICE simulation of the PT equivalent circuit applying the estimated model parameters. The slight difference between the experimental and reconstructed curves in the region of anti-resonant frequency is probably due to inaccuracies in estimating the input capacitance $C_{in.}$ An error in the value of this capacitance has a larger effect on f_a than on f_r because of the high impedance of the network in the anti-resonant region. The value of C_{in} can be corrected by iteration but this is not essential because the nominal operational region of the PT is near f_r where the matching between the measured and reconstructed admittance is excellent.

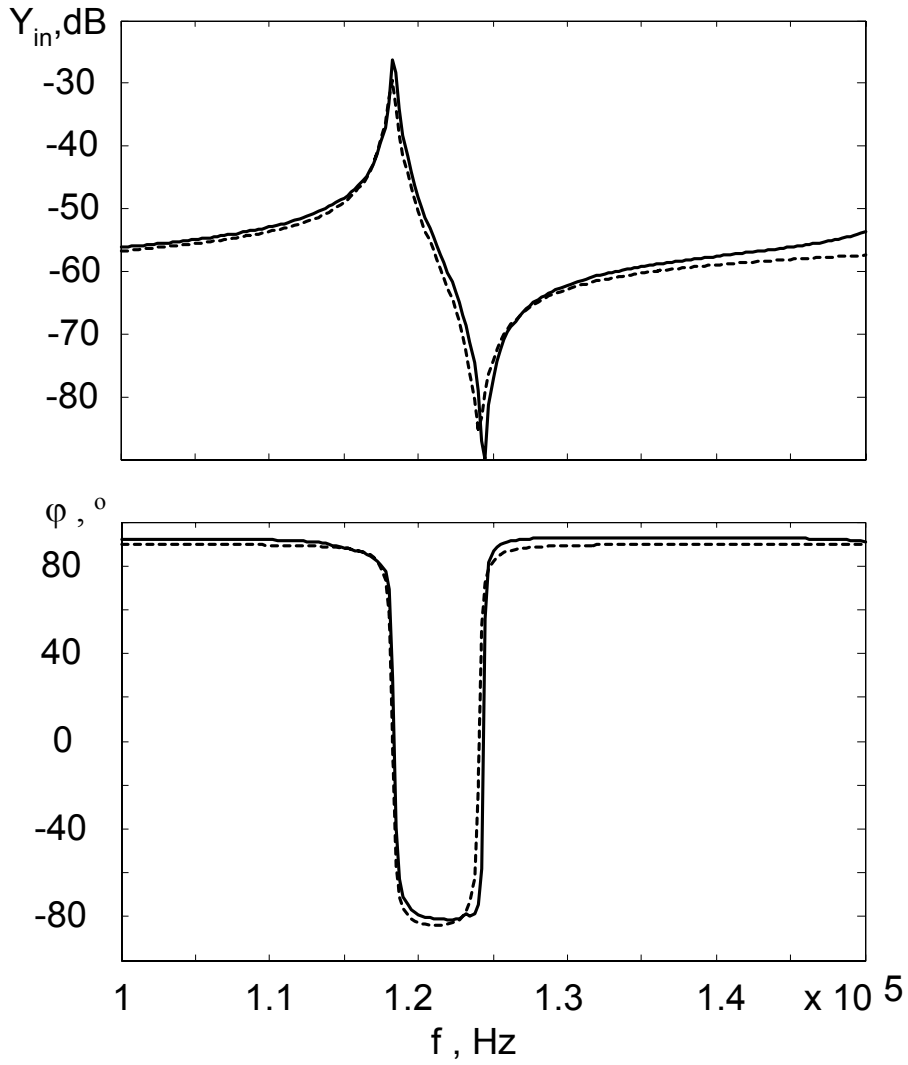

Fig. 2.3 Input admittance (upper – magnitude, lower – phase) of the experimental PT. Solid line – measured, dotted line – reconstructed by simulation of PT equivalent circuit based on the calculated equivalent circuit parameters.

2.4. TRANSFER FUNCTION TEST

In general, PT performance is dependent on the operating conditions (voltage/current) and load. When driving at a high level of vibration in a resonant mode with a strong electric field and high mechanical stress, parameters of piezoelectric materials become significantly non-linear.

Several attempts have been made to create a non-linear PT model or to correct the conventional equivalent PT circuit of PT [27-29], but no significant improvement was achieved. The majority of earlier methods for obtaining PT equivalent parameters are based on the short-circuit test, which imposes conditions that are far from real operational conditions. A few works [30 -31] used the transfer function test, but the process of extraction of the equivalent parameters from the experimental results, was too complicated. Furthermore, for high resistance loads and high output voltages (which are essential for Rosen-type PTs) the short circuit test could not estimate the parameters correctly because zero load resistance and zero output voltage could not meet nominal conditions. In addition, extraction of PT parameters using only two points from the entire measurement is not efficient. Although the equivalent circuit obtained from the two measured points of input impedance of shorted PT adequately characterizes the area around the chosen points, it might incorrectly estimate other areas.

To illustrate this shortcoming, we estimated the equivalent parameters of the Rosen-type PT (ELS-60) by algorithm presented in section 2.2. They were found to be: C_r=33pF, L_r=178mH, R_m=77.3Ω, n=5.06, C_{in}=700pF, C_o=11pF. Fig. 2.4, which shows the measured and calculated input impedance of the shorted PT, indicates that the area around the mechanical resonant frequency is estimated accurately, but in general there is poor agreement between the theoretical and measured results.

PT parameters are dependent on numerous conditions that cannot be taken into account in one simple analytical model. Therefore the only way to accurately estimate PT behavior in a network is to extract the equivalent parameters from an experiment carried out under nominal operational conditions (nominal voltage and load ranges). This can be accomplished by measuring the output to input voltage gain and phase of a loaded PT.

The objective of this section is to create a simple algorithm for obtaining the equivalent PT parameters from the measurements of the voltage ratio (amplitude and phase) of the loaded PT, and to verify the dependence of these PT parameters on the load resistance.

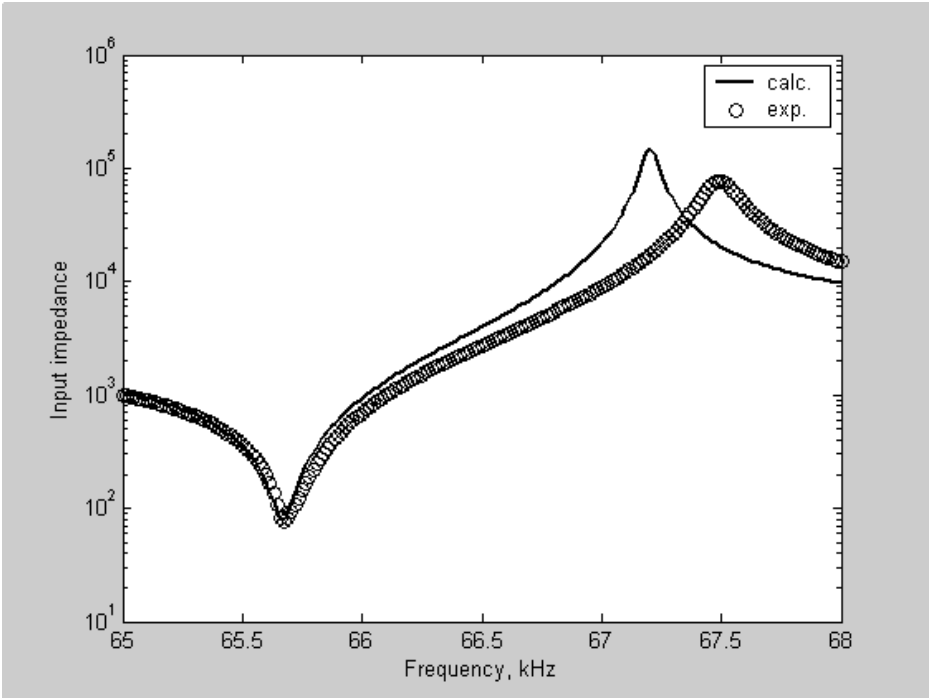

Fig. 2.4 Measured (circles) and calculated (solid line) input impedance of a PT with shorted output terminals. The PT equivalent parameters for the calculated curve were extracted from the short circuit test.

2.5. EXTRACTION OF MODEL PARAMETERS

Measurements are carried out from the input and output sides as the complementary terminals are loaded by the nominal load resistances (R_L at the output and R_L/n^2 at the input terminals). The voltage ratio (magnitude and phase) can be obtained by the setup shown in Fig. 2.5. The frequency is swept around the mechanical resonant frequency. The magnitude of voltage ratio V_{out}/V_{in} is recalculated from the measured data V_A/V_R as follows:

$$\frac{V_{out}}{V_{in}} = \frac{50 + R_{ref(i)}}{50 + R_{ref(j)}} 10^{\left(\frac{V_A}{V_R}\right)/20} \tag{2.6}$$

where i=2, j=1 for the forward voltage ratio and i=1, j=2 for the backward voltage ratio.

The forward voltage transfer ratio k_o of a PT with a voltage source connected at the input port and a load connected at the output port (Fig. 2.6, a) is

$$k_o = \frac{V_o}{V_{in}} = \frac{1}{n + \frac{nR_m}{R_f} + \frac{nC_o}{C_r} - \omega^2 nL_r C_o + j\left[\omega\left(\frac{nL_r}{R_f} + nR_m C_o\right) - \frac{n}{\omega C_r R_f}\right]} \tag{2.7}$$

where ω is the angular operating frequency ω=2πf, and $R_f=R_{ref2}+50\Omega$ is the forward load resistance.

The real and the imaginary parts of the inverted voltage ratio $k_f=1/k_o$ are

$$\begin{cases} \mathrm{Re}(k_f) = n + \frac{nR_m}{R_f} + \frac{nC_o}{C_r} - \omega^2 nL_r C_o \\ \mathrm{Im}(k_f) = \omega\left(\frac{nL_r}{R_f} + nR_m C_o\right) - \frac{n}{\omega C_r R_f} \end{cases} \tag{2.8}$$

The backward voltage ratio k_i of a PT with a voltage source connected at the output port and a load connected at the input port (Fig. 2.6, b) is

$$k_i = \left(\frac{V_o}{V_{in}}\right) = \frac{1}{\frac{1}{n} + \frac{nR_m}{R_r} + \frac{nC_{in}}{C_r} - \omega^2 nL_r C_{in} + j\left[\omega\left(\frac{nL_r}{R_r} + nR_m C_{in}\right) - \frac{n}{\omega C_r R_r}\right]} \tag{2.9}$$

where $R_r=R_{ref1}+50\Omega$ is the backward load resistance.

The real and imaginary parts of the inverted ratio $k_r=1/k_i$ are given respectively by the following equations:

$$\begin{cases} \mathrm{Re}(k_r) = \dfrac{1}{n} + \dfrac{nR_m}{R_r} + \dfrac{nC_{in}}{C_r} - \omega^2 nL_r C_{in} \\ \mathrm{Im}(k_r) = \omega\left(\dfrac{nL_r}{R_r} + nR_m C_{in}\right) - \dfrac{n}{\omega C_r R_r} \end{cases} \tag{2.10}$$

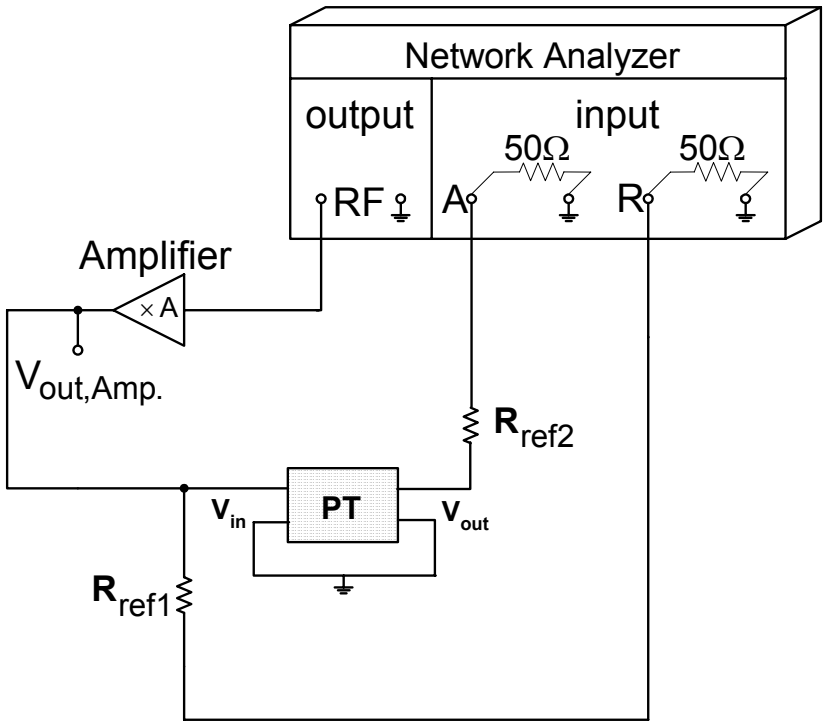

Fig. 2.5. Experimental setup for PT equivalent parameter measurements. The amplifier is connected to the input/output sides while the complementary terminals are loaded by the nominal load resistances – R_{ref2} and R_{ref1}.

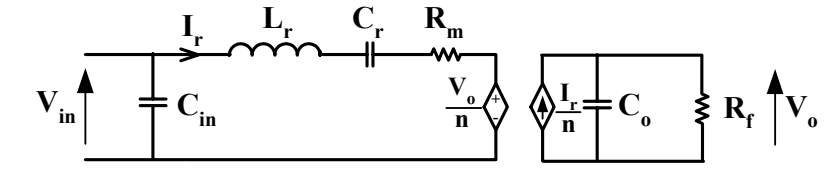

(a)

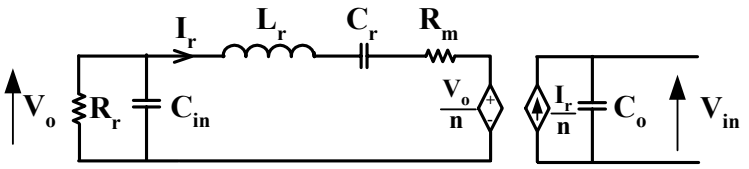

(b)

Fig. 2.6. The equivalent circuit of the loaded PT: (a) – when the voltage source is connected at the input port and load the resistance is connected at the output port, (b) – when the voltage source is connected at the output port and the load resistance is connected at the input port.

Applying Eq. (2.8) and (2.10) we obtain expressions for tangents of the phases of the forward and backward voltage ratios as follows:

$$\tan(\varphi_f) = \frac{\mathrm{Im}(k_f)}{\mathrm{Re}(k_f)} = \frac{\omega\left(\frac{nL_r}{R_f} + nR_mC_o\right) - \frac{n}{\omega C_r R_f}}{n + \frac{nR_m}{R_f} + \frac{nC_o}{C_r} - \omega^2 nL_rC_o} \tag{2.11}$$

$$\tan(\varphi_r) = \frac{\mathrm{Im}(k_r)}{\mathrm{Re}(k_r)} = \frac{\omega\left(\frac{nL_r}{R_r} + nR_mC_{in}\right) - \frac{n}{\omega C_r R_r}}{\frac{1}{n} + \frac{nR_m}{R_r} + \frac{nC_{in}}{C_r} - \omega^2 nL_rC_{in}} \tag{2.12}$$

These expressions can be transformed into

$$\tan(\varphi_f)=\frac{\omega^2\left(L_rC_r+R_mC_oC_rR_f\right)-1}{\omega\left(C_rR_f+R_mC_r+C_oR_f\right)-\omega^3L_rC_oC_rR_f} \tag{2.13}$$

$$\tan(\varphi_r)=\frac{\omega^2\left(L_rC_r+R_mC_{in}C_rR_r\right)-1}{\omega\left(\frac{1}{n^2}C_rR_r+R_mC_r+C_{in}R_r\right)-\omega^3L_rC_{in}C_rR_r} \tag{2.14}$$

Applying

$$a_1=L_rC_oC_rR_f \qquad a_2=L_rC_r+R_mC_oC_rR_f \qquad a_3=C_rR_f+R_mC_r+C_oR_f \tag{2.15}$$

and

$$b_1=L_rC_{in}C_rR_r \qquad b_2=L_rC_r+R_mC_{in}C_rR_r \qquad b_3=\frac{1}{n^2}C_rR_r+R_mC_r+C_{in}R_r \tag{2.16}$$

we simplify (2.13-2.14) to

$$\begin{cases} a_1\omega^3\tan(\varphi_f)+a_2\omega^2-a_3\omega\tan(\varphi_f)=1 \\ b_1\omega^3\tan(\varphi_r)+b_2\omega^2-b_3\omega\tan(\varphi_r)=1 \end{cases} \tag{2.17}$$

Solving (2.17) by the least mean square method using the measured phase of the transfer function and applying the attained a-b values to (2.15-2.16) we obtain six equations that allow us to make an initial estimation of six PT parameters. However, because of the rational behavior of the phase tangent the estimated amplitude is proportional to the actual amplitude of the voltage ratio with a constant coefficient “k”. A constant “k” can be obtained from the measured voltage ratio $k_{o(exp)}$ and the estimated voltage ratio $k_{o(est)}$ as $k=k_{o(exp)}/k_{o(est)}$. Applying (2.11)-(2.12), taking into account that phase angle is estimated correctly and assuming that C_o and C_{in} do not depend on the load resistance, we can see that parameters R_m and L_r are proportional to k^2, C_r is proportional to $1/k^2$ and n is proportional to k. Hence, the actual PT equivalent parameters are recalculated from the initial estimation as follows: $R_m=k^2R_{m(ini)}$, $L_r=k^2L_{r(ini)}$, $C_r=C_{r(ini)}/k^2$, $n=kn_{(ini)}$.

2.6. MEASUREMENT OF A ROSEN-TYPE PT SAMPLE

The experimental setup applied a HP4395A Network Analyzer. The experimental sample was a Rosen-Type PT, ELS-60. The objective of this test was to find the load dependence of the PT parameters. The experiment was carried out under the Following conditions:

1) The rms voltage applied to the input port was about $V_{in\ rms}$=4V. The rms voltage applied to the output port was adjusted so as to obtain $4V_{rms}$ at the input at resonance frequency.

2) The frequency was swept from 62 to 75 kHz.

3) The load resistances R_{ref2} connected at the output port while measuring the output/input voltage ratio varied from 10kΩ to 500kΩ.

4) Correspondingly, the load resistances connected at the input port while measuring the input/output voltage ratio varied from 400 to 20kΩ.

5) The measured data V_A/V_R (Fig. 2.4) was recalculated to find the actual magnitude of the voltage ratio.

6) Parameters were calculated from the phase measurements and then corrected following the procedure described above.

To confirm the obtained results, the measured and calculated voltage ratios and phase were compared. The calculated voltage ratio and phase values were obtained by applying (2.7) and (2.9). Fig. 2.7 shows measured and calculated amplitude and phase of voltage ratio before and after correction of the PT parameters (R_L=56.9kΩ). One can see that after correction, there is good agreement between the calculated and measured voltage ratios.

For verification of the proposed method an independent measurement of the loaded PT input impedance was carried out. Fig. 2.8 depicts the measured impedance and the impedance calculated from the parameters obtained for R_L=56.9kΩ. There is good agreement between the experiment and the calculation.

Fig. 2.9 shows the PT parameters n, R_m, Cr, L_r, and the mechanical resonant frequency as a function of the load resistance R_L. As can be seen, parameters L_r and C_r are slightly dependent on the load while the mechanical resonant frequency is noticeably dependent on it. The parameter n is somewhat independent from the load resistance whereas R_m is strongly dependent on it.

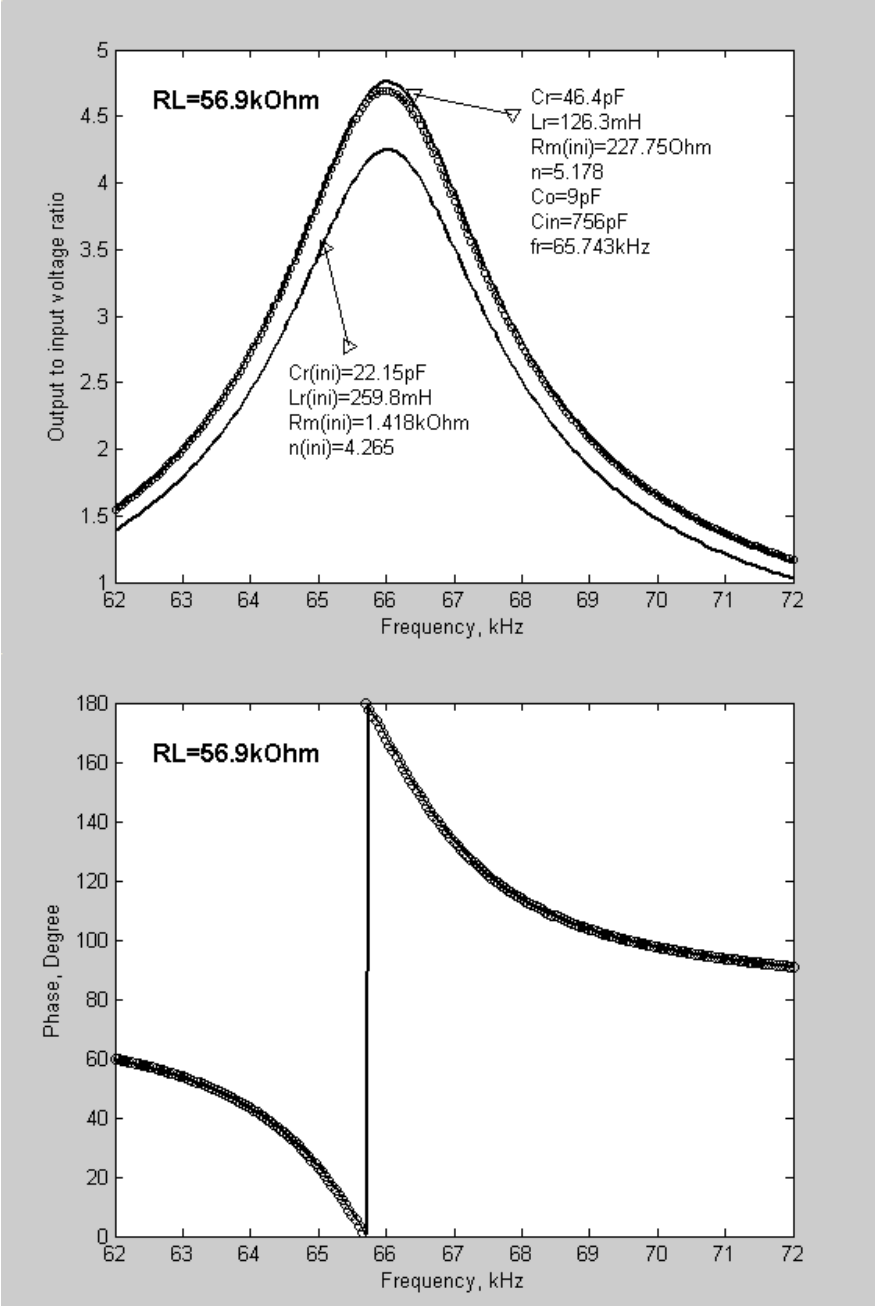

Fig. 2.7. Measured and reconstructed voltage ratio and phase as a function of frequency. Solid lines are the calculated and circles are the experimental results. Lower solid line in the voltage ratio plot (parameters with subscript ini) is obtained before parameter correction, upper solid line is obtained after parameter updating,

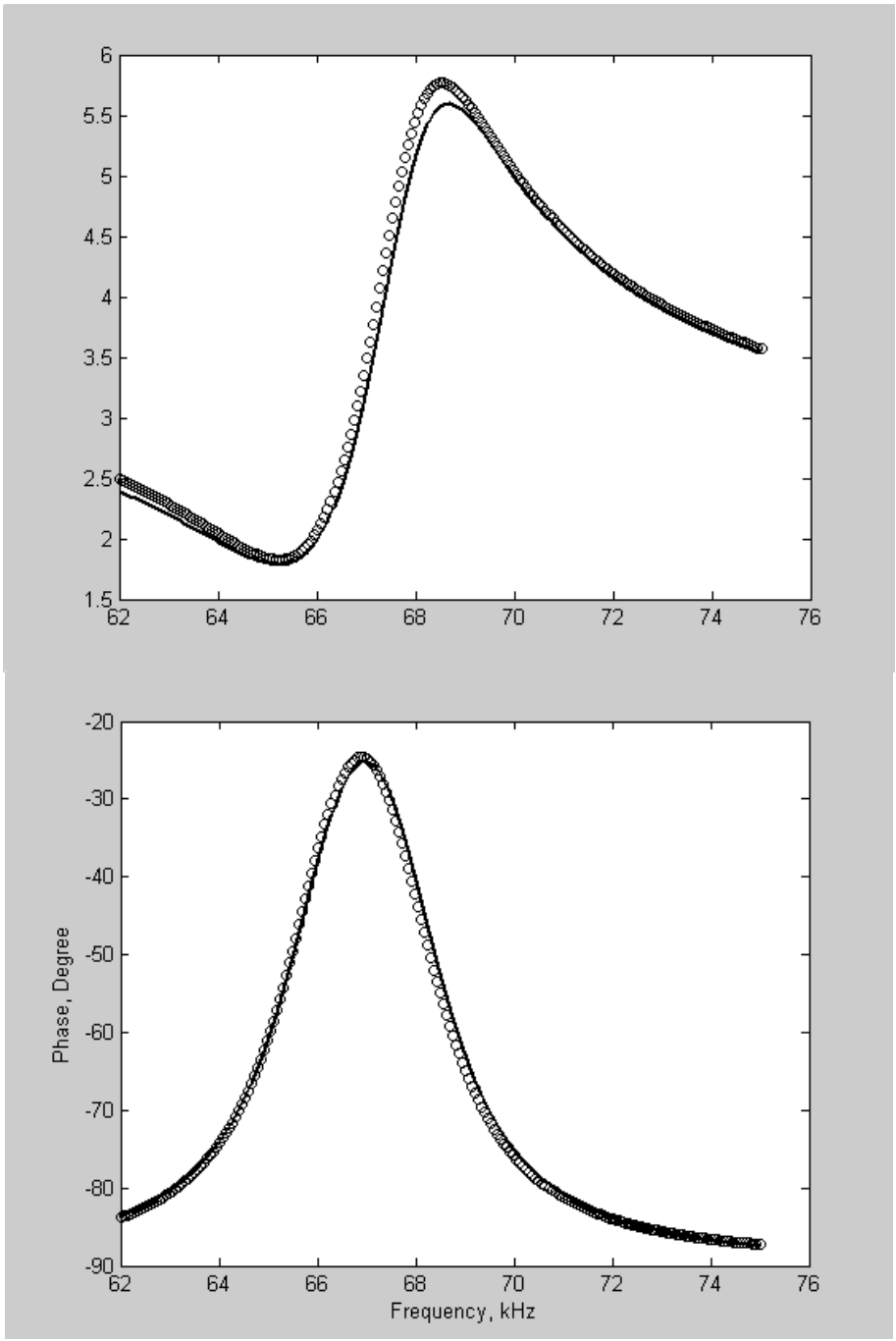

Fig. 2.8. Measured and calculated input impedance (a – amplitude, b – phase) as a function of frequency.

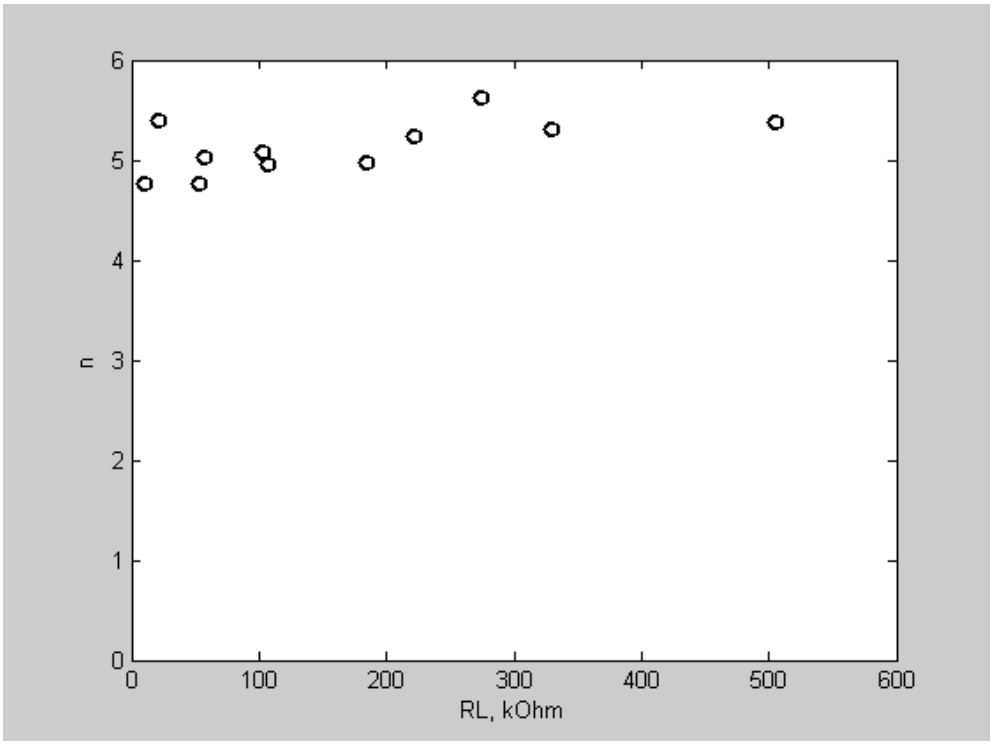
n
RL, kOhm
0
1
2
3
4
5
6
0
100
200
300
400
500
600

(a)

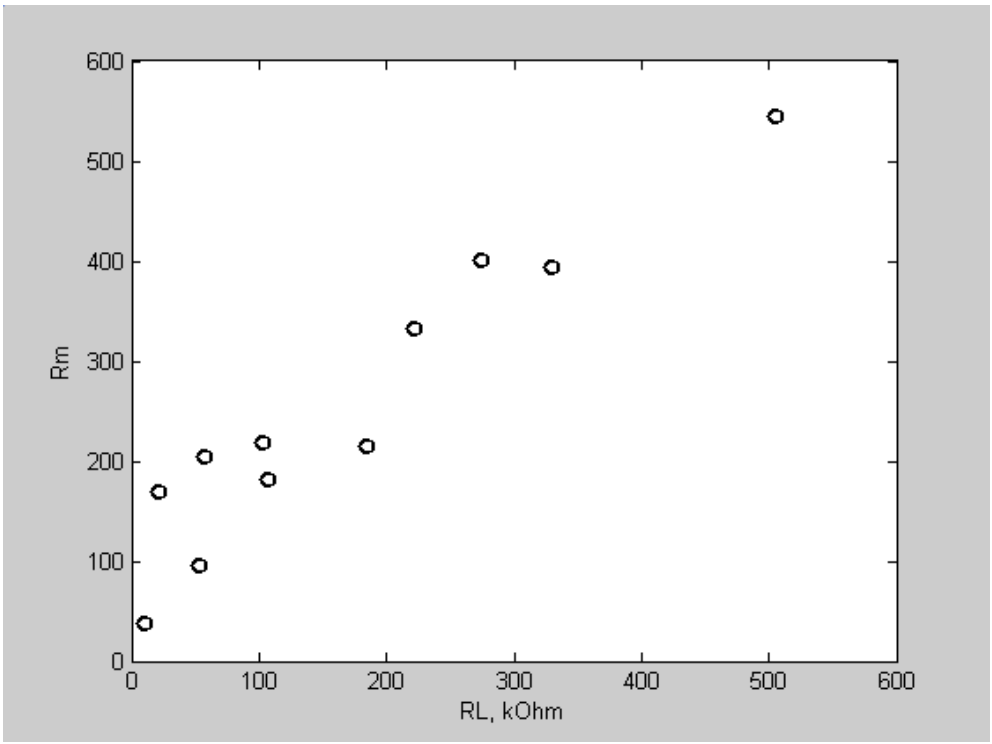
Rm
RL, kOhm
0
100
200
300
400
500
600
0
100
200
300
400
500
600

(b)

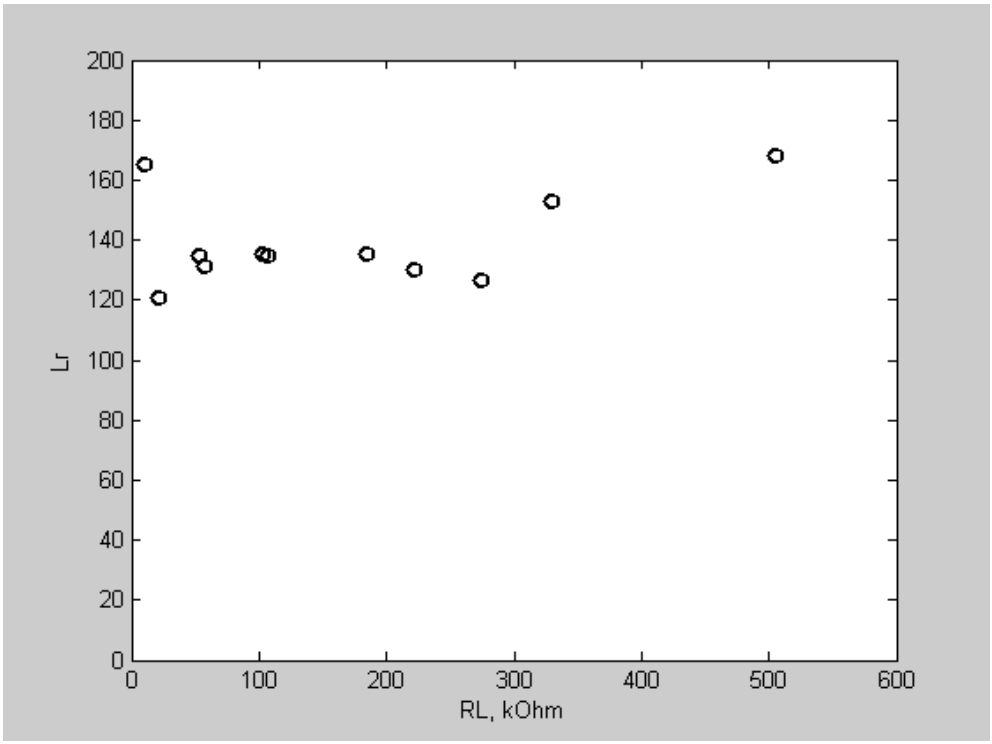
Lr
RL, kOhm
0
20
40
60
80
100
120
140
160
180
200
0
100
200
300
400
500
600

(c)

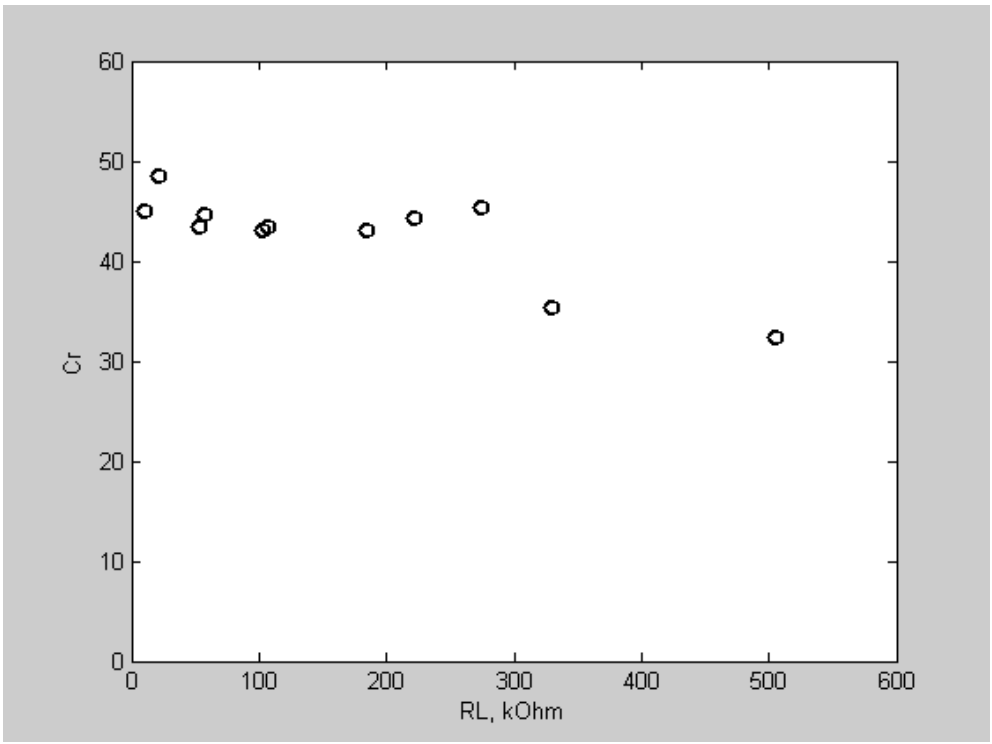
Cr
RL, kOhm
0
10
20
30
40
50
60
0
100
200
300
400
500
600

(d)

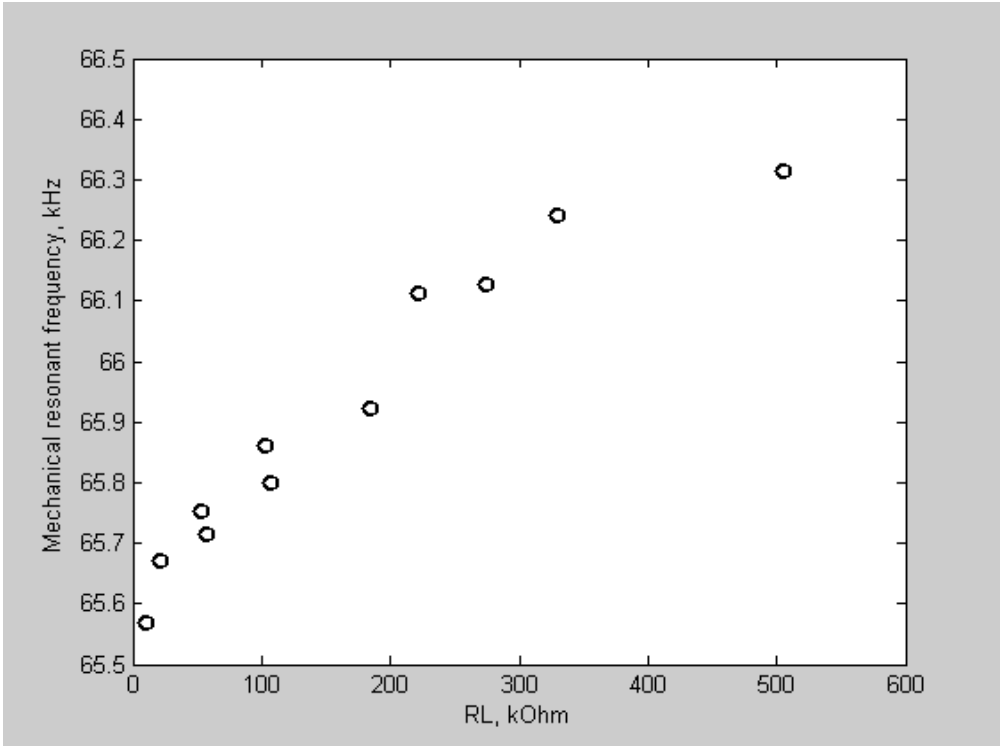

(e)

Fig. 2.9. PT equivalent parameters n, R_m, C_r, L_r – (a)-(d), and the mechanical resonant frequency of PT – (e) as a function of the load resistance.

2.7. CONCLUSIONS

Two ways for obtaining PT equivalent parameters from physical measurements: the short circuit test and the transfer function tests are proposed in this section. Each test was verified by simulation and experiment.

It was shown that the short circuit test, which is based on utilizing the characteristic points of the input impedance, although easier to implement, is recommended for those PTs that are not sensitive to voltage levels. On the other hand, the transfer function test, which is based on the all the information obtained from the measurements of the voltage transfer ratio (amplitude and phase), is more accurate and suits every type of PT.

We also demonstrated the dependence of PT equivalent parameters on the load resistance.

CHAPTER 3

A PIEZOELECTRIC TRANSFORMER DC/DC CONVERTERS' OUTPUT NETWORKS I

With the advance development of PT technology, this transformer may turn into a viable alternative to electromagnetic transformers in various applications such as DC/DC converters. The issue of optimal PT converter design becomes, therefore, an important issue that needs to be addressed.

3.1. Analysis and Design of a Piezoelectric Transformer DC/DC Converter in a Low Voltage Application

The typical output rectifier networks that can be applied to PT converters, as discussed in Chapter 1 (Figs. 1.1-1.4) are

1) The current doubler rectifier;
2) The half-way rectifier with two diodes and an LC-filter;
3) The full-way four diodes rectifier with the capacitive filter;
4) The voltage doubler rectifier with the capacitive filter.

PT power converters commonly operate in one of two modes: at a mechanical resonant frequency or at a frequency of maximum output voltage (or power, which is the same). When we use a half-way, two diode rectifier with an LC filter at the output (Fig. 1.2) we have to ensure that there is a direct current path because a DC current cannot flow through the output terminals of the PT. To deal with this problem we connected an additional inductance L_o parallel to the PT output. This inductance has to be chosen so that the parallel branch L_oC_o and the series branch L_rC_r have the same resonant frequencies, so as to minimize the circulating energy in the reactive elements of the circuit. For this reason, the converter should be operating at a mechanical resonant frequency [4-5, 20].

To date, only one operational mode of this converter has been comprehensively studied, namely the mode with no overlapping intervals of the diodes' currents. However, when carrying out experiments on this circuit, one sees that the output voltage is dependent on the load, in contrast to what was expected according to the simple theoretical model. When the load resistance decreases the output voltage becomes strongly dependent on the load resistance.

In this chapter the behavior of a low voltage PT converter with a half-bridge two-diode rectifier over the full load range is investigated. We develop a closed-form equations model that embraces all operating modes of the converter.

3.2. PRINCIPLE OF OPERATION OF A HALF-WAY TWO DIODES RECTIFIER

The conventional equivalent circuit of the PT was used to analyze the low voltage DC/DC converter topology (Fig. 3.1). This circuit is composed of $L_r, C_r, R_m, C_{in}, C_O$, a voltage source $\frac{v_{Co}}{n}$ and a current source $\frac{i_r}{n}$ (n is the transformer turn ratio) [32]. A halfway rectifier Rect and an inductor L_o are connected at the output of the PT. The rectifier includes two diodes (D_1, D_2) and an L_f, C_f filter. R_L is the load resistance. The function of L_o in this circuit is to provide a path for the DC current and also to cancel the circulating energy caused by C_o [5]. The resonant frequency of the parallel circuit L_o, C_o has to be equal to the series resonant frequency of the PT.

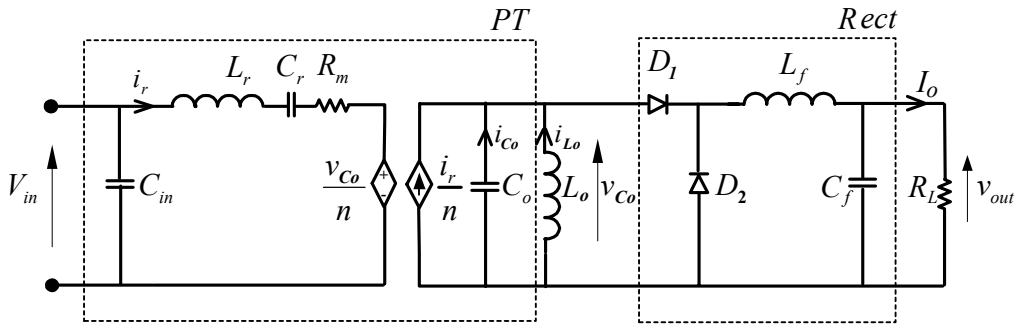

Fig. 3.1 The PT converter loaded by a halfway two diodes rectifier.

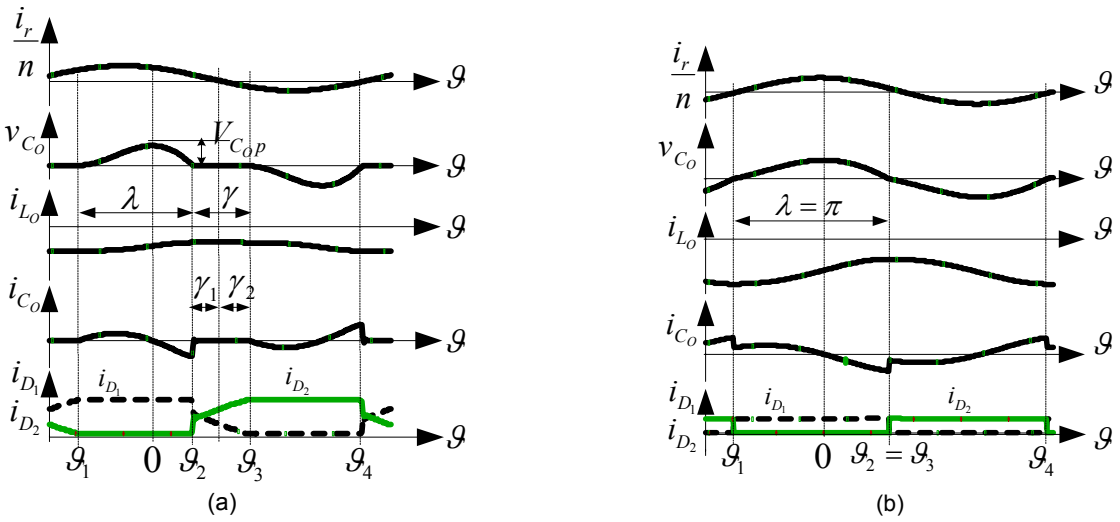

Fig. 3.2 Rectifier's current and voltage waveforms in the overlapping (a) and non-overlapping (b) modes.

The simulated current and voltage waveforms of the rectifier operating in overlapping and non-overlapping modes are shown in Fig. 3.2 a, b ($\vartheta = \omega t$ is the normalized time and ω is the operating angle frequency). The PT current i_r is assumed to be sinusoidal in both modes because of the high Q_m of practical PTs. The capacitor C_o voltage is practically sinusoidal in the non-overlapping mode but has a discontinuous behavior (intervals of zero voltage) in the overlapping mode. In this chapter we focus on the overlapping mode.

During the interval $\vartheta_1\vartheta_2 = \lambda$ the voltage v_{Co} across the capacitor C_o is positive, therefore the diode D_1 is ON and the diode D_2 is OFF. At ϑ_2, the polarity of the voltage v_{Co} changes and therefore D_2 turns on. If just before ϑ_2, the instant current of D_1 (i_{D1}) is higher than the absolute value of the capacitor C_o current (i_{Co}) the rectifier will operate under overlapping conditions. In this case the diodes D_1 and D_2 conduct simultaneously during the interval $\vartheta_2\vartheta_3$, and the current i_{D2} increases while the current i_{D1} decreases (due to changing i_r).

During this overlapping interval, the current i_{Co}=0, because the diodes have shorted the capacitor. At ϑ_3, i_{D1}=0 and D_1 turns off. During $\vartheta_3\vartheta_4$, only D_2 is ON and v_{Co}<0. Inductance

L_o charges by the input supply and it's current increases. At ϑ_4, v_{Co} changes polarity and an overlapping interval occurs again, but now i_{D1} increases while i_{D2} decreases, and so on.

3.3. UNIFIED ANALYSIS OF OVERLAPPING AND NON-OVERLAPPING MODES

The operation frequency of the converter, ω, is equal to the mechanical resonant frequency of a PT and to the resonant frequency of the parallel network C_oL_o

$$\omega = \frac{1}{\sqrt{L_r C_r}} = \frac{1}{\sqrt{L_o C_o}} \tag{3.1}$$

The analysis is carried out under the following assumptions:

1) The diodes and reactive elements are ideal.
2) The output filter is ideal ($L_f = \infty$, $C_f = \infty$).
3) The current i_r has a sinusoidal waveform.
4) The impulses of v_{Co} have a sinusoidal shape and the duration of each impulse is approximately λ.

A. Lossless PT (R_m=0)

According to the last assumption, the voltage v_{Co} is

$$v_{Co}(\vartheta) = V_{C_{OP}} \cos\left(\frac{\pi}{\lambda}\vartheta\right) \tag{3.2}$$

where $V_{C_{OP}}$ is the peak of the voltage across the capacitor C_o.

The peak of the first harmonic of this voltage is

$$V_{C_{O(1)P}} = \frac{4}{\lambda} V_{C_{OP}} \frac{\cos\left(\frac{\lambda}{2}\right)}{\left(\frac{\pi}{\lambda}\right)^2 - 1} \tag{3.3}$$

The average output voltage V_{out} is equal to the DC component of the positive value of v_{Co} and is expressed as

$$V_{out} = V_{C_{OP}} \frac{\lambda}{\pi^2} \tag{3.4}$$

Combining (3.4) in (3.3) we obtain

$$V_{C_O(1)p} = 4V_{out} \frac{\cos\left(\frac{\lambda}{2}\right)}{1-\left(\frac{\lambda}{\pi}\right)^2} \tag{3.5}$$

Since the operating frequency is equal to the resonant frequency of the series circuit C_r, L_r

$$\frac{V_{C_O(1)p}}{n} = V_{in.p} \tag{3.6}$$

The transfer ratio of the output voltage of the rectifier V_{out} to the peak of the input voltage $V_{in.p}$ for an ideal PT is

$$ko_{ideal} = \frac{V_{out}}{nV_{in.p}} = \frac{1-\left(\frac{\lambda}{\pi}\right)^2}{4\cos\left(\frac{\lambda}{2}\right)} \tag{3.7}$$

In the non-overlapping mode

$$ko_{ideal}^{NOM} = \lim_{\lambda\to\pi}(ko_{ideal}) = \frac{1}{\pi} \tag{3.8}$$

At the instant ϑ_2 the diode D_2 carries a current that was flowing via capacitor C_o. This current that starts as a step can be found from (3.2)

$$\left|I_{ch}\right| = \omega C_o \left.\frac{dv_{Co}}{d\vartheta}\right|_{\vartheta_2} = \frac{\pi}{\lambda}\omega C_o V_{C_{OP}} \tag{3.9}$$

or applying (3.4)

$$\left|I_{ch}\right| = \frac{\pi^3}{\lambda^2} V_{out}\omega C_o \tag{3.10}$$

The output current I_o at ϑ_2 may be written as

$$I_O = |I_{ch}| + \frac{I_m}{n}\sin(\gamma_1) + i_{L_O} \tag{3.11}$$

where $\frac{I_m}{n}\sin\gamma_1$ is the current $\frac{i_r}{n}$ at the instant ϑ_2, I_m is the peak of the input current, γ_1 - see Fig. 3.2 (a), and i_{L_O} is the inductor L_o current. The inductor L_o is shorted by the diodes D_1 and D_2 during the whole interval $\vartheta_2\vartheta_3$. That is why its voltage is practically zero and its current i_{L_O} has a constant value up to the instant ϑ_3 when D_1 turns off. Taking into account this condition, we use ϑ_3 to derive i_{L_O}. At ϑ_3 $i_{C_O} = i_{D_1} = 0$ and therefore

$$i_{L_O} = \frac{i_r}{n} = \frac{I_m}{n}\sin(\gamma_2) \tag{3.12}$$

where γ_2 - see Fig. 3.2 (a).

Consequently, the current balance at ϑ_2 (3.11) may be written as

$$I_O = \frac{\pi^3}{\lambda^2}V_{out}\omega C_o + 2\frac{I_m}{n}\sin\left(\frac{\gamma}{2}\right)\cos\left(\frac{\gamma_1 - \gamma_2}{2}\right) \tag{3.13}$$

where $\gamma = \gamma_1 + \gamma_2$ is the overlapping angle, $\gamma = \pi - \lambda$.

Taking into account that $\sin\left(\frac{\gamma}{2}\right) = \cos\left(\frac{\lambda}{2}\right)$ and assuming that $\cos\left(\frac{\gamma_1 - \gamma_2}{2}\right) \approx 1$ equation (3.13) can be simplified to

$$I_O = \frac{V_{out}}{R_L} = \frac{\pi^3}{\lambda^2}V_{out}\omega C_o + 2\frac{I_m}{n}\cos\left(\frac{\lambda}{2}\right) \tag{3.14}$$

From the energy balance it follows that

$$\frac{V_{in.p}I_m}{2} = \frac{{V_{out}}^2}{R_L} \tag{3.15}$$

Solving (3.7), (3.14) and (3.15) together, we obtain the equation for duration of the impulses of the voltage v_{Co} in the overlapping mode:

$$\lambda = \sqrt[4]{\pi^5 \omega C_o R_L} \qquad (3.16)$$

In the non-overlapping mode $\lambda = \pi$.

Duration of the capacitance C_o voltage impulses λ as a function of the load factor $\omega C_o R_L$ based on (3.16) is depicted in Fig. 3.3. The rectifier operates in overlapping mode when $\omega C_o R_L < \frac{1}{\pi}$.

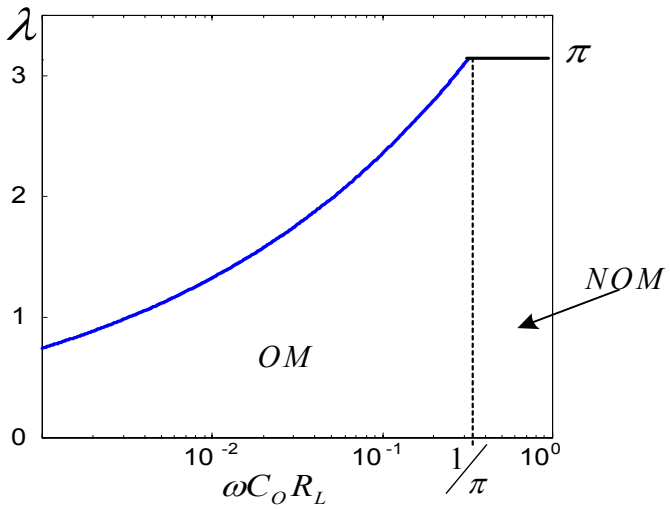

Fig. 3.3 Duration λ as a function of the normalized load factor $\omega C_o R_L$. OM - overlapping mode, NOM- non-overlapping mode.

B. Real PT (R_m>0).

We use the following additional assumptions:

1) The voltage across the resonant circuit L_r, C_r is zero.
2) The voltage across R_m and the first harmonic of the input voltage of the rectifier are in phase with the input voltage of the PT.

Under these assumptions

$$V_{in.p} - I_m R_m = \frac{V_{C_O(1)p}}{n} \qquad (3.17)$$

or, according to (3.5)

$$V_{in.p} - I_m R_m = \frac{4V_{out}}{n} \frac{\cos\left(\frac{\lambda}{2}\right)}{1-\left(\frac{\lambda}{\pi}\right)^2} \tag{3.18}$$

It can be shown that equation (3.14) derived above for an ideal PT, is also correct for a lossy PT. Taking $\cos\left(\frac{\lambda}{2}\right)$ from (3.14) and inserting it to (3.18) we obtain

$$\frac{V_{in.p} I_m}{2} - \frac{{I_m}^2 R_m}{2} = \frac{\frac{{V_{out}}^2}{R_L} - {V_{out}}^2 \omega C_O \frac{\pi^3}{\lambda^2}}{1-\left(\frac{\lambda}{\pi}\right)^2} \tag{3.19}$$

Since the left side of this equation is the output power, (3.19) may be rewritten as

$$\frac{{V_{out}}^2}{R_L} = \frac{\frac{{V_{out}}^2}{R_L} - {V_{out}}^2 \omega C_o \frac{\pi^3}{\lambda^2}}{1-\left(\frac{\lambda}{\pi}\right)^2} \tag{3.20}$$

Equation (3.20) can now be used to obtain the conduction angle λ, whose expression is identical to that of (3.16). We find here that even in the lossy case, λ is independent of the equivalent loss resistance of the PT -R_m.

C. Diode Losses

In low output voltage rectifiers the voltage drops of the diodes have be taken into account for designing the converter.

The power losses P_D in each diode are calculated from the following equation [43]:

$$P_D = V_F I_{D(ave)} + R_F I^2_{D(rms)} \tag{3.21}$$

where: $I_{D(ave)}$ and $I_{D(rms)}$ are the average and the rms diode currents, and R_F and V_F are the diode parameters (R_F is the equivalent forward resistance and V_F is the forward voltage).

According to Kirchoff's law, the diodes' currents i_{D_1} and i_{D_2} during the overlapping intervals can be described by the following equations:

$$i_{D_1} = i_{L_O} + \frac{i_r}{n} \tag{3.22}$$

$$i_{D_2} = I_O - i_{L_O} - \frac{i_r}{n} \tag{3.23}$$

During the non-overlapping intervals, the current of one of the diodes is I_o and the current of the other diode is zero.

The average diode current $I_{D(ave)}$ is approximately equal to half of the output DC current ($I_{D(ave)}$=0.5I_o). The rms diode current $I_{D(rms)}$ was determined using the assumption that during the overlapping intervals the diode currents are changing linearly.

Applying (3.10), (3.14) and (3.20), following expression for $I_{D(rms)}$ is obtained:

$$I_{D(rms)} = \frac{I_O}{\sqrt{2}}\varphi(\lambda) \tag{3.24}$$

where

$$\varphi(\lambda) = \sqrt{\frac{1}{\pi}\left\{\left[\frac{\lambda^2}{\pi^2} + \frac{2}{3}\left(1 - \frac{\lambda^2}{\pi^2}\right)^2\right](\pi - \lambda) + \lambda\right\}} \tag{3.25}$$

Hence, the general equation of the power losses in each diode P_D (3.21) can be rewritten in the following form:

$$P_D = \frac{1}{2} I_O V_F + \frac{1}{2} I_O^2 R_F (\varphi(\lambda))^2 \tag{3.26}$$

In non-overlapping mode this equation is simplified to

$$P_D^{NOM} = \frac{1}{2} I_O V_F + \frac{I_O^2 R_F}{2} \tag{3.27}$$

Assuming that the diode's power dissipations is the major power loss, the rectifier efficiency is expressed as

$$\eta_{rect} = \frac{P_{out}}{P_{out} + 2P_D} \tag{3.28}$$

where

$$P_{out} = V_{out} I_O \tag{3.29}$$

is the output power.

Applying (3.26) we transform (3.28) into

$$\eta_{rect} = \frac{1}{1 + \frac{V_F}{V_{out}} + \frac{R_F (\varphi(\lambda))^2}{R_L}} \tag{3.30}$$

The value of R_F in modern diodes is usually small and in most practical cases it is much lower than the load resistance of the rectifier R_L. This consideration and the fact that the function $\varphi(\lambda) \leq 1$ for every λ suggest that the term $R_F(\varphi(\lambda))^2/R_L$ in the last equation can be neglected. Hence,

$$\eta_{rect} \approx \frac{1}{1 + \frac{V_F}{V_{out}}} \tag{3.31}$$

As this equation shows, the rectifier efficiency η_{rect} decreases as the output voltage V_{out} gets lower. This is especially noticeable when V_{out} becomes closer to the diodes' forward voltage V_F.

D. Voltage Range and Power Characteristics of a Real Converter

Applying the power balance condition we can replace the loaded output rectifier by an equivalent resistance R_{eq} connected to the output of the PT (Fig. 3.4) [18, 36, 39, 42]. The power balance condition including the rectifier losses can be expressed as

$$\frac{V_{CO(1)p}^2}{2R_{eq}} = \frac{V_{out}^2}{R_L} + V_F I_O = \frac{V_{out}^2}{R_L \eta_{rect}} \tag{3.32}$$

from which

$$R_{eq} = \left(\frac{V_{CO(1)p}}{V_{out}} \right)^2 \frac{R_L \eta_{rect}}{2} \tag{3.33}$$

We found that the voltage ratio of the last equation can be calculated by an expression that is similar to (3.5), but which takes into account the rectifier's efficiency

$$\frac{V_{C_O(1)p}}{V_{out}} = \frac{4}{\eta_{rect}}\left[\frac{\cos\frac{\lambda^*}{2}}{1-\left(\frac{\lambda^*}{\pi}\right)^2}\right] \tag{3.34}$$

The angle λ^* is defined by an expression similar to (3.16)

$$\lambda^* = \sqrt[4]{\frac{\pi^5 \omega C_o R_L}{\eta_{rect}}} \tag{3.35}$$

In the non-overlapping mode, expressions (3.33) and (3.34) converge to

$$R_{eq}^{NOM} = \frac{\pi^2}{2\eta_{rect}} R_L \tag{3.36}$$

Applying (3.31)-(3.34), we obtain the output to input voltage ratio of a converter with losses in the rectifier and the PT as follows:

$$ko = \frac{0.25\eta_{rect}\left[1-\left(\frac{\lambda^*}{\pi}\right)^2\right]}{\left(1+\frac{n^2 R_m}{R_{eq}}\right)\cos\left(\frac{\lambda^*}{2}\right)} \tag{3.37}$$

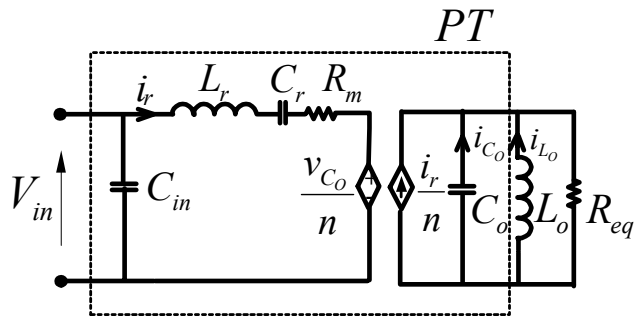

Fig. 3.4 A simplified equivalent circuit of the converter.

The dependences of ko_{ideal} (3.7) and ko (3.37) on the normalized load factor ($\omega C_o R_L$) are depicted in Fig. 3.5 a, b. Fig. 3.5 shows that a decrease in the load factor $\omega C_o R_L$ causes a decrease of the voltage ratio ko in the overlapping mode even in ideal case of a lossless PT (R_m=0). However, this decrease is much more pronounced in the real case (R_m>0, P_D>0).

Fig. 3.6 depicts the normalized output power $P_O^* = \frac{V_{out}^2}{R_L} \frac{2\sqrt{\frac{L_r}{C_r}}}{V_{in.p}^2}$ as a function of the normalized load factor $\omega C_o R_L$.

Efficiency of the PT η_{PT} and efficiency of the whole converter η can be easily calculated if we know R_{eq} as

$$\eta_{PT} = \frac{R_{eq}}{n^2 R_m + R_{eq}} \tag{3.38}$$

$$\eta = \frac{P_{out}}{P_{in}} = \eta_{PT} \eta_{rect} \tag{3.39}$$

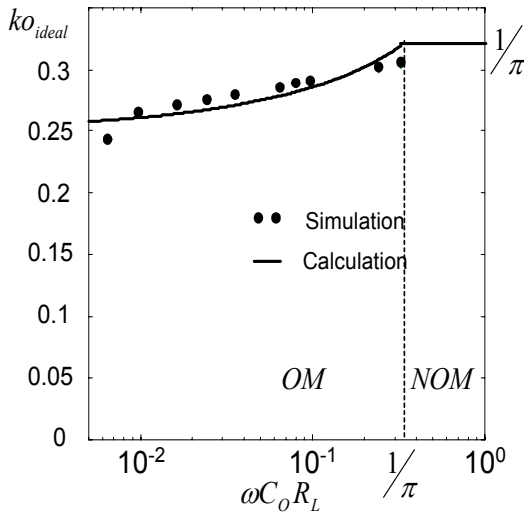

(a)

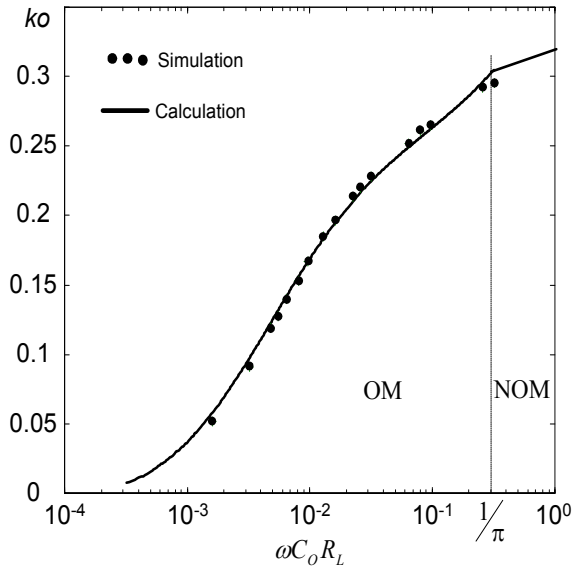

(b)

Fig. 3.5 Voltage ratio as a function of normalized load factor $\omega C_O R_L$: (a) lossless PT, ideal diodes, (b) real PT ($\omega C_o R_m$=0.034), real diodes (MBR160P). The peak input voltage $V_{in.p}$=30V. OM – overlapping mode, NOM – non-overlapping mode.

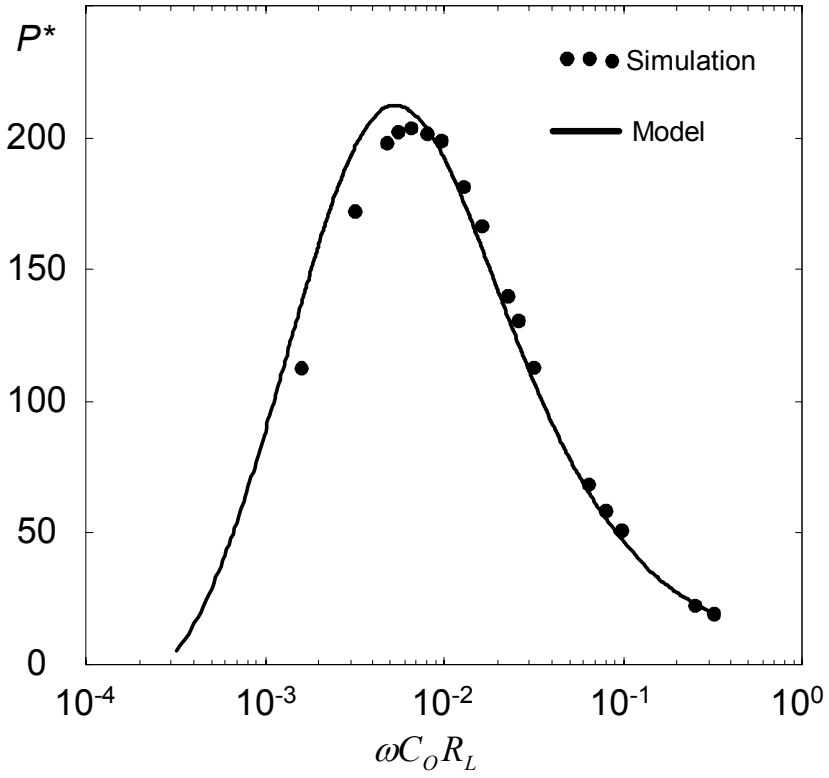

Fig. 3.6 Normalized output power P* as a function of normalized load factor $\omega C_O R_L$. Real PT and real diodes (the same parameters as in Fig. 3.5 b).

3.4. EXPERIMENTAL RESULTS

A Philips PT (RT 35x8x2 PXE43-S) with a thickness polarization mode was used in the experiment. The PT's main parameters (Fig. 3.1) were measured to be L_r=165mH, C_r=15.1pF, C_{in}=C_o=510pF, R_m=105Ω, n=1. The operation frequency was equal to the resonant frequency. The parallel resonant inductance was $L_o = 4.88\text{mH}$ and the diodes were a Schottky diode (MBR160P). The experiments were carried out for a load resistance R_L range of 30Ω to 1kΩ. The range of the peak of the input voltage was $V_{in.p} = 5 - 30\text{V}$. The experimental and the theoretical voltage ratios as a function of the load resistance are shown in Fig. 3.7, which clearly indicate that the analytical equations derived in this study are in excellent agreement with the simulations and experimental results.

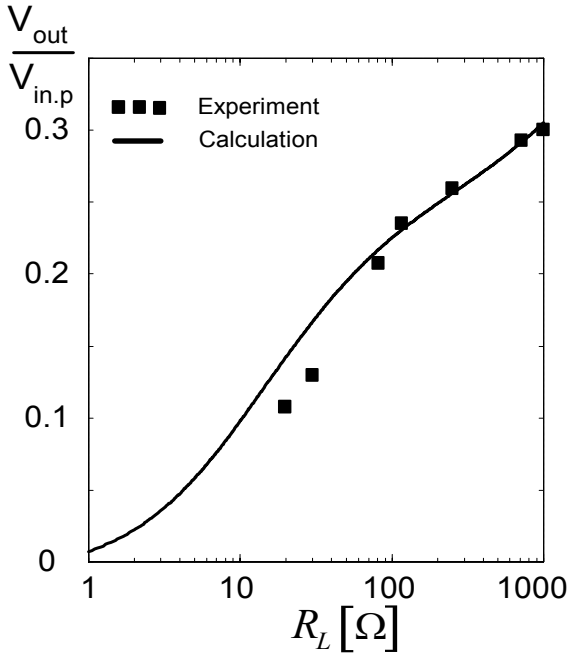

Fig. 3.7 Experimental and theoretical voltage ratio $V_{out}/V_{in.p}$ as a function of load resistance R_L. $V_{in.p}$=30V, $\omega C_o R_L$=0.034.

3.5. CONCLUSIONS

It was shown that a PT power converter with a halfway two-diode rectifier can operate in two modes: NOM - the operational mode described earlier in which there is no overlap between the conduction intervals of the diodes, and OM – the newly discovered mode with overlaping between the conduction intervals of the diodes. It was found that the operation mode is dependent on the normalized load factor $\omega C_o R_L$. The load factor is a function of the PT parameters and the load resistance.

This section pointed out the effect of the load and parasitic resistances on the output voltage and the losses for both modes. The analytical investigations were supported by simulation and experiment results, and were found to be in excellent agreement.

It is important to note that a design that is based on the known NOM may result in a considerable error if the rectifier operates in OM.

The analytical equations derived in this study can be used in engineering design. An example of a design procedure is given in the example presented below. In this design example we assume that the PT is given and we calculate the required input voltage to meet the out specifications (P_{out}, V_{out}). If the calculated input voltage is not equal to the available input source, a trial and error procedure is implemented until the correct PT is found. Alternatively, the PT parameters (e.g. n) can be adjusted to meet the requirements and by this we can define a set of PT parameters that will meet the given specifications.

The results of this chapter have been published in [40].

DESIGN EXAMPLE

Given: DC/DC PT converter output requirements (V_{out}, P_{out}), PT parameters ($L_r, C_r, C_{in}, C_o, R_m, n$), and diodes to be used in converter.

Variables to be evaluated: the input voltage V_{in} that ensures the required output attributes of the power converter and the input power P_{in}.

Design steps:

1) Define the resonant frequency ω_r, the load resistance R_L, the resonant inductance $L_O = \frac{L_r C_r}{C_o}$ and the load factor $\omega C_o R_L$ from the output specifications and the PT parameters.
2) Find the forward diode voltage V_F from the data sheet and evaluate the rectifier efficiency η_{rect} (3.31).
3) Calculate the parameter λ^* (3.35). The rectifier is operating in non-overlapping mode when $\lambda^* = \pi$ and in overlapping mode when $\lambda^* < \pi$.
4) Define the equivalent load resistance of the converter R_{eq} (3.33) and (3.34).
5) Obtain the voltage ratio ko of the real converter (3.37).
6) Calculate the peak input voltage according to $V_{in(p)} = \frac{V_{out}}{ko}$.
7) Find the PT and the converter efficiencies η_{PT} and η (3.38), (3.39).
8) Determine the input power $P_{in} = \frac{P_{out}}{\eta}$.

CHAPTER 4

A PIEZOELECTRIC TRANSFORMER DC/DC CONVERTERS' OUTPUT NETWORKS II

Since a PT is a low power device, it seems to be preferable to derive maximum power from the converter, which means the PT converter should be run at a frequency of the maximum output voltage/power. Under these conditions, a PT converter with a half-way rectifier operates similarly to a PT converter with a current-doubler rectifier. Likewise, a PT converter with a full-way rectifier and a capacitive filter operates similarly to a PT converter with a voltage-doubler rectifier. Therefore, we compared only two types of rectifiers: a current-doubler and a voltage-doubler rectifier. The subject of the present chapter is to decide which particular output network is the best for running the PT converter.

4.1. A COMPARISON OF PIEZOELECTRIC TRANSFORMER DC/DC CONVERTERS WITH CURRENT-DOUBLER AND VOLTAGE-DOUBLER RECTIFIERS

Figures 1.1, 1.4 show the current doubler (CD) and the voltage doubler (VD) rectifiers. In the VD, the average current of the diodes is equal to the average load current while in the CD the average current of the diodes is twice lower than the load current. On the other hand, the peak of the diodes' voltage in the VD is equal to the load voltage while in the CD the peak of the diodes' voltage is twice higher than the load voltage. Therefore, for high currents and low voltages (low resistance loads) the CD rectifier is a superior choice, whereas for high voltages and low currents (high resistance load) the VD rectifier is a better choice. The problem is, however, that the load regions between these two rectification schemes are not well defined: what rectifier should be applied when the load resistance is neither high nor low? What are the voltage and the power capabilities of each rectifier when they are connected at the output of the PT? What are their advantages and disadvantages?

This chapter presents a comparative analysis of PT based power converters that apply these types of rectifiers. The comparison methodology follows an approach developed earlier

[18, 36, 41, 42] by which the output capacitor of PT and the rectifier sections are represented by an equivalent circuit. The equivalent circuit is linear and is composed of a parallel RC network that loads the PT as the corresponding rectifier does.

4.2. COMPARATIVE CIRCUITS AND COMPARISON PRINCIPLES

We assume that both converters are operated at a maximum output voltage mode, that is, at a frequency that produces the maximum output voltage. As was shown earlier [32, 44], the frequency of maximum output is different from the mechanical resonant frequency. The operation of the VD rectifier when running at a maximum output voltage mode was studied in [18] and is further developed in the present work. A current doubler rectifier operating at a mechanical resonant frequency was studied in [5, 35]. The present work studies its operation at a frequency of a maximum output voltage.

In order to generalize the model of the PT converter, the following normalized parameters are applied:

1) Normalized load factor

$$K_{PT}=R_L/n^2R_m \tag{4.1}$$

2) Normalized PT factor

$$A_{PT}=\omega_r C_o n^2 R_m \tag{4.2}$$

3) PT mechanical quality factor

$$Q_m=1/(\omega_r C_r R_m) \tag{4.3}$$

where R_L is the load resistance, R_m-L_r-C_r-C_o are the parameters of the PT equivalent circuit; n is the transfer ratio, and $\omega_r = 1/\sqrt{L_r C_r}$ is the mechanical resonant frequency. These parameters refer to the elements of a conventional PT lumped model [5, 24, 26].

The normalized load factor K_{PT} is a convenient parameter to analyze the effect of the load resistance R_L on the operating conditions of the converter and rectifier (output voltage, power, and efficiency). Analytical and experimental results presented below were obtained for a K_{PT} ranging: from 0.5 to $3\cdot10^5$.

The normalized PT parameter A_{PT} and the PT mechanical quality factor Q_m are independent of the load resistance. These parameters are useful for analyzing the operational conditions of the PT. In particular, A_{PT} can be used to obtain the dependence of the output voltage on the output capacitance of the PT, C_o, which has a marked effect on the operation of the PT based converter. Analytical and experimental results presented below were obtained for an A_{PT} ranging from 0.01 to 0.05 and varying Q_m from 50 to 5000. It was found, however, that the effect of Q_m on the operational characteristics of the converter is insignificant when $Q_m>900$.

The current and voltage waveforms of the two rectifiers being compared in the study are presented in Fig. 4.1. The parameters marked in Fig. 4.1 are defined as follows: $\vartheta = \omega t$ is the normalized time, ω is the operating angular frequency, θ is the duration of the VD rectifier input current pulses, and λ is the duration of the CD rectifier input voltage pulses (i.e. the pulses of the PT output capacitor voltage).

Despite the fact that the output voltage of the PT converter v_{Co} includes high harmonics components, the current waveform within the PT equivalent circuit (i_r) is assumed to be sinusoidal due to the high quality factor of the resonant circuit. Consequently, power transfer to the output is affected only by the fundamental harmonics component. For that reason, the rectifier can be studied by the first harmonics approximation as follows:

1) The rectifier with the output capacitor and the load are replaced by an equivalent parallel network C_{eq}-R_{eq} (at the secondary side of the PT). In the case of ideal and lossless rectifiers the values of the parameters can be derived from the power considerations as

$$\frac{V_{Co(1)pk}^2}{2R_{eq}} = \frac{V_L^2}{R_L} \tag{4.4}$$

$$C_{eq} = \frac{\tan\varphi_{(1)}}{\omega R_{eq}} \tag{4.5}$$

where R_L is the load resistance, V_L is the load (DC) voltage, $V_{Co(1)pk}$ is the peak of the first harmonics component of the capacitor C_o voltage v_{Co}, and $\varphi_{(1)}$ is the phase angle between the voltage $v_{Co(1)}$ and the PT current i_r flowing through R_m-C_r-L_r.

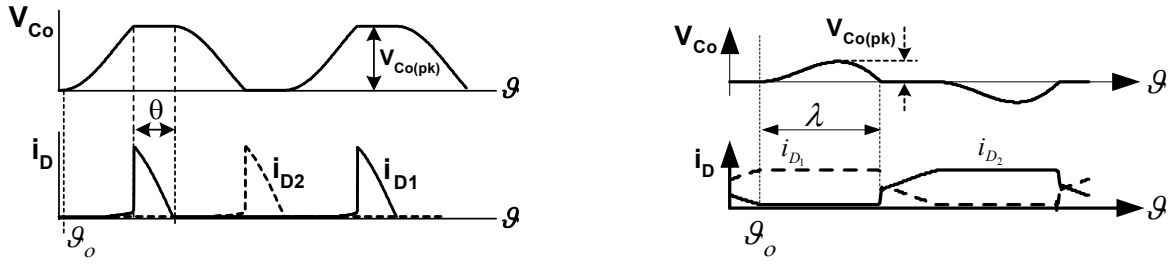

(a) (b)

Fig. 4.1 The output voltage of the PT (across C_o) and the diode currents: a) voltage doubler rectifier, b) current doubler rectifier.

2) This equivalent parallel network is then reflected to the primary side as shown on Fig. 4.2a, where C'_{eq} - R'_{eq} are the reflected values of C_{eq} and R_{eq}, and $C'_{eq}=C_{eq}n^2$, $R'_{eq}=R_{eq}/n^2$.

3) The reflected parallel network is then converted to an equivalent series network C''_{eq} - R''_{eq} (Fig. 4.2, b) [18, 32] by applying the following relationships:

$$\begin{cases} R''_{eq} = R'_{eq}\cos^2\varphi_{(1)} \\ C''_{eq} = \dfrac{C'_{eq}}{\sin^2\varphi_{(1)}} \end{cases} \qquad (4.6)$$

This presentation is used in the following analysis to obtain generalized expressions for the voltage ratio, power relationships, and efficiency in a similar form for the two converters. All expressions are normalized and applied per unit system.

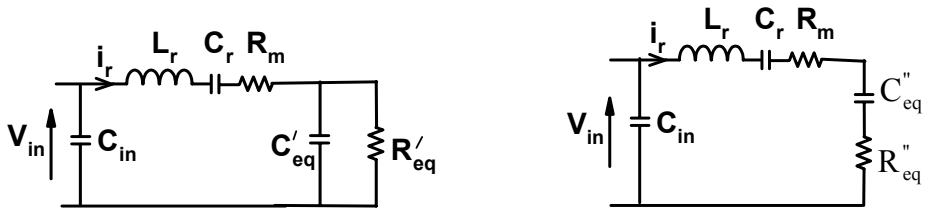

Fig. 4.2 Series-parallel (a) and series (b) equivalent circuits of a PT AC-DC converter reflected to the primary. The parallel C_{eq}' and R_{eq}' and series R_{eq}'' and C_{eq}'' networks emulate the loading effect of the rectifier (C_{eq} includes the output capacitance of the PT – C_o).

A. Voltage-Doubler Rectifier

Following [18], the duration of the impulses of the diode currents θ (Fig. 4.1a) is

$$\theta = 2\tan^{-1}\sqrt{\frac{2\pi}{\omega^* q}} \tag{4.7}$$

where $q=\omega_r C_o R_L=A_{PT}K_{PT}$ is the PT load parameter, $\omega^*=\omega/\omega_r$ and ω is the operating frequency corresponding to the frequency of the maximum voltage transfer ratio. According to [18],

$$\omega^* = \sqrt{1+\frac{C_r}{n^2 C_{eq}}\sin^2\varphi_{(1)}} \tag{4.8}$$

The waveform coefficient $k_{(1)}$ and the phase angle $\varphi_{(1)}$ of the first harmonics of the PT's output capacitance C_o voltage, referred to the instant $\vartheta_o = 0$ (Fig. 1a) are

$$k_{(1)} = \frac{V_{Co(1)pk}}{V_{Co(pk)}} = \sqrt{a_{(1)}^2 + b_{(1)}^2} \tag{4.9}$$

$$\varphi_{(1)} = \tan^{-1}\left(\frac{a_{(1)}}{b_{(1)}}\right) \tag{4.10}$$

where $V_{Co(pk)}$ is the peak value of the voltage v_{Co} (Fig. 3.1a), $a_{(1)}$ and $b_{(1)}$ are the first components of the Fourier series expansion:

$$a_{(1)} = -\frac{2}{\pi}\left[\frac{\pi - \theta + 0.5\sin(2\theta)}{1+\cos\theta}\right] \tag{4.11}$$

$$b_{(1)} = \frac{2}{\pi}(1-\cos\theta) \tag{4.12}$$

The VD rectifier conduction angle θ, the phase angle $\varphi_{(1)}$ and the voltage waveform coefficient $k_{V(1)}$ as a function of the load parameter $\omega C_o R_L$ are shown in the Fig. 4.3.

The equivalent resistance and capacitance [18] are

$$\begin{cases} R_{eq}^{VD} = \dfrac{1}{8}k_{(1)}^2 R_L \\ C_{eq}^{VD} = \dfrac{\tan\varphi_{(1)}}{\omega R_{eq}^{VD}} \end{cases} \tag{4.13}$$

The voltage transfer function of the rectifier is

$$k_{rect} = \frac{V_L}{V_{Co(1)pk}} = \frac{2}{k_{(1)}} \tag{4.14}$$

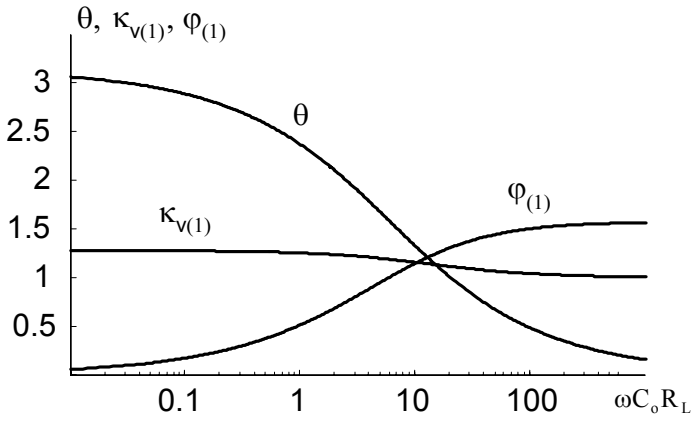

Fig. 4.3 VD rectifier conduction angle θ, phase angle $\varphi_{(1)}$ and voltage waveform coefficient $k_{V(1)}$ as a function of the PT load parameter $\omega C_o R_L$.

B. Current-Doubler Rectifier

When connected to the output of the PT converter, the CD rectifier can operate in either an overlapping (OM) or a non-overlapping mode (NOM) with respect to the diode currents [41]. Fig. 4.4 shows the waveforms of the PT current i_r/n and the input current to the rectifier $i_{in(rect)}$ in the OM (Fig. 4.4, a) and NOM (Fig 4.4, b).

It is assumed that the load current I_L and the inductors' L_1, L_2 currents have negligible ripple and therefore the waveform $i_{in(rect)}$ is clamped to the inductors' currents that are equal to the half the value of the load current. The difference between currents i_r/n and $i_{in(rect)}$ is the current i_{Co} of the PT output capacitor C_o.

$$i_{Co} = I_m \sin \vartheta - 0.5 I_L \tag{4.15}$$

where I_m is the peak of the i_r/n current and $\vartheta=\omega t$ is normalized time referred to the instant ϑ_o (Fig. 4.4). The current i_{Co} charges and discharges the capacitor C_o during the time interval λ when the capacitor is not shorted through the conducting diodes. In the OM (Fig. 4.4a), the capacitor current does not include a step at the instant ϑ_1 when the preceding overlapping period terminates. At this instant

$$\frac{i_r}{n} = \frac{I_L}{2} = I_m \sin \psi \tag{4.16}$$

where ψ is shown in Fig. 4.4. In NOM (Fig. 4.4, b) $i_{in(rect)}$ has a rectangular waveform. The steps of this current correspond to the instants when the capacitor voltage changes polarity.

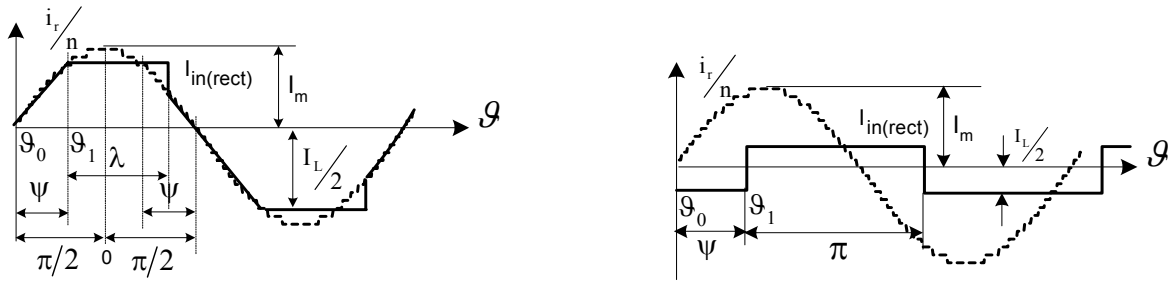

(a) (b)

Fig. 4.4 Current doubler rectifier input current (solid line) and sinusoidal PT resonant current (dotted line) a – OM, b - NOM.

In a steady state, the average charge during the time period λ is zero. Therefore in the OM

$$\int_{\psi}^{\psi+\lambda}\left(I_m \sin\vartheta - I_m \sin\psi\right)d\vartheta = 0 \tag{4.17}$$

The solution of this equation is

$$\psi = \tan^{-1}\left(\frac{1-\cos\lambda}{\lambda-\sin\lambda}\right) \tag{4.18}$$

The voltage across C_o is obtained from (4.15), (4.16). Taking into account that $v_{Co}=0$ at $\vartheta=\psi$,

$$v_{Co} = \frac{I_m}{\omega C_o}\left[\cos\psi - \cos\vartheta + (\psi-\vartheta)\sin\psi\right] \tag{4.19}$$

and the average output voltage of the rectifier is found as

$$V_L = \frac{1}{2\pi}\int_{\psi}^{\psi+\lambda} v_{Co}\,d\vartheta \tag{4.20}$$

On the other hand,

$$V_L = I_L R_L = 2I_m R_L \sin\psi \tag{4.21}$$

By combining (4.18)-(4.21) we derive an equation that relates the duration λ of the capacitor C_o voltage pulses to the parameter $q\omega^*=\omega C_o R_L$

$$\frac{0.5\lambda}{\tan(0.5\lambda)} = 1-\sqrt{2\pi q\omega^*} \tag{4.22}$$

where

$$\omega^* = \sqrt{1+\frac{C_r}{n^2 C_{eq}}\sin^2\varphi_{(1)}} \tag{4.23}$$

It follows from (4.22) that the condition $\omega C_o R_L < 1/2\pi$ is corresponded to the OM.

Replacing the real voltage pulses v_{Co} by an equivalent sine wave with the same duration λ and the same peak $V_{Co(pk)}$ we define $k_{(1)}$, $\varphi_{(1)}$ and $V_L/V_{Co(pk)}$ as follows:

$$k_{(1)} = \frac{4}{\lambda} \frac{\cos\left(\frac{\lambda}{2}\right)}{\left(\frac{\pi}{\lambda}\right)^2 - 1} \tag{4.24}$$

$$\varphi_{(1)} = \psi + \lambda/2 - \pi/2 \tag{4.25}$$

$$\frac{V_L}{V_{Co(pk)}} = \frac{\lambda}{\pi^2} \tag{4.26}$$

In the NOM (Fig. 4.4b) $\lambda=\pi$.

$$\frac{1}{\pi} \int_{\psi}^{\psi+\pi} \left(I_m \sin\vartheta - \frac{I_L}{2} \right) d\vartheta = 0 \tag{4.27}$$

It follows from this expression that:

$$\cos\psi = \frac{\pi}{4} \frac{I_L}{I_m} \tag{4.28}$$

$$\begin{cases} k_{(1)} = 1 \\ \varphi_{(1)} = \psi \end{cases} \tag{4.29}$$

$$\frac{V_L}{V_{Co(pk)}} = \frac{1}{\pi} \tag{4.30}$$

$$\omega C_o V_{Co(1)pk} = I_m \sin\psi \tag{4.31}$$

From (4.28), (4.30) and (4.31) we obtain

$$\tan\psi = 4\omega C_o R_L = 4q\omega^* \tag{4.32}$$

The duration of the PT output capacitor voltage pulses λ, the CD rectifier voltage waveform coefficient $k_{V(1)}$, the phase angle $\varphi_{(1)}$, and the conduction angle ψ as a function of $\omega C_o R_L$ are depicted in Fig. 4.5.

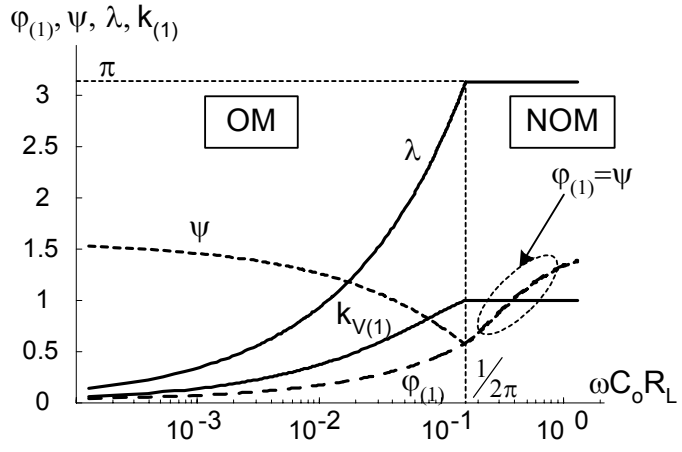

Fig. 4.5 CD rectifier: duration of the capacitor C_o voltage pulses λ, rectifier voltage waveform coefficient $k_{V(1)}$, phase angle $\varphi_{(1)}$ and angle ψ (see Fig. 4.4) as a function of the PT load parameter $\omega C_o R_L$.

From (4.9), (4.24) and (4.26) we obtain the voltage transfer ratio of the rectifier in the OM:

$$k_{rect} = \frac{V_L}{V_{Co(1)pk}} = \frac{\lambda}{\pi^2 k_{(1)}} \tag{4.33}$$

In the NOM applying $\lambda=\pi$ and $k_{(1)}=1$, we obtain

$$k_{rect} = \frac{1}{\pi} \tag{4.34}$$

Based on (4.4), (4.5). (4.9) and (4.26), the equivalent load resistance and capacitance in the OM (Fig. 4.2, a) are

$$\begin{cases} R_{eq}^{CD} = \dfrac{1}{2}\left(\dfrac{\pi^2}{\lambda}\right)^2 k_{(1)}^2 R_L \\ C_{eq}^{CD} = \dfrac{\tan\varphi_{(1)}}{\omega R_{eq}^{CD}} \end{cases} \tag{4.35}$$

From (4.29) and (4.35) when $\lambda=\pi$, the equivalent resistance and capacitance in the NOM are

$$\begin{cases} R_{eq}^{CD} = \dfrac{\pi^2}{2} R_L \\ C_{eq}^{CD} = \dfrac{\tan\varphi_{(1)}}{\omega R_{eq}^{CD}} = \dfrac{8}{\pi^2} C_o \end{cases} \tag{4.36}$$

C. Characteristics of the Compared Rectifiers

Figs. 4.6-4.8 show the ratios R_{eq}/R_L, C_{eq}/C_o and the rectifier gain k_{rect} as a function of the PT load parameter $\omega C_o R_L$ for the VD and CD rectifiers. Fig. 4.6 shows that in the CD rectifier the equivalent resistance is an order of magnitude higher than R_L while in the VD rectifier it is in order lower. For this reason, for low load resistance one should use the CD rectifier to obtain better efficiency while for high R_L a VD rectifier is more suitable. Fig. 4.7 demonstrates that for high load parameter $\omega C_o R_L$ the equivalent capacitance C_{eq} of the CD rectifier is less than C_o. Fig. 4.8 shows that the rectifier gain is about four times higher in the VD than in the CD.

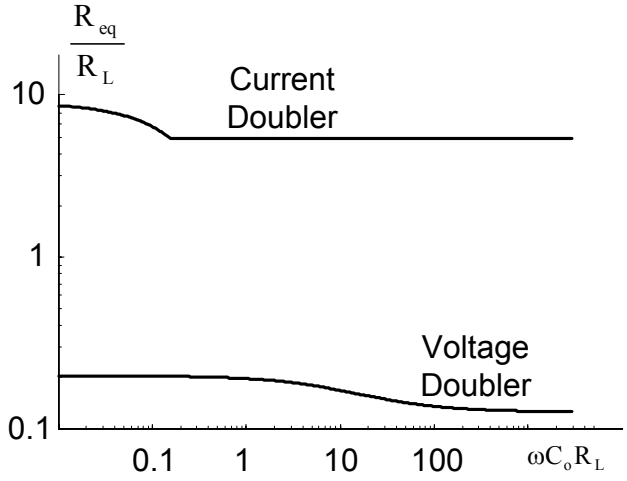

Fig. 4.6 Normalized equivalent resistance R_{eq}/R_L as a function of the PT load parameter $\omega C_o R_L$ for the two rectifiers.

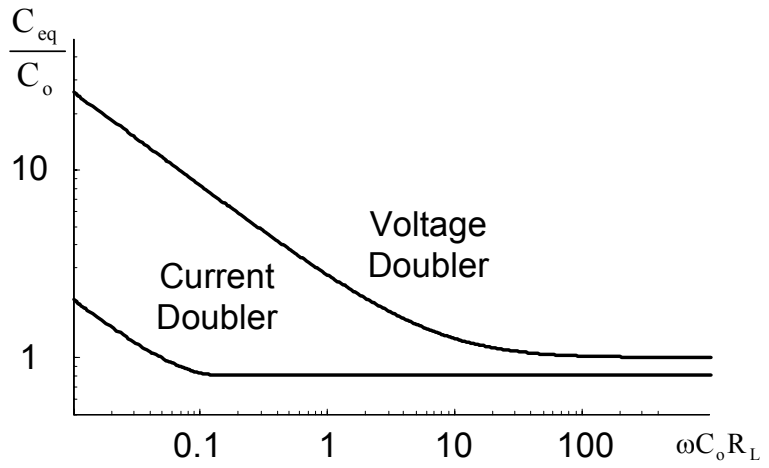

Fig. 4.7 Normalized equivalent capacitance C_{eq}/C_o as a function of the PT load parameter $\omega C_o R_L$ for the two rectifiers.

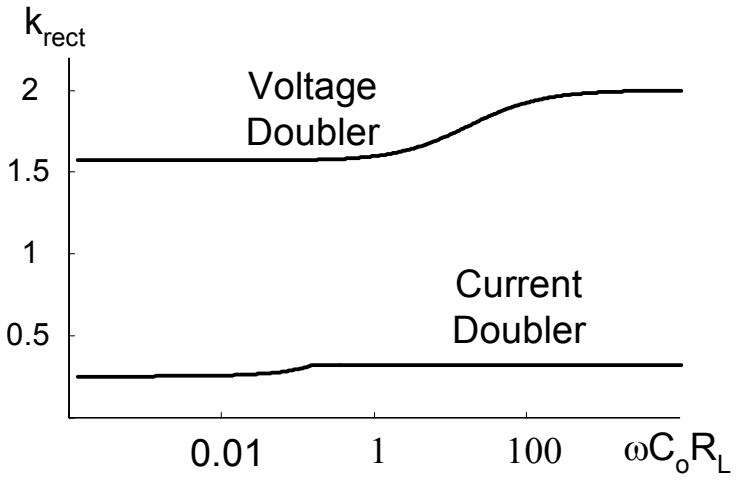

Fig. 4.8 VD and CD rectifier voltage gain as a function of the PT load parameter $\omega C_o R_L$.

4.3. General Equations of a PT Loaded by an Output Rectifier

For both rectifiers, the referred to the primary side of PT voltage transfer ratio at the frequency of maximum output voltage gain ω^* [18] is

$$k_{21m} = \frac{V_{Co(pk)}}{nV_{in(pk)}} = \frac{1}{\cos\varphi_{(1)} + \frac{1}{K_{PT}\cos\varphi_{(1)}}} \tag{4.37}$$

where $V_{in(pk)}$ is the peak input voltage.

As proven in [32], $1<\omega^*<1.1$. For such a narrow frequency range, the changes in the values of the parameters $\varphi_{(1)}$ and C_{eq} are insignificantly small. Consequently, ω^* was obtained under the assumption that the values of $\varphi_{(1)}$ and C_{eq} are independent of ω.

The DC output to peak input voltage transfer ratio k_o is

$$k_o = \frac{V_o}{V_{in(pk)}} = nk_{21m}k_{rect} \tag{4.38}$$

The efficiency of the PT for both rectifiers is given by [18]:

$$\eta_{PT} = \frac{1}{1+\frac{R_m}{R''_{eq}}} = \frac{1}{1+\frac{R_L}{K_{PT}R_{eq}\cos\varphi_{(1)}}} \tag{4.39}$$

The ratio of the output power P_o to the power dissipation of the PT P_{PD} for both rectifiers is

$$\Delta_{PT} = \frac{P_o}{P_{PD}} = \frac{\eta_{PT}}{1-\eta_{PT}} = \frac{R_{eq}}{R_L}K_{PT}\cos\varphi_{(1)} \tag{4.40}$$

For the case of non-ideal rectifier one has to take into account the diode losses. The rectifier efficiency is

$$\eta_{rect} = \frac{1}{1+\frac{P_D}{P_o}} \tag{4.41}$$

where P_D are the diode power losses, which in both rectifiers are approximated by

$$P_D = 2\left(I_{D(ave)}V_F + I^2_{D(rms)}R_s\right) \tag{4.42}$$

where $I_{D(ave)}$ is the average diode current, V_F is the forward diode voltage, $I_{D(rms)}$ is the effective diode current and R_s is the diode's incremental resistance. In the CD rectifier $I_{D(ave)}=0.5I_L$, where I_L is load current. In the VD rectifier $I_{D(ave)}=I_L$.

The efficiency of the rectifiers when connected at the PT output is

$$\eta^{CD}_{rect} \approx \frac{1}{1+\frac{V_F}{V_L}\left[1+\left(\frac{I_{D(rms)}}{I_{D(ave)}}\right)^2\frac{V_L}{V_F}\frac{R_s}{2R_L}\right]} \tag{4.43}$$

$$\eta^{VD}_{rect} \approx \frac{1}{1+\frac{2V_F}{V_L}\left[1+\left(\frac{I_{D(rms)}}{I_{D(ave)}}\right)^2\frac{V_L}{V_F}\frac{R_s}{R_L}\right]} \tag{4.44}$$

where V_L is the average load voltage and $\frac{I_{D(rms)}}{I_{D(ave)}}$ is the ratio of rms and average diode currents:

$$\left.\frac{I_{D(rms)}}{I_{D(ave)}}\right|_{CD} = \sqrt{\frac{1}{\pi}\left\{\left[\frac{\lambda^2}{\pi^2}+\frac{2}{3}\left(1-\frac{\lambda^2}{\pi^2}\right)^2\right](\pi-\lambda)+\lambda\right\}} \tag{4.45}$$

$$\left.\frac{I_{D(rms)}}{I_{D(ave)}}\right|_{VD} = \sqrt{\frac{\pi\left[\theta-\frac{1}{2}\sin(2\theta)\right]}{[1-\cos(\theta)]^2}} \tag{4.46}$$

Taking into account the rectifier losses, the overall efficiency will be

$$\eta = \eta_{rect}\eta_{PT} \tag{4.47}$$

4.4. Main Comparison Results

Fig. 4.9, which is based on (4.39), (4.40) shows the power handling capability Δ_{PT} as a function of the normalized load factor $K_{PT}=R_L/n^2R_m$ for different values of the normalized PT parameter $A_{PT}=\omega_r C_o n^2 R_m$. Since the efficiency (as it follows from (4.40)) equals $\Delta_{PT}/(\Delta_{PT}+1)$, the maximum of Δ_{PT} corresponds to the point of maximum efficiency. The generic data of

Fig. 4.9 suggest that for any given PT (i.e. a specific A_{PT}) the efficiency that can be achieved with a CD rectifier is higher than that can be achieved with the VD rectifier. The data also show that for a given PT, the load resistance R_L that corresponds to maximum efficiency is lower in the CD rectifier than in the VD rectifier. Consequently, for a given PT, maximum efficiency will be obtained in the VD rectifier at higher voltages than in the CD rectifier. From Fig. 4.9 one can observe the borderline between load values that will produce a higher efficiency with a CD rectifier, to the load range that is more compatible to the VD rectifier. Fig. 4.10 delineates the borderlines between the CD and VD regions for different PT's for a range of A_{PT} values. This plot can be used as a tool for choosing the rectifier most suitable for given load conditions. From the figure we can surmise that, for a given PT, one should use a VD rectifier when the load factor K_{PT} is higher then the dotted line, and a CD – when the load factor is lower. The plots (Fig. 4.9) are built for a mechanical quality factor of PT Q_m=966. For larger values of Q_m, the Δ_{PT} does not changed significantly.

It follows from (4.9), (4.14) and (4.23), (4.33), (4.34) that for a high voltage gain the VD has higher k_{rect} than CD, therefore VD is better option.

It was further found that for low load resistances, higher voltage transfer ratios k_o can be obtained with the CD rectifier. This is because the efficiency of a CD with low load resistances is higher than the VD. Likewise, the efficiency of CD rectifier η_{rect}^{CD} is higher than VD η_{rect}^{VD}, because the ratio of $I_{D(rms)}/I_{D(ave)}$ in the CD is lower.

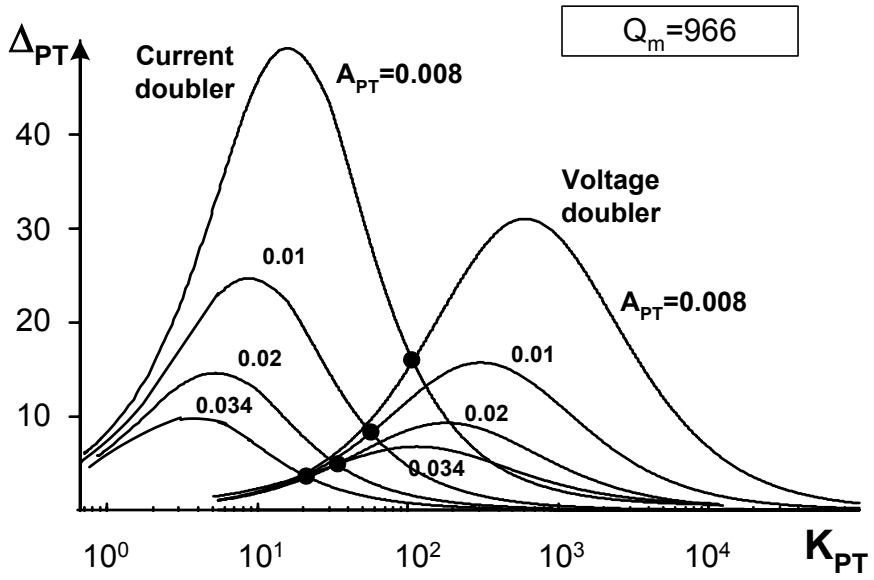

Fig. 4.9 The ratio of the output power P_o to the PT power dissipation P_{PD} (Δ_{PT}) as a function of the normalized load resistance $K_{PT}=R_L/n^2R_m$ for different $A_{PT}=\omega_r C_o R_m n^2$.

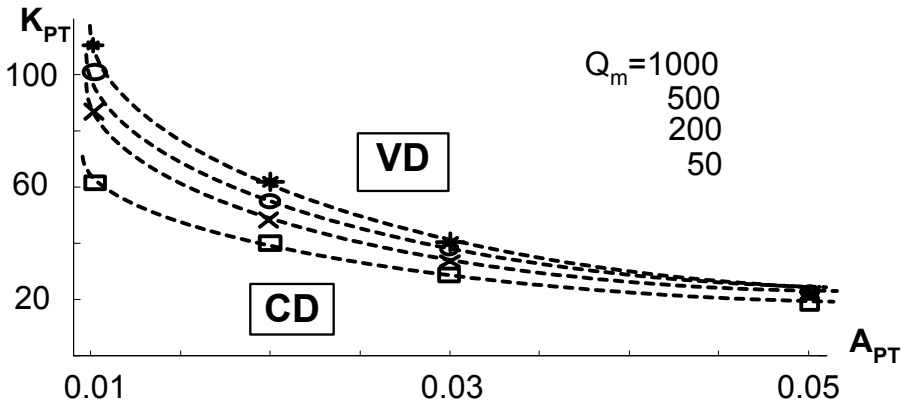

Fig. 4.10 Boundaries between preferred operating regions that provide higher efficiency for VD and CD rectifiers for the different values of the mechanical quality factor Q_m.

4.5. SIMULATION AND EXPERIMENTAL RESULTS

The experimental setup included a LeCroy WaveRunner Scope LT264M DSO with APO15 Current Probe, using the PMA1 Power Measure Analysis Software for calculating the input power of the PT. The experiments were carried out in the maximum output voltage mode with frequency adjusting.

The experimental PT was a radial vibration mode PT, Face Co., VA, USA. The equivalent PT parameters were found to be as follows: C_{in}=1.72nF, C_o=1.33nF, L_r=10.5mH, C_r=172.5μF, R_m=21Ω, n=1.08. Thus, the series resonant frequency of the PT is calculated to be 118.3kHz, the mechanical quality factor is Q_m=371.5, and the normalized PT factor is A_{PT}=0.0242.

The output power of CD converter varied from 4W to 11W, keeping mostly around 6-7W. Load resistances varied from 30Ω to 10kΩ, that corresponds to K_{PT} values of 1.22 to 410, respectively. In order to prevent the PT from overheating the input current of the CD converter was limited to 250mA (rms).

The output voltage of the VD converter was kept constant at V_L=170V for loads values of 2kΩ to 100kΩ. For lower resistances, the current conditions were kept similar to the CD case.

Figs. 4.11-4.12 show the experimental and simulation results as well as the calculated results: the output to input voltage transfer ratio (Fig. 4.11) and the converter efficiency (Fig. 4.12) as a function of the load resistance. Note that efficiency (Fig. 4.12) was calculated with the assumptions that the forward diode voltage V_F is constant and that the diode's incremental resistance R_s is negligibly small. Under these experimental conditions the forward voltage of the MUR440 V_F was about 0.7V for most of the measurements and therefore this value was chosen for diode loss calculations. In general, good agreement was found between the experimental, simulation and theoretical results (Figs. 4.11-4.12).

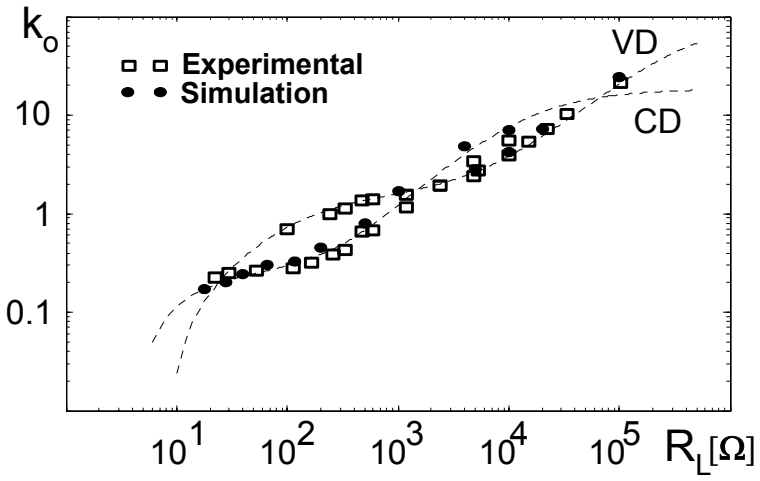

Fig. 4.11 Theoretical (dotted lines), experimental and simulation results of output to input voltage ratio of the PT converter for the two types of rectifiers as a function of the load resistance. Normalized parameters: A_{PT}=0.0242, Q_m=371.5; K_{PT} varies from 0.5 to $3 \cdot 10^5$.

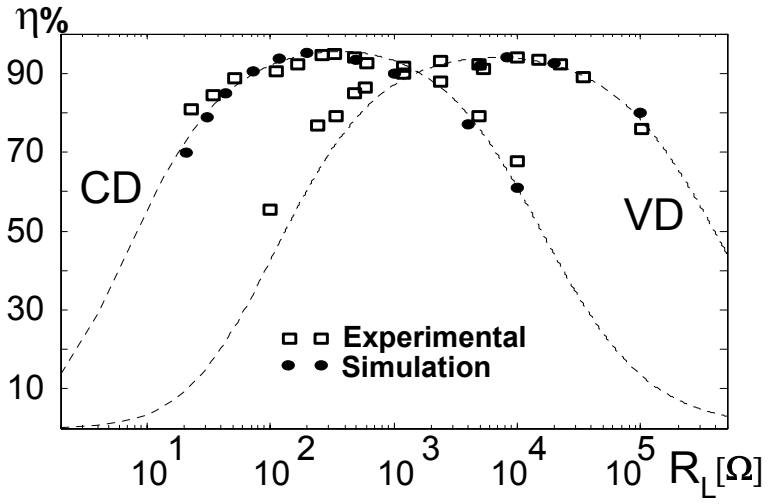

Fig. 4.12 Theoretical (dotted lines), experimental and simulation results of the efficiency of the PT converter with VD and CD rectifiers as a function of the load resistance R_L. Normalized parameters are the same as in Fig. 4.11

4.6. CONCLUSIONS

This section compared two popular rectifiers used in PT power converters: a current doubler rectifier and a voltage doubler rectifier. The advantages and disadvantages of each rectifier were assessed resulting in a recommendation of the preferred application areas for each rectifier in terms of output current and voltage, power handling capability, and load resistance.

The results of this study are general and are not confined to any particular PT since we apply here generic parameters for the PT and the load. The PT is characterized by the normalized parameters: A_{PT}, Q_m, and n, while the load is presented as a normalized factor K_{PT}. These fundamental parameters are used to develop the relationship for the maximum voltage transfer function and Δ_{PT} (which is the ratio of the output power to the power dissipated by the PT). Since the maximum allowable PT power dissipation is one of the most important design constraints, the value of the parameter Δ_{PT} in any given application can determine the maximum output power of the system.

We showed that for low load resistances R_L, higher voltage transfer ratios can be obtained when using the CD rather than the VD rectifier whereas for achieving high gain the VD rectifier is much more suitable.

In general, the results of simulations, experiments and the theoretical results were found to be in a good agreement. Some discrepancies were probably due to experimental errors.

The analytical methodology developed and applied in this study and the closed-form analytical expressions that were derived provide generic information on PT converters that apply the CD and VD rectifiers. The analytical expressions were also summarized in generic graphs shed additional light on PT characteristics. As such, these graphs can be useful for selecting a PT for a given application and for designing a PT for a specific system.

The results of this section have been published in [39, 40].

CHAPTER 5

DESIGN CONSIDERATIONS FOR ACHIEVING ZERO VOLTAGE SWITCHING

Power supplies that employ PTs rather than the classical magnetic transformers have a potential to be made smaller in size. This attribute is relevant for a number of applications such as battery chargers, laptop computers supplies, fluorescent lamp drivers etc. However, earlier designs of PT-based converters/inverters used additional series inductors to meet the zero voltage switching (ZVS) conditions [23, 24], which destroyed the ability of PTs to decrease the size of power supplies. It was already shown in [23] that by using specific characteristics of the PT, ZVS could be achieved without any additional elements. This can be accomplished when the circuit is operating at a frequency that is higher than the resonance frequency of the PT and sufficient energy is available to charge and discharge the PT's input capacitance during the switching dead time. Thus, by utilizing the characteristics of the PT, the switches of the inverter can operate under ZVS conditions without the need of a series inductor. In addition, the inherent input capacitance of the PT works as a turn-off snubber for the power switches, which too decreases the turn-off voltage spikes and thus the turn-off losses of the switches.

This chapter presents a comprehensive analysis of the inherent soft switching capability of PTs. Closed-form equations estimate the load and the frequency boundaries that allows soft switching in a power inverter/converter built around a given PT.

5.1. ANALYSIS AND DESIGN OF ZVS PT POWER INVERTER

A. Analysis of ZVS Conditions for a Half-Bridge Inverter

The analysis is carried out on a half bridge inverter (see Fig.5.1). The inverter has two bi-directional switches Q_1 and Q_2 including anti-paralleled diodes D_1, D_2, and a PT. The PT is represented by an equivalent series-parallel resonant circuit $R_m - L_r - C_r - C_O' - R_L' - n$. The parameters L_r, C_r, R_m represent the mechanical behavior of the PT, C_{in} is the input PT capacitance and the output capacitance of the switches, $C_O' = \frac{C_O}{n^2}$ is the reflected output capacitance, where C_o is the output dielectric capacitance and n is the gain, and $R_L' = n^2 R_L$ is the reflected load resistance R_L.

The switches Q_1 and Q_2 (Fig. 5.1) will normally be power MOSFETs and will include inherent anti-parallel diodes D_1 and D_2. The switches are driven alternately by rectangular voltages V_{GS1} and V_{GS2} with a sufficiently long dead time. Fig. 5.2 depicts steady-state current and voltage waveforms in the inverter for an operating frequency that is higher than the resonance frequency.

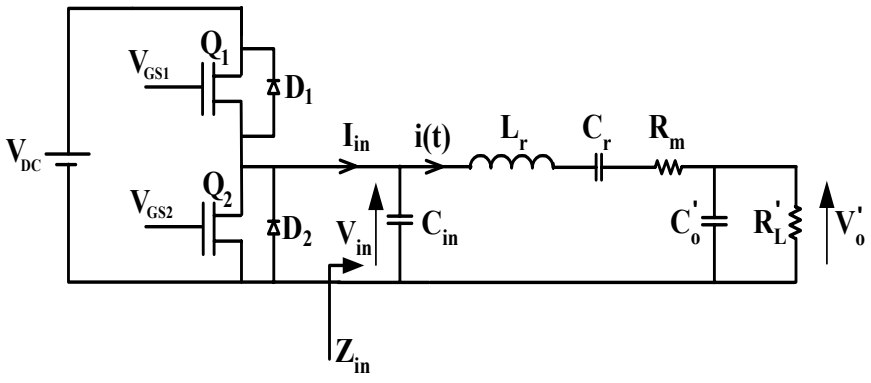

Fig.5.1 Equivalent circuit of a half-bridge inverter driving a PT around a resonant frequency.

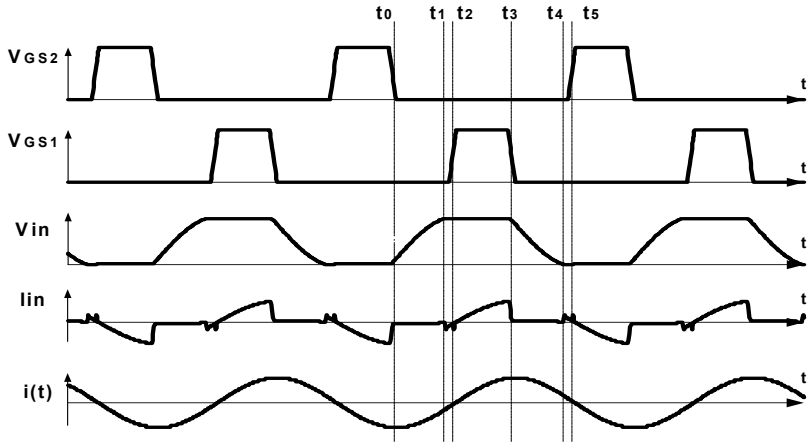

Fig. 5.2 Steady-state current and voltage waveforms of the ZVS PT inverter.

The charging process of the capacitor is considered with reference to Fig. 5.2. At the instant t_o the drive voltage V_{GS2} turns OFFQ_2. Transistor Q_1 is still kept in the OFF state by the drive voltageV_{GS1}. Both diodes are reversed biased and remain in the OFF condition.

Assuming that the quality factor of the network is high, the sinusoidal current waveform of the resonant circuit can be represented by:

$$i(t) = I_m \sin(\omega t - \psi) \tag{5.1}$$

where I_m and ψ are the current peak and initial phase respectively. When transistor Q_2 is turned OFF at the instant t_0 this current is diverted from transistor Q_2 to the capacitor C_{in}. Thus, the current through the shunt capacitor during $t_0 < t < t_1$ is:

$$i_{C1}(t) = -i(t) = -I_m \sin(\omega t - \psi) \tag{5.2}$$

This current charges the capacitor C_{in} so that the voltage across the capacitor (and hence across the switch Q_2) gradually increases from zero to V_{DC}. If the current i_{S2} through transistor Q_2 is forced to drop quickly to zero (by an appropriate gate driver) switching losses in the transistor Q_2 will be low. At t_1, the voltage across the capacitor C_{in} reaches V_{DC}, therefore the diode D_1 turns ON, the current i(t) is diverted from the shunt capacitor C_{in} to the diode D_1, and the voltage across the top switch becomes zero. The diode D_1 conducts during the interval t_1t_2. When the voltage V_{in} decreases to V_{DC} at the instant t_2, the drive voltage V_{GS1} turns the upper

transistor ON. The transistor Q_1 is ON during the time interval t_2t_3. At t_3, it turns OFF again. Since transistor Q_2 is still OFF, the current of the resonant circuit discharges the shunt capacitor C_{in}, decreasing V_{DS2} and thereby increasing V_{DS1}. The discharging process of C_{in} is taking place during the time interval of t_3-t_4. When the voltage across C_{in} reaches zero, the diode D_2 starts to conduct at t_4 and the voltage across the top switch S_2 becomes zero. Since the charging-discharging process takes place when the switch current is zero (both switches are OFF) the switching losses can be made small. In fact, the capacitor C_{in} works as a turn-off snubber for the switches Q_1 and Q_2 of the half-bridge inverter.

B. The Main Assumptions

The analysis of the inverter is carried out under the following assumptions:

1) The capacitor charging time is shorter than the switching dead time.
2) The capacitor is charged by a constant current.
3) The input voltage $V_{in}(t)$ is a symmetrical rectangular waveform (instead of trapezoidal). This assumption is relevant because the difference between the first harmonic amplitude of the rectangular and trapezoidal waveforms is small.
4) The power losses of the PT are limited to 5-10% of the output power.

In order to ensure ZVS for the switches, the input capacitor has to be charged-discharged within the switching dead time whose duration is less than T/4 (where T is the period of the resonant current that is developed during the dead time (see below)).

The charging process begins at t_0. If the charging time t_r is much shorter than the cycle T=1/f, the charging current can be assumed to be constant and is given approximately by

$$I = i_{Cin}(0) = I_m \sin\psi \tag{5.3}$$

The charging process ends when the capacitor voltage reaches V_{DC}. Hence, the charging time is approximately [24]

$$t_r = \frac{C_{in}V_{DC}}{I_m \sin\psi} = \frac{\pi}{2}\frac{C_{in}V_{in(1)p}}{I_m \sin\psi} = \frac{\pi}{2}C_{in}\frac{|Z_{in}|}{\sin\psi} < \frac{1}{4}T \tag{5.4}$$

where $V_{in(1)p}$ is the fundamental component of the rectangular waveform, and Z_{in} is the input impedance of the resonant tank (not including C_{in}).

In order to transfer sufficient energy to the output, the inverter has to operate close to the frequency of maximum output power and under high efficiency conditions [32]. Furthermore, the power dissipated by the PT has to be limited to 5-10% of the output power in order to achieve efficiencies of the order of 90-95%. For example, if the power dissipation of a PT is limited to be 1W, the output power of 10W will be obtained with 90% efficiency (assuming here a lossless inverter).

C. Normalized Model for a Soft Switching PT Inverter

In order to generalize the analysis, we developed a normalized model for a PT inverter which is applicable to any PT that can be described by the resonant network of Fig. 5.1. All parameters of the inverter considered in this study are normalized as follows:

1) The main initial parameters are defined as:

$$a = \frac{C_o'}{C_r};\ b = \frac{C_{in}}{C_o'};\ \omega_r = \frac{1}{\sqrt{L_r C_r}};\ Q = \omega_r C_o' R_L';\ Q_m = \frac{1}{\omega_r C_r R_m} \tag{5.5}$$

2) The normalized input impedance Δ_{Zin} is defined as the ratio of the input impedance of the PT - Z_{in} to the reflected load resistance R_L':

$$\Delta_{Zin} = \frac{Z_{in}}{R_L'} = \frac{R_m + j\omega L_r + \frac{1}{j\omega C_r} + \frac{R_L'}{1 + j\omega C_O' R_L'}}{R_L'} = \frac{A + jB}{1 + j\frac{\omega}{\omega_r}Q} \tag{5.6}$$

where:

$$\begin{cases} A = 1 + \dfrac{a}{QQ_m} - a\left[\left(\dfrac{\omega}{\omega_r}\right)^2 - 1\right] \\ B = \dfrac{\omega_r}{\omega}\dfrac{a}{Q}\left[\left(\dfrac{\omega}{\omega_r}\right)^2 - 1\right] + \dfrac{\omega}{\omega_r}\dfrac{a}{Q_m} \end{cases} \tag{5.7}$$

3) The normalized charging time Δ_r is defined as the ratio of the charging time t_r to the switching period T. (Note that Δ_r has to be less than 1/4 - [23-14, 43]):

$$\Delta_r = \frac{t_r}{T} = \frac{\pi}{2T} C_{in} \frac{|Z_{in}|}{\sin\psi} = \frac{1}{4}\frac{\omega}{\omega_r} bQ \frac{|\Delta_{Zin}|}{\sin\psi} \tag{5.8}$$

where ψ is the normalized input impedance phase angle, which is opposite to the initial current phase (5.1):

$$\psi = \arg\left(\frac{Z_{in}}{R_L'}\right) \tag{5.9}$$

4) The voltage transfer ratio ko is the ratio of the output voltage V_{out} to the peak of the first harmonic of the input voltage $V_{in(1)p}$ (Fig. 5.1):

$$ko = \frac{V_{out}}{V_{in(1)p}} = \frac{1}{\left|\Delta_{Zin}\right|\sqrt{\left[1+\left(\frac{\omega Q}{\omega_r}\right)^2\right]}} \tag{5.10}$$

5) The normalized power dissipated by the PT, Δ_{PD} is defined as the ratio of the PT power dissipated by the P_{PD} to the output power P_{out}:

$$\Delta_{PD} = \frac{P_{PD}}{P_{out}} = \frac{a}{QQ_m}\left[1+\left(\frac{\omega}{\omega_r}Q\right)^2\right] \tag{5.11}$$

6) The inverter efficiency is the ratio is defined as of the output power P_{out} to the input power P_{in}:

$$\eta = \frac{P_{out}}{P_{in}} = ko^2\,\frac{\Delta_{Zin}}{\cos\left(\Delta_{Zin}\right)} \tag{5.12}$$

7) The maximum output voltage is reached at the equivalent resonant frequency ω_m. Since the equivalent resonant frequency is close to the series resonant frequency ω_r, one can replace the normalized resonant frequency $\frac{\omega_m}{\omega_r}$ by the factor $1+\varepsilon$, where ε is a small number that represents a deviation from the normalized series resonant frequency. By equating the derivative of (5.10) to zero we obtain the following approximate expression for ε:

$$\varepsilon \approx \frac{1}{2a\left(1+1/Q^2\right)} \tag{5.13}$$

8) The normalized operating frequency $\frac{\omega}{\omega_r}$ (the ratio of the operating frequency ω to the series resonant frequency ω_r) can now be expressed as:

$$\frac{\omega}{\omega_r} = \frac{\omega}{\omega_m}\frac{\omega_m}{\omega_r} = k(1+\varepsilon), \tag{5.14}$$

where the normalized frequency factor $k=\omega/\omega_m$ is the ratio of the operating frequency to the frequency of the maximum output power.

D. Design guidelines

Given: the PT inverter output voltage V_{out} and the PT parameters $L_r, C_r, C_{in}, C_o, R_m, n$.

To be evaluated: the frequency range, the output power and the load boundaries for soft switching.

The general design steps:

1) On the basis of the specifications of the given PT we calculate the parameters a, b, Q_m (5.5).
2) For different Qs we plot $\Delta_r(k)$ (5.6), (5.8), (5.14), (5.15).
3) For the same Qs we calculate $\Delta_{PD}(k)$ (5.11).
4) Soft switching is achieved in the k range where $\Delta_r(k) < 0.25$. The upper boundary for Q is stated by the requirement $\Delta_r(k) = 0.25$ and the lower boundary for Q is bounded by the PT power dissipation limit Δ_{PD}.
5) From the parameter Q and parameters of PT we calculate the load resistance R_L':

$$R_L' = \frac{Q}{\omega_r C_O'} \tag{5.16}$$

6) Based on the soft switching boundaries of the normalized frequency factor k, the series resonant frequency ω_r and the normalized load factor Q, we calculate the frequency boundaries for ZVS:

$$f = \frac{1}{2\pi} k \left(1 + \frac{1}{2a\left(1 + \frac{1}{Q^2}\right)} \right) \omega_r \qquad (5.17)$$

For $k = \text{const}$ one can calculate the transfer function $ko = f(R_L)$ or for $R_L = \text{const}$ - the transfer function $ko = f(k)$.

EXAMPLE 1.

Given: The PT is a radial vibration mode piezoelectric transformer (T1-2, Transoner^R) [10], the power dissipation of PT is limited to Δ_{PD}=10% and the required peak output voltage is $V_{out(p)}$=30V.

To be evaluated: the frequency range, the input voltage range and the load range that ensures soft switching.

This PT has one layer at the input side and one layer at the output side. The diameter of the PT is 19 mm; the thickness of the input layer is 1.52 mm, and the thickness of the output layer is 2.29 mm.

Applying the HP4395A Impedance Analyzer, the parameters of the simplified electrical equivalent circuit for a narrow frequency range around its mechanical resonant frequency are estimated to be:

$$R_M = 11.6\Omega,\ C_{in} = 2.19\text{nF},\ C_O = 1.547\text{nF},\ C_r = 120\text{pF},$$
$$L_r = 15.1\text{mH},\ f_{res} = 118.3\text{kHz},\ n \approx 1$$

For these circuit parameters the normalized model parameters are calculated to be: a=12.9, b=1.416, Q_m=966.5.

As a preparation for the design we generate the following plots:

a) Fig. 5.3, which is based on equation (5.8), shows the normalized charge time Δ_r as a function of the normalized frequency factor k for different normalized load factor Q. It can be seen that the upper limit for Q to comply with $\Delta_r < 0.25$ is $Q \approx 0.37$. The lower boundary for the load factor is determined by $\Delta_{PD} < 0.1$ ($Q \approx 0.13$) (4.11).

b) Fig. 5.4, which is based on equation (5.10), depicts the transfer function $\mathrm{ko} = \frac{V_{out}}{V_{in}}$ as a function of the normalized frequency factor k for the same normalized load factors Q.

These plots are then used to calculate the input voltage range and power range for which ZVS can be achieved taking into account the design constraints and the maximum power dissipation on PT.

For any given load (Q-factor) the corresponding plots from Fig. 5.3 and Fig. 5.4 can be combined into a single plot. For example Fig. 5.5 is built for Q=0.15. The same plots can be constructed for different R_L values so as encompass the desired power range. In this case the soft switching frequency boundaries are 1.003<k<1.025 (or, from (17): 118770<f<121360 Hz). And for this frequency region the transfer function ko is approximately 0.8>ko>0.22. Hence, the range of the peak input voltage $V_{in(p)} = \frac{V_{out(p)}}{\mathrm{ko}}$ is $37.5\mathrm{V} < V_{in} < 136\mathrm{V}$ respectively (Fig. 5.6).

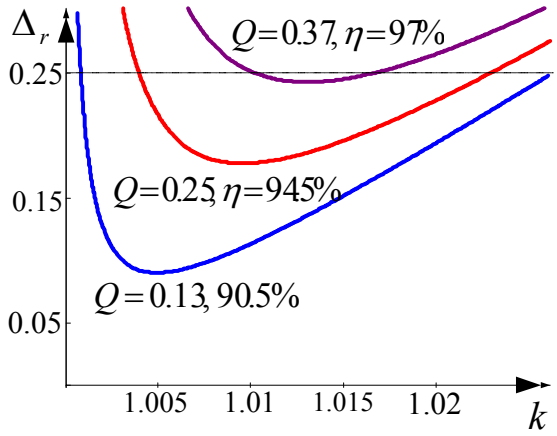

Fig. 5.3 Normalized charging time as a function of the normalized frequency factor k for different normalized load factors Q in the range Q=0.13 to Q=0.37. Data is for a T1-2, Transoner[R].

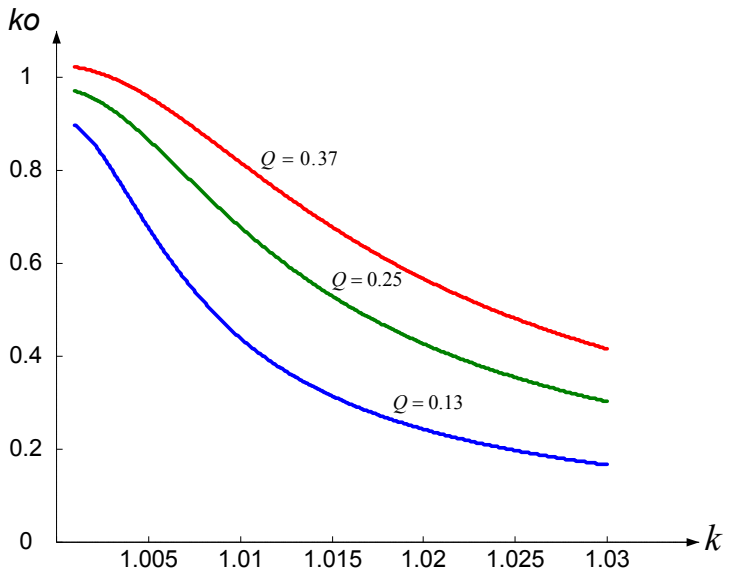

Fig. 5.4 Voltage transfer function ko as a function of the normalized frequency factor k for different normalized load factors Q in the range of Q=0.13 to Q=0.37. Data is for a T1-2, Transoner[R].

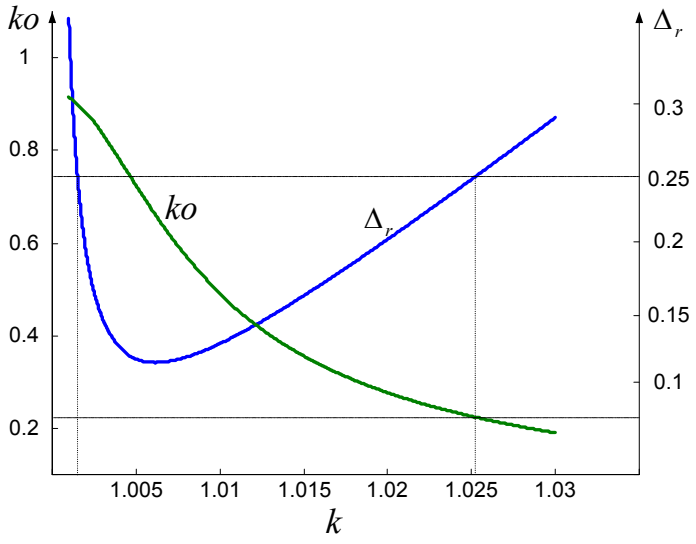

Fig. 5.5 Voltage transfer function ko and the normalized charging time Δ_r as a function of the normalized frequency factor k for normalized load factor Q=0.15 (R_L=130Ω).Data is for a T1-2, Transoner[R].

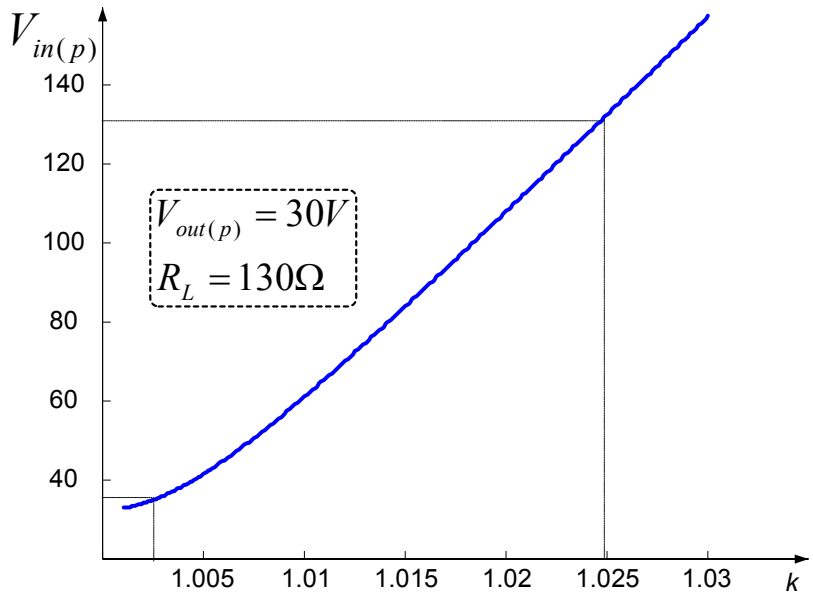

Fig. 5.6 Peak input voltage $V_{in(p)}$ as a function of the normalized frequency factor *k* for the constant output peak voltage $V_{out(p)}$=30V and the load resistance R_L=130Ω. Data is for a T1-2, Transoner[R].

EXAMPLE 2.

Given: the same PT as in Example 1, the power dissipation on PT is limited to 10% of the output power, the peak input voltage $V_{in(p)}$=50V and load resistance R_L=130Ω.

To be evaluated: the boundaries of the output voltage and output power for soft switching operation.

The frequency boundaries for soft switching is evaluated from Fig. 5.5 to be $1.003 < k < 1.025$ (or, from (5.17), $118770 < f < 121360\,\text{Hz}$). The power dissipation of the PT for this load factor and this frequency range is approximately 9%. The transfer function ko that corresponds to this frequency region is 0.8>ko>0.22 (the same as in Example 1.). Consequently, the range of peak output voltage that can be obtained (under soft switching

conditions) $V_{out(p)} = ko \cdot V_{in}$ is $40V > V_{out(p)} > 11V$, and the range of output power $P_{out} = \frac{V_{out(p)}^2}{2R_L}$ is $6.1W > P_{out} > 0.46W$ respectively (Fig. 5.7).

The same procedure can be carried out for different load resistances in the soft switching conditions to obtain the whole range of output voltages and powers.

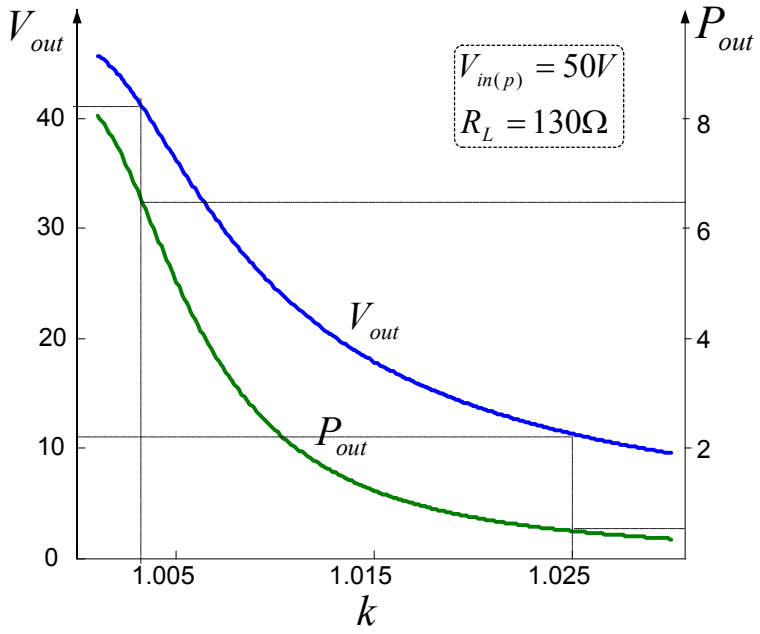

Fig. 5.7 Peak output voltage $V_{out(p)}$ and output power P_{out} as a function of the normalized frequency factor k for peak input voltage $V_{in(p)}$=50V and load resistance $R_L = 130\Omega$. Data is for a T1-2, Transoner^R.

5.2. SIMULATION AND EXPERIMENTAL RESULTS

The proposed model was verified by simulations and experiments. Fig. 5.2 shows the switching timing diagram of a half-bridge inverter (Fig. 5.1) obtained by simulation. The operation frequency was assumed to be f=120kHz (k=1.014) and the load resistance $R_L = 130\Omega$ (Q=0.15). The calculated normalized charging time was $\Delta_r = 0.16$ while the simulated normalized charging time was $\frac{t_r}{T} \approx 0.167$ (Fig. 5.2).

Fig. 5.8 presents the experimental setup. The circuit operates as follows: the input pulse voltage is applied to the dual power MOSFET driver MIC426 where it is divided into two separate complementary pulse voltages, which in turn are connected to the "dead time" networks. The delayed pulses are fed to the high voltage MOS gate driver IR2110, and finally to the gates of the half-bridge inverter MOSFETs. "Dead time" networks are built on resistors, capacitors, and Schotky diodes. Capacitors of the "dead time" networks are charged through the high resistances (330Ω) delaying front sides of pulses, and then quickly discharged through the low resistances (33Ω) and the diodes. In this way the width of the pulses is shortened, producing dead time.

The experimental PT is a radial vibration mode PT (Face Co., VA, USA). Maximum input voltage was 35V. The operation frequency and the load resistance were the same as in the simulation.

Fig. 5.9 shows the experimental voltage curves. The experimental normalized charging time was found to be $\frac{t_r}{T} \approx 0.175$.

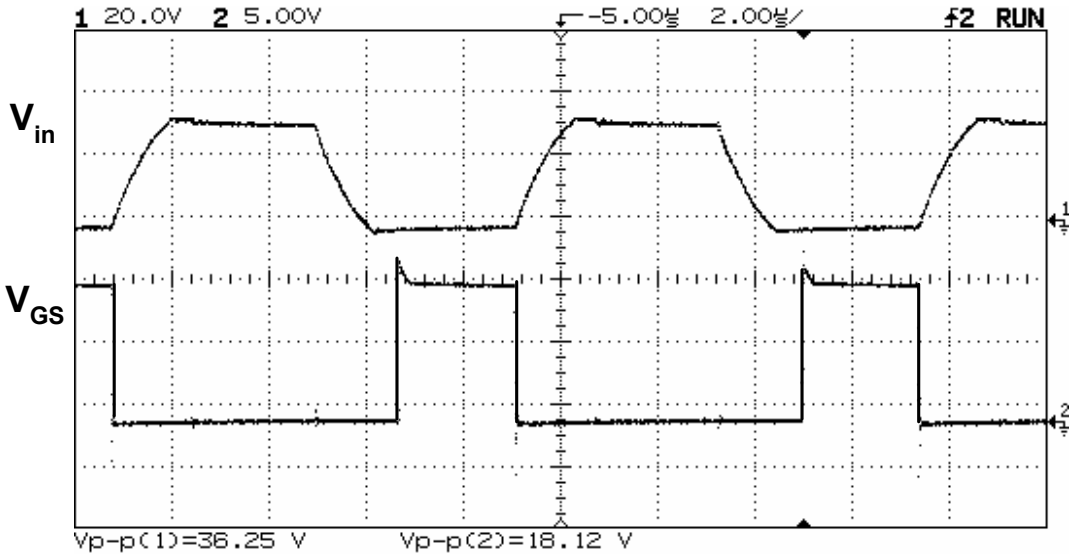

Fig. 5.9 Experimental voltage waveforms of a half-bridge inductor-less PT inverter: V_{GS} (upper plot), V_{IN} (lower plot). Operating frequency f=120 kHz, load resistance R_L=130 Ohm. Data is for T1-2, Transoner^R).

5.3. CONCLUSION

In this chapter we presented a comprehensive analysis of the inherent soft switching capability of PTs. The closed-form equations, developed in this study, were used to estimate the load and frequency boundaries that allow soft switching in a power inverter built around a given PT.

A general procedure for maintaining soft switching in an inductor-less half-bridge piezoelectric transformer inverter was studied analytically and verified by simulations and experiments. The results of the simulations and experiments were in a good agreement with the theoretical predictions.

The results of this study were published in [44].

CHAPTER 6

COMBINED OPERATION OF PIEZOELECTRIC TRANSFORMERS

At present, the power that can be handled through commercial PTs is limited. A possible solution to this problem is to connect several PTs [4, 5, 17]. However, since two different PTs are never absolutely identical, it is crucial to ensure current sharing when the PTs are feeding the same load.

The objective of this section was to define the requirements for combined PTs, and in particular, to identify and quantify the effect of non-identities in PT parameters on current sharing and overall efficiency. This is necessary to avoid overheating of one or more of the combined PTs. The influence of each PT parameter on the operation of parallel-parallel connected PTs is examined and tested by simulations and experiment.

6.1. PARAMETERS OF A SINGLE PT

The equivalent circuit of the PT reflected to the primary side is given in Fig. 6.1, where C_{in} is the input capacitance of PT, $C_o' - R_L'$ are the reflected values of the PT output capacitance and the load resistance, and C_r-L_r-R_m are the equivalent electrical parameters that represent the mechanical resonant circuit of the PT.

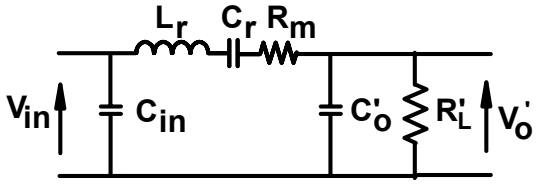

Fig. 6.1 Equivalent circuit of a PT after reflecting the secondary to the primary side.

The study applies the principles of the Generic PT Model. All the parameters of the model are normalized. It is assumed that the PT inverter operates at the frequency of the maximum output voltage [18, 32, 44]. The normalized parameters of the base PT are defined as follows:

$$\begin{cases} a = \dfrac{C_o'}{C_r} \\ \omega_r = \dfrac{1}{\sqrt{L_r C_r}} \\ Q = \omega_r C_o' R_L' \\ Q_m = \dfrac{1}{\omega_r C_r R_m} \end{cases} \tag{6.1}$$

where ω_r is the mechanical resonant frequency of the PT, Q is the normalized load factor, and Q_m is the mechanical quality factor.

Following [44], the frequency corresponding to the maximum output voltage ω_m, the efficiency η, the voltage transfer ratio k_{21}, and the output power P_o are obtained as

$$\omega_m = \omega_r \left[1 + \frac{1}{2a\left(1 + Q^{-2}\right)} \right] \tag{6.2}$$

$$\eta = \frac{1}{1 + \dfrac{a}{Q_m}\left[\dfrac{1}{Q} + \left(\dfrac{\omega_m}{\omega_r} \right)^2 Q \right]} \tag{6.3}$$

$$k_{21} = \frac{1}{\sqrt{\left\{ 1 + \dfrac{a}{QQ_m} - ax \right\}^2 + \left\{ \dfrac{\omega_r}{\omega_m} \dfrac{a}{Q} x + \dfrac{\omega_m}{\omega_r} \dfrac{a}{Q_m} \right\}^2}} \tag{6.4}$$

$$P_o = \frac{V_o^2}{R_L} = k_{21}^2 \frac{V_{in}^2}{R_L} \tag{6.5}$$

where $x = \left[\left(\dfrac{\omega_m}{\omega_r} \right)^2 - 1 \right]$

6.2. POSSIBLE CONNECTION OF PTS FOR COMBINED OPERATION (IDENTICAL PTS)

Generally, the PT can be considered as a two port network. There are four possible ways of interconnecting PTs for combined operation [45]: parallel input – parallel output, series input – series output, series input – parallel output, and parallel input – series output (Fig. 6.2, a-d). It should be noted that last two types of connections are realizable only in the case of ground isolated PTs. Otherwise input or output circuit will be shorted.

We consider these interconnections under the assumption that all the PTs are identical. In order to achieve multiple power in the output, the following conditions for the load resistance R_{LT}, input V_{inT} and output V_{oT} voltages of the total (combined) circuit were derived for each type of connection:

a) Parallel-parallel connection (Fig. 6.2, a).

In this case $V_{inT}=V_{in1}=\ldots=V_{inN}$ and $V_{oT}=V_{o1}=\ldots=V_{oN}$. The voltage gain $k_{21T}=k_{21}$. The load resistance and the output power of the combined circuit are

$$R_{LT} = R_L / N \tag{6.6}$$

$$P_{oT} = \frac{N(V_o)^2}{R_L} = NP_o \tag{6.7}$$

b) Series-series connection (Fig. 6.2, b).

The input and output voltages of the total circuit V_{inT} and V_{oT}, and the load resistance R_{LT} are distributed equally between the PTs. Therefore:

$$\begin{aligned} V_{inT} &= NV_{in} \\ V_{oT} &= NV_o \\ R_{LT} &= NR_L \end{aligned} \tag{6.8}$$

The voltage gain of the total circuit k_{21T} is

$$k_{21T} = \frac{V_{oT}}{V_{inT}} = \frac{NV_o}{NR_L} = k_{21} \tag{6.9)}$$

The output power of the combined circuit is

$$P_{oT} = \frac{(NV_o)^2}{NR_L} = NP_o \tag{6.10}$$

c) Series-parallel connection (Fig. 6.2, c).

Similarly to the first two cases, the input voltage for N PTs has to be N times higher than that of a single unit, the output voltage is the same as for a single PT, and the load resistance is $R_{LT}={}^{R_L}\!/_{N}$.

d) Parallel-series connection (Fig. 6.2, d).

The input conditions in this case are the same as for the parallel-parallel connection and the output conditions are the same as for the series-series connection.

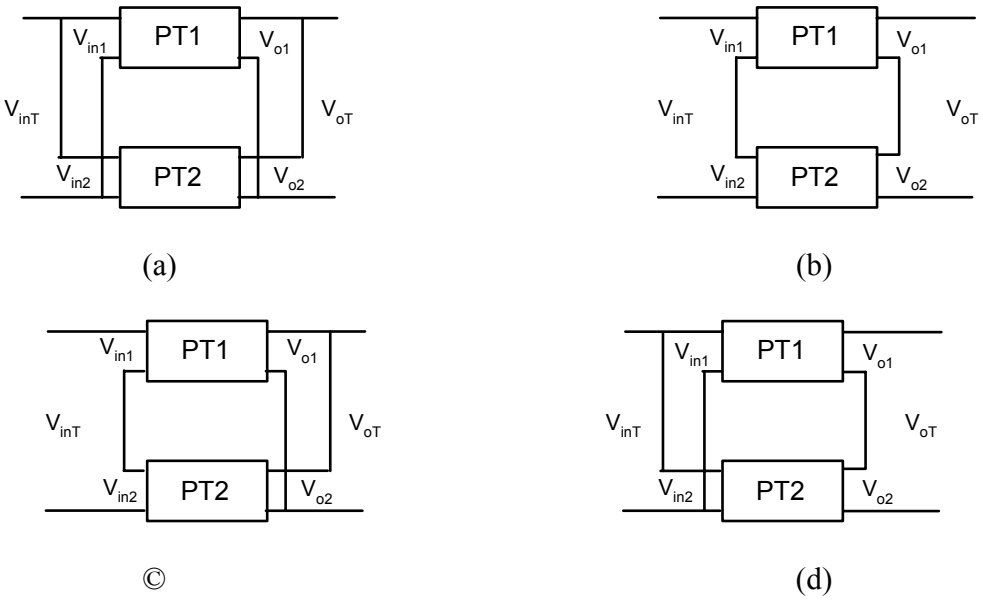

Fig. 6.2 Possible ways of interconnecting PTs (illustrated for two units): a) parallel-parallel, b) series-series, c) series-parallel, and d) parallel-series

Table 6.1 summarizes results the results of the above analysis.

TABLE 6.1: LOAD AND VOLTAGE RATIO CONDITIONS FOR DIFFERENT CONNECTIONS OF COMBINED PTS.

Topology	Figure	R_{LT}/R_L	V_{inT}/V_{in}	V_{oT}/V_o
Parallel-Parallel	2a	1/N	1	1
Series-Series	2b	N	N	N
Series-Parallel	2c	1/N	N	1
Parallel-Series	2d	N	1	N

6.3. PARALLEL-PARALLEL CONNECTION OF NON-IDENTICAL PTS

In general, two PTs are never identical, that is their parameters are usually slightly different. In the following, we make a detailed analysis of the influence of each parameter deviation on parallel-parallel connected PTs by comparing the output power P_{oT} and efficiency η_T of the combined PTs with the output power P_o and efficiency η of a single PT.

The equivalent circuit of two parallel-parallel connected PTs, after reflecting the secondary side to the primary side, is given in Fig. 6.3a. If the combined network operates at a frequency close to its mechanical resonant frequency, this circuit can be simplified to the one shown in Fig. 6.3b by replacing the two networks by a single one. In the following analysis we replace the two parallel branches Z_1 and Z_2 (that is, L_r-C_r-R_m networks) by the equivalent impedance Z_T and derive the parameters of the 'new' PT from the expression of Z_T. This is used to quantify the effect of non-equality in the PT parameters on the overall operation of the parallel-connected PTs.

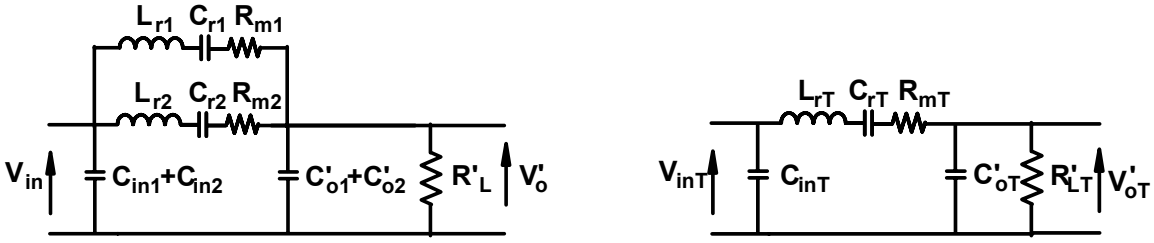

(a) (b)

Fig. 6.3 The equivalent circuits of parallel-parallel connected PTs: (a) common case, (b) operation close to the resonant frequency.

A. The Influence of the Non-Equality of C_o

A deviation in C_o is expressed as follows:

$$C'_{o1} = C'_o$$
$$C'_{o2} = C'_o + \Delta C'_o = C'_o(1+\delta_c) \qquad (6.11)$$

$$C'_{oT} = C'_{o1} + C'_{o2} = 2C'_{o}\left(1 + \frac{\delta_c}{2}\right) \tag{6.12}$$

where C'_{o1} and C'_{o2} are the output capacitances of the parallel PTs reflected to the primary side, ΔC_o and $\delta_c = \Delta C_o / C_o$ are the absolute and relative deviation of the parameter C_o from the nominal value, and C'_{oT} is the reflected capacitance of total PT. We analyze the influence of δ_c for the case when the impedances of the RLC networks Z_1 and Z_2 are the same:

$$Z_1 = Z_2 = R_{m1} + j\omega L_{r1} + \frac{1}{j\omega C_{r1}} = R_{m2} + j\omega L_{r2} + \frac{1}{j\omega C_{r2}} \tag{6.13}$$

If the capacitance deviation is not too great, one can assume that the reflected load resistance of the circuit under consideration is the same as in ideal case (Table 6.1): $R'_{LT} = 0.5R'_{L}$. The impedance and the parameters of the total network are

$$Z_T = Z_1 || Z_2 = 0.5Z_1 \tag{6.14}$$

$$\begin{cases} R_{mT} = 0.5R_m \\ C_{rT} = 2C_r \\ L_{rT} = 0.5L_r \end{cases} \tag{6.15}$$

The normalized parameters (6.1) for this case are

$$\begin{cases} a_T = \dfrac{C'_{oT}}{C_{rT}} = a\left(1 + \dfrac{\delta_c}{2}\right) \\ \omega_{rT} = \omega_r \\ Q_T = \omega_{rT} C'_{oT} R'_{LT} = Q\left(1 + \dfrac{\delta_c}{2}\right) \\ Q_{mT} = Q_m \end{cases} \tag{6.16}$$

By substituting these normalized parameters into equations (6.2)-(6.5) we can calculate the optimal operating frequency for maximum power transfer ω_{mT}, the efficiency η_T, the voltage transfer ratio k_{21T}, and the output power P_{oT}.

Fig. 6.4 represents the relation of the efficiencies (η_T/η) of the combined and single PTs as a function of the normalized non-equality $\Delta C_o/C_o$ for different values of the normalized load parameter Q when the mechanical quality factor is assumed to be Q_m=900. From these plots one can see that the efficiency is decreasing with an increase in $\Delta C_o/C_o$. This

phenomenon can be explained as follows: an increase of the output capacitance C_o causes a larger current in the L_r-C_r-R_m network, which in turn, causes a rise in the losses of R_m and hence a decrease in efficiency. This effect is similar to the case of a single PT with a larger C_o. The larger the output capacitance the lower will be the PT's efficiency. However, substantial deviation in the values of the output capacitances of the PTs (up to 30%) results in minor changes in the overall efficiency.

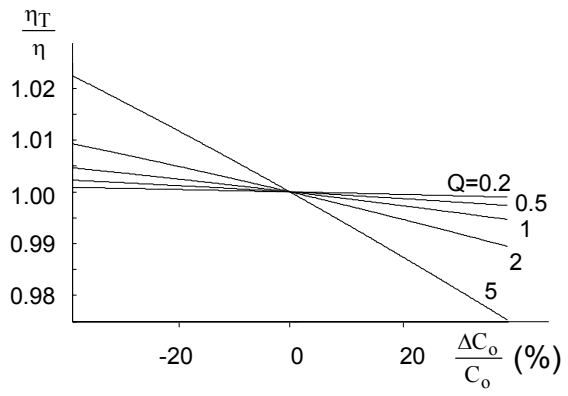

Fig. 6.4 The relation of efficiency to nominal efficiency of the combined circuit as a function of the relative deviation of the output capacitance C_o for Q ranging between 0.2 - 5 and Q_m=900.

B. The Influence of Non-Equality of R_m

The deviation in R_m is:

$$\begin{cases} R_{m1} = R_m \\ R_{m2} = R_m + \Delta R_m = R_m(1+\delta_m) \end{cases} \tag{6.17}$$

where ΔR_m and $\delta_m=\Delta R_m/R_m$ are the absolute and the relative deviation of the loss resistance from its nominal value. Assuming that the rest of parameters are identical

$$\begin{cases} C'_{o1} = C'_{o2} \\ L_{r1} = L_{r2} \\ C_{r1} = C_{r2} \end{cases} \tag{6.18}$$

the total impedance of the network ($Z_T=Z_1||Z_2$) is

$$Z_T \approx \frac{R_m}{2}\left(1+\frac{\delta_m}{2}\right)+\frac{1}{2}j\omega L_r+\frac{1}{2j\omega C_r}+\varphi\left(R_m, C_r, \omega, \delta_m^2\right) \tag{6.19}$$

The function φ (R_m, C_r, ω,δ_m^2) in (6.19) has a relatively small value and can be neglected. Therefore the equivalent series components of the total PT are

$$\begin{cases} R_{mT} = 0.5R_m\left(1+0.5\delta_m\right) \\ L_{rT} = 0.5L_r \\ C_{rT} = 2C_r \end{cases} \tag{6.20}$$

The total output capacitance C_{oT}=2C_o. The load resistance is the same as for the case A. Using these parameters, we recalculate the normalized parameters of the total circuit as follows:

$$\begin{cases} a_T = a \\ \omega_{rT} = \dfrac{1}{\sqrt{L_{rT}C_{rT}}} = \omega_r \\ Q_T = \omega_{rT}C_{rT}R_{LT} = Q \\ Q_{mT} = \dfrac{1}{\omega_{rT}C_{rT}R_{mT}} = \dfrac{Q_m}{1+0.5\delta_m} \end{cases} \tag{6.21}$$

Substituting these normalized parameters into (6.2)-(6.5), we can obtain the expressions for the operating frequency, efficiency, voltage transfer ratio, and output power of the equivalent inverter.

The plots of the output power and efficiency ratios of the combined PT to the single PT P_{oT}/P_o and η_T/η (Fig. 6, a, b) as a function of the non-equality $\Delta R_m/R_m$ for different values of load resistance (parameter Q) show that fairly large changes in the parameter R_m (up to 20%) cause rather small changes in the output characteristics.

Since the impedances of the parallel networks are different, we compare the power losses in the networks Z_1 and Z_2. The loss relation P_{Loss1}/P_{Loss2} can be calculated using the parameters of each PT as follows:

$$\begin{aligned} P_{Loss1} &= I_1^2 R_m = \left(\frac{V_{z1}}{Z_1}\right)^2 R_m \\ P_{Loss2} &= I_2^2 R_m\left(1+\delta_m\right) = \left(\frac{V_{z2}}{Z_2}\right)^2 R_m\left(1+\delta_m\right) \end{aligned} \tag{6.22}$$

where I_1 and I_2 are the rms currents, and V_{z1} and V_{z2} are the rms voltages across the series parts (Z_1 and Z_2). Since $V_{z1} = V_{z2}$, the loss relation λ_m is

$$\lambda_m = \frac{P_{Loss1}}{P_{Loss2}} = \frac{1}{1+\delta_m}\left(\frac{Z_2}{Z_1}\right)^2 \tag{6.23}$$

where

$$\left(\frac{Z_2}{Z_1}\right)^2 = \frac{(1+\delta_m)^2 + \left\{Q_m \frac{\omega_r}{\omega}\left[\left(\frac{\omega}{\omega_r}\right)^2 - 1\right]\right\}^2}{1 + \left\{Q_m \frac{\omega_r}{\omega}\left[\left(\frac{\omega}{\omega_r}\right)^2 - 1\right]\right\}^2} \tag{6.24))}$$

When R_m increases, the current through the RLC network decreases. Hence, the effect on the product I^2R_m (that is, the losses) could be positive or negative. In order to examine the behavior of the loss sharing, we derivate (6.23) with respect to δ_m

$$\frac{\partial \lambda_m}{\partial \delta_m} = \frac{(1+A)\left\{(1+\delta_m)^2 - A\right\}}{(1+\delta_m)^2(1+A)^2} \tag{6.25))}$$

where

$$A = \left\{Q_m \frac{\omega_r}{\omega}\left[\left(\frac{\omega}{\omega_r}\right)^2 - 1\right]\right\}^2 \tag{6.26}$$

It should be noted that a change in R_m has practically no impact on the maximum output voltage frequency [3-4]. Hence, A is independent of δ_m. The sign of the derivative $\frac{\partial \lambda_m}{\partial \delta_m}$, which is defined by the sign of the expression $(1+\delta_m)^2 - Q_m^2\left(\frac{\omega}{\omega_r} - \frac{\omega_r}{\omega}\right)^2$, determines the slope of the loss ratio curves.

If Q_m is very high, then the derivative is negative and the plots of the loss ratio will go down. If Q_m is very low, then the derivative is positive and the plots of losses ratio will go up. Otherwise, the slope of the loss ratio is dependent on the load factors (the load resistance) and can even change the polarity for a given δ_m.

Plots of the loss ratio as a function of the ratio $\Delta R_m/R_m$ for different values of the load resistance (parameters Q varying from 0.056 to 0.2) and Q_m=370 (Fig. 6.5, c) show that the loss relationship in the parallel parts of the PTs varies less than 5-10% when $\Delta R_m/R_m$ changes by more than 15%. Since the mechanical quality factor of the PT is intermediate (Q_m=370, as in PT2-1, Face Co., VA, USA), the slopes of the curves change polarity from one load resistance to another.

The boundaries of the loss ratio deviation can be obtained by analyzing (6.23)

$$\lambda_m = \frac{1}{1+\delta_m}\frac{R_m^2(1+\delta_m)^2 + X^2}{R_m^2 + X^2} = \frac{\left(\frac{R_m}{X}\right)^2(1+\delta_m)^2 + 1}{\left[\left(\frac{R_m}{X}\right)^2 + 1\right](1+\delta_m)} \tag{6.27}$$

where $X = \omega L_r - \frac{1}{\omega C_r}$

If $\left(\frac{R_m}{X}\right)^2 << 1$, than $\frac{P_{Loss1}}{P_{Loss2}} \approx \frac{1}{1+\delta_m}$

If $\left(\frac{R_m}{X}\right)^2 >> 1$, than $\frac{P_{Loss1}}{P_{Loss2}} \approx 1+\delta_m$

Therefore

$$\frac{1}{1+\delta_m} < \frac{P_{Loss1}}{P_{Loss2}} < 1+\delta_m \tag{6.28}$$

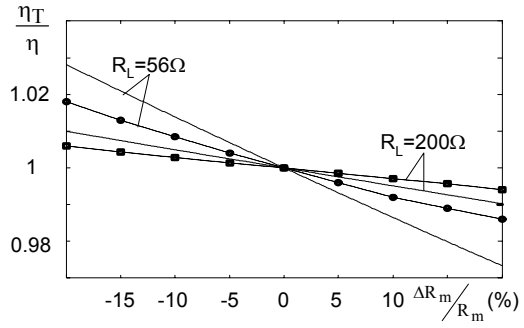

(a)

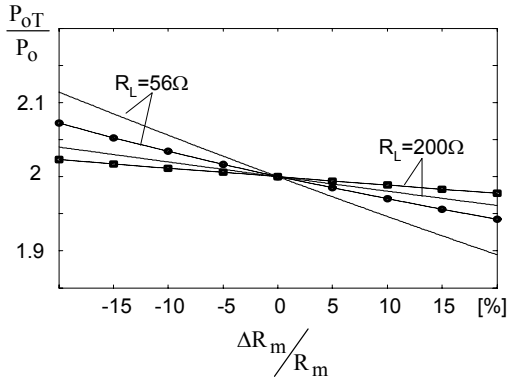

(b)

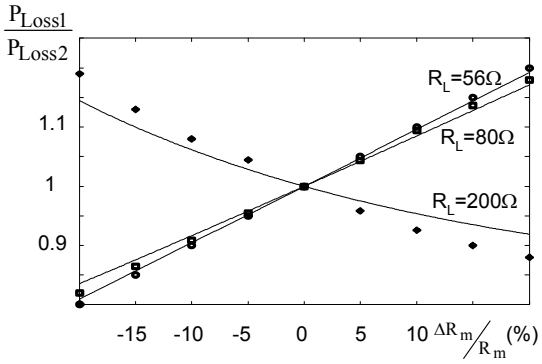

(c)

Fig. 6.5 The efficiency, (a), output power, (b), and losses ratio, (c) as a function of the relative deviation of the loss resistance R_m for different values of the load resistances R_L. Solid line – theoretical prediction, dots – PSPICE simulation results. Simulation was carried out assuming that PTs nominal parameters are identical to those of PT2-1, Face Co., VA, USA.

C. The Influence of Non-Equality of ω_r

The main problem of the case when the mechanical resonant frequencies are different is that the currents in the parallel branches of the PTs are strongly unequal, which causes a large difference in the losses. The losses ratio $\lambda_\omega$is

$$\lambda_\omega = \frac{1+\left\{Q_m \frac{\omega_r}{\omega}\left[\frac{\left(\frac{\omega}{\omega_r}\right)^2(1+\delta_\omega)-1}{(1+\delta_\omega)}\right]\right\}^2}{1+\left\{Q_m \frac{\omega_r}{\omega}\left[\left(\frac{\omega}{\omega_r}\right)^2-1\right]\right\}^2} \qquad (6.29))$$

where δ_ω is the normalized mechanical resonant frequency deviation ($\delta_\omega=\Delta\omega_r/\omega_r$).

Fig. 6.6 shows the losses ratio as a function of the frequency deviation for different values of the parameter Q when Q_m=370. One can see that even minor deviations in the resonant frequency of the PTs (less than 2-3%) cause a great difference in the losses (up to ten times and more), which renders combined operation impractical.

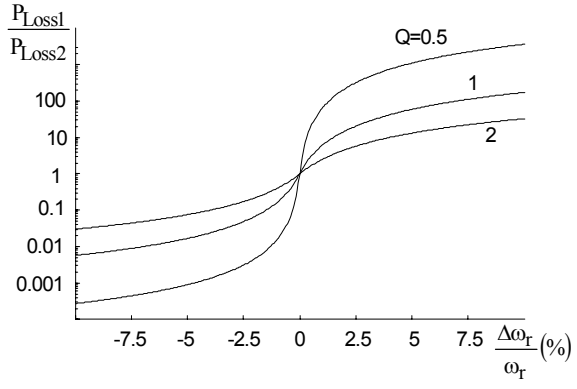

Fig. 6.6 The loss ratio in the parallel connected PTs as a function of the relative change of the mechanical resonant frequencies of PTs for different values of Q (Q_m=900).

D. The Influence of Non-Equality of C_r and L_r while ω_r is Kept Constant

In order to examine how non-equality of the parameters C_r and L_r in parallel parts of the PTs (when ω_r are the same) impacts the output characteristics of the combined PTs we assume that the series capacitance and inductance of the second PT are different from the parameters of the first (nominal) PT while the series resonant frequency of the parallel parts remains constant (δ_{Cr} and δ_{Lr} are relative variations of C_r and L_r)

$$\begin{aligned} C_{r2} &= C_{r1}(1-\delta_{Cr}) \\ L_{r2} &= L_{r1}(1+\delta_{Lr}) \end{aligned} \qquad (6.30))$$

when $\omega_{r1}=\omega_{r2}$

$$C_{r1}L_{r1} = C_{r2}L_{r2} \qquad (6.31)$$

or

$$\delta_{Lr} = \frac{\delta_{Cr}}{1-\delta_{Cr}} \qquad (6.32)$$

The total series impedance is

$$\begin{aligned} Z_T \approx{}& \frac{\left(2+2\delta_{Lr}+\delta_{Lr}^2\right)R_m}{(2+\delta_{Lr})^2} + \frac{1}{2j\omega C_r(1-0.5\delta_{Cr})} \\ &+ \frac{1}{2} j\omega L_r \frac{1+\delta_{Lr}}{1+0.5\delta_{Lr}} \end{aligned} \qquad (6.33)$$

which implies that

$$\begin{cases} R_{mT} \approx 0.5R_m \\ L_{rT} \approx 0.5L_r(1+0.5\delta_{Lr}) \\ C_{rT} \approx 2C_r(1-0.5\delta_{Cr}) \end{cases} \qquad (6.34)$$

The losses ratio λ_r is

$$\lambda_r \approx \frac{\frac{1}{Q_m^2} + \left[\frac{\frac{\omega}{\omega_r} - \frac{\omega_r}{\omega}}{1-\delta_{Cr}}\right]^2}{\frac{1}{Q_m^2} + \left[\frac{\omega}{\omega_r} - \frac{\omega_r}{\omega}\right]^2} \tag{6.35}$$

Analyzing (33) we obtain the boundary of the loss ratio deviation.

$$\text{If } \frac{1}{Q_m^2} << \left[\frac{\omega}{\omega_r} - \frac{\omega_r}{\omega}\right]^2, \text{ then } \frac{P_{Loss1}}{P_{Loss2}} \approx \frac{1}{(1-\delta_{Cr})^2} \tag{6.36}$$

$$\text{If } \frac{1}{Q_m^2} >> \left[\frac{\omega}{\omega_r} - \frac{\omega_r}{\omega}\right]^2, \text{ then } \frac{P_{Loss1}}{P_{Loss2}} \approx 1 \tag{6.37}$$

The loss ratio as a function of relative non-equality of C_r and L_r for two load resistances is shown in Fig. 6.7. The plots reveal that for non-equality of the parameters C_r and L_r by 15% the loss ratio varies up to 1.5 times.

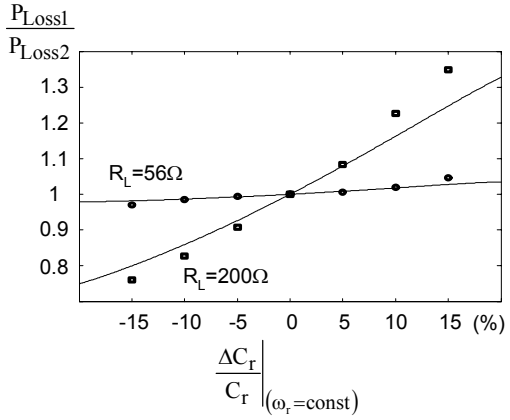

Fig. 6.7 The loss ratio in the parallel-connected PT as a function of the relative change of the parameters C_r (complementary to L_r) while mechanical resonant frequencies ω_r=118.4kHz are identical. Solid line – theory, dots – simulation results. Simulation was carried out assuming that the PTs nominal parameters are identical to those of PT2-1, Face Co., VA, USA

6.4. SIMULATIONS AND EXPERIMENTS

The equivalent circuit parameters of the experimental PTs, (PT2-1 Face Co., VA, USA) were measured [6] to be as follows: R_m=21Ω, C_r=172.5pF, L_r=10.5mH, C_o=1.33nF, C_{in}=1.78nF, n=1.08. (Q_m=370, a=8.33). The influence of deviations of different PT parameters on output power, efficiency and loss sharing in the combined circuit were tested by time domain PSPICE simulation, and were found to be in a good agreement with the theoretical predictions (Figs. 6.5 and 6.7).

Experiments were carried out on two radial vibration mode PTs. The mechanical resonant frequencies of the PTs were found to be 118.43kHz and 118.38kHz (less than 0.06% difference). The maximum efficiency achieved in both individual and combined operation of the PTs was 96.5%. Parallel operation provided double output power as compared to the single PT.

For experimental verification of the theoretical predictions, two pseudo PTs were built in the form of two LCC series-parallel resonant networks with no output transformer.

The experimental setup used the following data:

1) The series inductances and capacitances were C_{r1}=1.011nF, L_{r1}=2.087mH, C_{r2}=0.945nF, L_{r2}=2.25mH. Measured series resonant frequencies were f_{r1}=108.6kHz and f_{r2}=109.3kHz. Thus, the parameter deviations were δ_{Cr}≈−6.5%, δ_{Lr}≈7.8%, and the mechanical frequency deviation δ_ω was about 0.65%.
2) The parallel capacitances were equal: C_{o1}=C_{o2}=10nF (capacitances ratio a=9.9).
3) The measured ac resistances of the inductances and the capacitances in the experimental setup were R_{m1}=13.67Ω, R_{m2}=17Ω which means a parameter deviation of δ_m=24.4%.
4) Mechanical quality factor was Q_m≈105.
5) Experimental resistances were 56Ω and 200Ω (load factor Q was equal to 0.77 and 2.75), the capacitances ratio, a, was about 10 (similar to that of the experimental PT).
6) The experiment involved low input power (up to 5W). The two LCC networks were connected in a parallel-parallel scheme.

The results of the measurements were as follows:

1) R_L=56Ω. Currents in the RLC networks were: I_{r1}=185mA, I_{r2}=153mA, which caused P_{Loss1}=0.468W and P_{Loss2}=0.4W, and hence the loss ratio λ was 1.17
2) R_L=200Ω. The measured currents were I_{r1}=152mA, I_{r2}=132mA, losses: P_{Loss1}=0.317W, P_{Loss2}=0.296W, and loss ratio λ=1.07.

It can be shown that for a small deviation such as $\lambda \approx 1$ the total losses ratio λ_T can be approximated by

$$\lambda_T = 1-(1-\lambda_m)-(1-\lambda_\omega)-(1-\lambda_{Cr}) \qquad (6.38)$$

Using expressions (6.23), (6.29) and (6.35) the theoretical predictions were found to be as follows:

For R_L=56Ω

λ_T=1−(1−1.37)−(1−0.835)−(1−0.89)=1.085

For R_L=200Ω

λ_T=1−(1−1.2)−(1−0.85)−(1−0.883)=0.94

As can be seen, the experimental results are in good agreement with the theoretical prediction.

6.5. CONCLUSIONS

In this chapter we carried out detailed analysis of the influence of each PT parameter deviation on the effectiveness of parallel-parallel operation of PTs. It was found that the requirements for equality of R_m and C_o in two parallel-connected PTs are not strong. The most critical parameter that can harm parallel operation is ω_r – the mechanical resonant frequency. For good current sharing, the mechanical resonant frequencies of the parallel-connected PTs have to be very close while C_r and L_r may be slightly different.

Our main conclusion is that effective parallel connection of PTs can be achieved if the mechanical resonant frequencies of the parallel units are matched, because current sharing in

parallel parts is dependent on the impedances of the parallel branches. The impedance of the L_r-C_r-R_m network, Z, is a function of the characteristic impedance Z_r of the network and its series resonant frequency:

$$Z \approx \sqrt{R_m^2 + \left(Z_r \frac{2\Delta\omega}{\omega_r} \right)^2} \tag{6.39}$$

where $\Delta\omega=\omega_m-\omega_r$ and $Z_r = \sqrt{\frac{L_r}{C_r}}$

Z_r in practical PTs is very high. For the experimental units Z_r is about 7.5kΩ, although it may reach 100kΩ [32] and above. Consequently, a small deviation in ω_r, that will cause a corresponding shift in $\Delta\omega$, will result in a large difference in Z and hence in the loss ratios.

As discussed in [5, 24, 26], the equivalent parameters of PT are dependent on the transformer dimensions and ceramic constants. When two PTs are produced from the same ceramic material under the same technological process, their dimensions are equal with high accuracy, the sound velocity in the PTs are practically the same (that is, the same mechanical resonant frequencies), and their masses and all mechanical properties are the same. Thus their equivalent parameters L_rC_r are probably very similar, which suggest equal characteristic impedances. This means that the main requirement for proper combined operation could be fulfilled in practical piezoelectric transformers.

The results of this chapter have been published in [46].

CONCLUSIONS AND FUTURE WORK

A generic approach towards the design and analysis of PT converters has been developed in this research. Our main results can be summarized as follows:

1. Two novel methods for determining PT equivalent circuit parameters were proposed and verified. The first method was based on measurements of the input impedance of a short circuited PT and the second on measurements of the voltage transfer function (amplitude and phase) of a loaded PT. It was shown that the short circuit method is easier, but can only be recommended for those PTs that are not sensitive to the voltage level. As such, it is not suitable for the Rosen-type PT. On the other hand, the second method is more accurate and suits every kind of PT.

2. Analysis of DC/DC PT converters with different types of rectifiers operating at either mechanical resonant frequency or frequency of maximum output power yielded several models. It was found that a PT converter with half-way rectifier operates similarly to a PT converter with a current doubler rectifier, and a PT converter with a full-way rectifier operates similarly to a PT converter with voltage doubler rectifier.

2.1. Detailed examination of the converter with a half-way two-diode rectifier operating at a mechanical resonant frequency revealed that this type of converter can operate not only in the known non-overlapping mode where there is no overlap between the conduction intervals of the diodes, but also in the newly uncovered overlapping mode with overlap between the conduction intervals of the diodes. Both operation modes depend on the PT equivalent parameters and the load resistance. The study highlighted the effect of the load and parasitic resistances on the output voltage and losses for both modes.

2.2. Comparative examination of the current doubler and the voltage doubler rectifiers connected at the output of the PT converter, operating at a frequency of maximum output voltage, displayed the advantages and disadvantages of each rectifier configuration. This allowed us to recommend the preferred application areas for each rectifier in terms of output current and voltage, power handling capability, and load resistance.

3. A comprehensive analysis of the inherent soft switching capability of PTs resulted in the development of a general procedure for maintaining soft switching in an inductorless half-bridge PT inverter. The closed-form equations developed in the study estimated the

load and frequency boundaries that allow soft switching in a power inverter built around a given PT.

4. Detailed analysis of the influence of each PT parameter deviation on the effectiveness of parallel-parallel operation of PTs allowed us to determine the basic principles for achieving the combined operation of several PTs.

5. All the main problems considered in the research were complemented with practical recommendations for engineering design.

6. All the theoretical results were found to be in good agreement with the simulations and experiments.

7. The results of this work are general and are not restricted to any particular PT since generic parameters for the PT and load were applied.

Recommended Future Work

- Since a PT is a non-linear element, its performance depends on the operating conditions (voltage/current) and load. This dependence should be examined and equivalent PT parameters should be verified according to the operating conditions.
- A generic PT model is widely applied in PT converter/inverter design. However, many PT power supplies utilize a small inductance in the input networks for achieving soft switching. A generic model of this kind of PT operation should be developed. Accomplishing this target could be very useful for engineering design of PT power converters/inverters.
- This study examined conditions for successful operation of parallel-parallel connected PTs. Additional research on other kinds of combined operation of PTs could provide opportunities for exploiting various power supplies.

REFERENCES

[1]. E. M. Syed, F. P. Dawson, and E. S. Rogers, "Analysis and modeling of a Rosen-Type piezoelectric transformer," in *Proc. IEEE PESC,* 2001, pp.1761-1766.

[2]. Y. Sasaki, M. Yamamoto, A. Ochi, T. Inoue, and S. Takahashi, "Small multilayer piezoelectric transformers with high power density - characteristics of second and third-mode Rosen-Type transformers,*" Jpn. J. Appl. Phys*., Vol. 38 (1999), pp. 5598-5602.

[3]. K. Kanayama, N. Maruko, and H. Saigoh, "Development of the multilayer alternately poled piezoelectric transformer,*" Jpn. J. Appl. Phys.*, Vol. 37 (1998), pp. 2891-2895.

[4]. C. Y. Lin and F. C. Lee, "Piezoelectric transformer and its application," in *Proc. IEEE VPEC,* 1995, pp. 129-136.

[5]. C. Y. Lin, "*Design and analysis of piezoelectric transformer converters,*" Ph. D. Dissertation, Virginia Tech. July 1997.

[6]. K. Sacurai, K. Ohnishi and Y. Tomikawa, "Presentation of a new equivalent circuit of a piezoelectric transformer under high-power operation," *Jpn. J. Appl. Phys*., Vol. 38 (1999), pp. 5592-5597.

[7]. J. Hu, Y. Fuda, M. Katsuno, and T. Yoshida, "A study on the rectangular-bar-shaped multilayer piezoelectric transformer using length extension mode," *Jpn. J. Appl. Phys*., Vol. 38 (1999), pp. 3208-3212.

[8]. J. Navas, T. Bove, J. A. Cobos, F. Nuno, K. Brebol, "Miniaturized battery charger using piezoelectric transformer," in *Proc. IEEE PESC,* 2001, pp. 492-496.

[9]. A. Oliver, R. Prieto, M. Sanz, J. A. Cobos, and J. Uceda, "1D modeling of multi-layer piezoelectric transformers," in *Proc. IEEE PESC*, 2001, pp. 2097-2102.

[10]. M. J. Prieto, J. Diaz, J. A. Martin, F. Nuno, "A very simple DC/DC converter using piezoelectric transformer," in *Proc. IEEE PESC*, 2001, pp. 1755-1760.

[11]. T.Bove, W. Wolny, E. Ringgaard, K. Breboel, "New type of piezoelectric transformer with very high power density," in *Proc IEEE PESC*, 2002*,* pp. 2005-2009.

[12]. T. Zaitsu, O. Ohnishi, T. Inoue, M. Shoyama, T. Ninomiya, F. Lee, and G. Hua, "Piezoelectric transformer operating in thickness extensional vibration and its application to switching converter," in *Proc. IEEE PESC,* 1994, pp. 585-589.

[13]. J. Hu, H. Li, H. Chan, and C. Choy, "A ring-shaped piezoelectric transformer operating in the third symmetric extensional vibration mode," *Sensors and Actuators,* vol. 88 (2001), pp. 79-86.

[14]. K. Sacurai, T. Nakazawa, S. Shindou, K. Ohnishi and Y. Tomikawa, "Experimental investigation of a piezoelectric ceramic transformer using radial vibration of disks combined with a coupling element," *Jpn. J. Appl. Phys*., Vol. 37 (1998), pp. 2896-2900.

[15]. R. L. Lin, F. C. Lee, and E. Baker, “Characterization of piezoelectric transformers,” in *Proc. IEEE VPEC*, 2000, pp. 219-225.

[16]. R. L. Lin, P. L. Wong, and F. C. Lee, “An equivalent circuit model of radial vibration mode piezoelectric transformers,” in *Proc. IEEE VPEC,* 2000, pp. 120-125.

[17]. H. Kakehashi, T. Hidaka, T.Ninomiya, M. Shoyama, H. Ogasawara, Y. Ohta, “Electronic ballast using piezoelectric transformers for fluorescent lamps,” in *Proc. IEEE APEC,* 1998, pp. 29-35.

[18]. G. Ivensky, M. Shvartsas, and S. Ben-Yaakov, “Analysis and modeling of a piezoelectric transformer in high output voltage applications,” *IEEE Trans. Power Electron.,* vol. 19, pp. 542-549, Mar. 2004.

[19]. T. Zaitsu, T. Inoue, O. Ohnishi, and A. Iwamoto, “2 MHz power converter with piezoelectric ceramic transformer,” in *IEEE Intelec Proc.*, pp. 430-437, 1992.

[20]. O. Ohnishi, H. Kishie, A. Iwamoto, T. Zaitsu, and T. Inoue, “Piezoelectric ceramic transformer operating in thickness extensional mode for power supply,” *Ultrasonics Symposium,* pp. 483-488, 1992.

[21]. M. Shoyama, K. Horikoshi, T. Ninomiya, T. Zaitsu, and Y. Sasaki, "Steady-state characteristics of the Push-Pull piezoelectric inverter," *APEC-97*, pp. 715-721.J.

[22]. C. Y. Lin and F. C. Lee, "Development of a piezoelectric transformer converter," in *Proc. IEEE VPEC*, 1993, pp. 79-85.

[23]. R. L. Lin, F. C. Lee, E. M. Baker and D. Y. Chen, “Inductor-less piezoelectric electronic ballast for linear fluorescent lamp,” in *Proc. IEEE APEC*, 2001, pp. 664-669.

[24]. R. Lin, “*Piezoelectric transformer characterization and application of electronic ballast*,” Ph. D. Dissertation, Virginia Polytechnic Institute, 2001.

[25]. H. Kakedhashi, T. Hidaka, T. Ninomiya, M. Shoyama, H. Ogasawara and Y. Ohta, “Electronic ballast using piezoelectric transformers for fluorescent lamps,” in *Proc. IEEE PESC*, 1998, pp. 29-35.

[26]. A. A. Erofeev, “*Piezoelectritcheskie transformatory,*” Mashinostroenie, Leningrad, 1982, in Russian.

[27]. Y. Hsu, C. Lee, and W. Hsiao, "Optimizing piezoelectric transformer for maximum power transfer," *Smart Material and Structures,* pp. 373-383, 2003.

[28]. P. Gonnard, P. Schmitt, and M. Brissaud, "New equivalent lumped electrical circuit for piezoelectric transformers," *IEEE Symp. on the Appl. of Ferroelectrics,* May 2002, pp. 319-322.

[29]. A. Mezheritsky, "Invariants of coupling coefficients in piezoceramics," *IEEE Tranz. Ultrason., Ferroelect., and Freq. Cont.,* vol. 50, no. 12, pp. 1742-1751, 2003.

[30]. S. Lineykine and S. Ben-Yaakov, “Feedback isolation by piezoelectric transformers: a feasibility study,” in *Proc. IEEE PCIM*, 2000*,* pp.175-181.

[31]. S. Ben-Yaakov and N. Krihely, “Modeling and driving piezoelectric resonant blade elements,” in *Proc. IEEE APEC-2004,* pp. 1733-1739.

[32]. G. Ivensky, I. Zafrany, and S. Ben-Yaakov, “General operation characteristics of piezoelectric transformers,” *IEEE Trans. Power Electron,* vol. 17, pp. 1049-1057, Nov. 2002.

[33]. C.Y. Lin and F.C. Lee, “Design of a piezoelectric transformer converter and its matching networks,” in *Proc. IEEE PESC*, 1994, pp. 607-612.

[34]. T. Ninomiya, M. Shoyama, T. Zaitsu, T. Inoue, ‘Zero-voltage-switching techniques and their application to high frequency converter with piezoelectric transformer,’ in *Proc. IEEE IECON*, 1994, pp.1665-1669.

[35]. J. Sun and V. Mehrotra, “Unified analysis of half-bridge converters with current-doubler rectifier,”in *Proc. IEEE PESC*, 2001, pp. 514-520.

[36]. R. L. Steigerwald, “A comparison of half-bridge resonant converter topologies”, *IEEE Trans. Power Electron.*, vol. 3, vol. 3, pp.174 -182, Apr. 1988.

[37]. A. M. Flynn, S. R. Sanders, “Fundamental limits on energy transfer and circuit considerations for piezoelectric transformers,” in *Proc. IEEE VPEC*, 1998, pp. 1463-1471.

[38]. E. Wells, "Comparing magnetic and piezoelectric transformer approaches in CCFL applications," *Analog Application Journal,* Texas Instrument Inc., www.ti.com/sc/analogapps, pp. 12-17.

[39]. G. Ivensky, S. Bronstein, and S. Ben-Yaakov, “A comparison of piezoelectric transformer AC/DC converters with current-doubler and

voltage-doubler rectifiers," *IEEE Trans. on Power Electron.,* vol. 19, pp. 1446-1453, Nov. 2004.

[40]. G. Ivensky, S. Bronstein, and S. Ben-Yaakov, "A comparison of piezoelectric transformer AC/DC converters with current doubler and voltage doubler rectifiers," in *Proc. IEEE PESC*, 2003*,* pp. 365-370.

[41]. G. Ivensky, S. Bronstein, and S. Ban-Yaakov, "Analysis and design of a piezoelectric transformer AC/DC converter in a low voltage application," in *Proc. IEEE PESC,* 2002, pp. 409-414.

[42]. G. Ivensky, S. Bronstein and S. Ben-Yaakov, "Approximate analysis of the resonant LCL DC-DC converter," in *Proc. IEEEI*, 2004, pp. 44-47.

[43]. M. Kazimerczuk and D. Czarkowski, *Resonant power converters*, John Wiley & sons, Inc., 1995.

[44]. S. Bronstein, and S. Ben-Yaakov, "Design considerations for achieving ZVS in a half bridge inverter that drives a piezoelectric transformer with no series inductor," in *Proc. IEEE PESC*, 2002, pp. 585-590.

[45]. L. Weinberg, *"Network analysis and synthesis,"* McGraw-Hill Book Company, Inc. 1962.

[46]. S. Bronstein, G. Ivensky, S. Ben-Yaakov, "Parallel operation of piezoelectric transformers," in *Proc. IEEE PESC-2004,* pp. 1779-1785.

תקציר

השימוש הגובר של שנאים פיזואלקטריים באלקטרוניקת הספק מחייב באנליזה ותכנון מעמיקים של ממירי הספק פיזואלקטריים. בנוסף, יש מקום לבחון את האפשרויות להתגבר על יכולות מוגבלות של העברת הספק דרך שנאי פייזו ע״י חיבור מקבילי של מספר שנאים. התנאים המוזכרים יכולים לשפר את התכנון של התקני הספק מבוססים שנאי פייזואלקטרי.

מטרה המרכזית של עבודת מחקר זו הינה פיתוח מודלים כלליים של ממירי פייזו. אנו בוחנים מעגלי כניסה ויציאה של ממירי פייזו תוך שימוש במעגל תמורה של השנאי.

קבלת פרמטרי מעגל אקוויוולנטי של שנאי פייזו ממדידות פיסיקליות עדיין מהווה בעיה. לפיכך, נקודת ההתחלה של עבודת מחקר זו היא שיפור השיטות הקיימות ופיתוח שיטות חדישות לשערוך הפרמטרים של מעגל תמורה, על מנת להתאימם לכל סוג של שנאי פייזו ולתנאים בהם השנאי הנתון פועל. בעבודה זו אנו מציעים ובוחנים שתי גישות לפתרון בעיה זו.

מודלים כלליים של ממירי הספק AC/DC מבוססים שנאי פייזו מתקבלים דרך אנליזה השוואתית של מיישרים שונים המחוברים ביציאת השנאי. הגישה המיושמת בעבודה זו הינה כללית ומציגה מעגל ישור בעזרת רשת אקוויוולנטית בעלת עומס זהה.

המבנה המיוחד של שנאי פייזו מאפשר תכנון חדשני של ממירי פייזו המבטיחים מיתוג רך ללא צורך בסלילים נוספים בכניסה לשנאי. תכנון כזה עשוי להוריד נפח ומחיר של רכיבים במעגל. לפיכך, מטרה נוספת של המחקר הינה פיתוח שיטות כלליות לקבלת מיתוג רך ללא אלמנטים ראקטיביים נוספים.

בסיום העבודה מוגדרות דרישות כלליות להפעלה משותפת של מספר שנאים.

מלות מפתח: שנאי פייזואלקטרי, מעגל תמורה, הערכת פרמטרים, גישה כללית, מיישרים, מיתוג רך, ספקים.

שנאים פייזואלקטריים באלקטרוניקת הספק

מאת

סבטלנה ברונשטיין

הוגש לסינאת אוניברסיטת בן-גוריון בנגב

תשרי תשס״ו October 2005

באר-שבע